Predicting Temperature Profiles in Soil During Simulated Forest Fires

A Thesis Submitted to the College of
Graduate Studies and Research
in Partial Fulfillment of the Requirements
for the Degree of Master of Science in the
Division of Environmental Engineering at the
University of Saskatchewan
Saskatoon

By

Ebenezer Korsah Enninful

PERMISSION TO USE

In presenting this thesis in partial fulfillment of the requirements for a Postgraduate degree from the University of Saskatchewan, I agree that the Libraries of this University may make it freely available for inspection. I further agree that permission for copying of this thesis in any manner, in whole or in part, for scholarly purposes may be granted by the professor or professors who supervised my thesis work or, in their absence, by the Head of the Department or the Dean of the College in which my thesis work was done. It is understood that any copying or publication or use of this thesis or parts thereof for financial gain shall not be allowed without my written permission. It is also understood that due recognition shall be given to me and to the University of Saskatchewan in any scholarly use which may be made of any material in my thesis.

Requests for permission to copy or to make other use of material in this thesis in whole or part should be addressed to:

The Head of Division
Division of Environmental Engineering
57 Campus Drive
University of Saskatchewan
Saskatoon
S7N 5A9

ABSTRACT

Below-ground effects during forest fires are some of the important issues forest managers consider when conducting prescribed fire programs. Heat transfer models in soil are needed to predict temperatures in soil during forest fires. Many of the heat transfer models in soil that include the effects of moisture are complex and in most cases do not have very good predictive abilities. Researchers believe that simple heat transfer models in soil that neglect the effects of moisture could have very good predictive abilities.

This study presents a one-dimensional numerical model of heat transfer in dry homogenous sand. Both constant and temperature dependent thermal properties of the sand were used in order to determine which had better predictive abilities. The constant thermal properties model was also extended to a model of two-layer dry soil. A computer code written in Fortran was used to generate results from the model. A number of experiments were conducted with dry sand to validate the model. A comparison of the numerical and experimental results indicated that the temperature dependent properties model had better predictive abilities than the constant properties model. The models were found to do a good job of predicting temperature profiles and depth of lethal heat penetration at heat fluxes indicative of forest fires.

Experiments were also conducted to determine the effect of moisture on temperature profiles and the depth of lethal heat penetration in sand and the effect of inorganics on the spread rate of smoldering combustion in peat moss. An experimental correlation of the effects of inorganic content on the spread rate of smoldering combustion in peat moss was developed. Additionally, laboratory methods of validating models of heat transfer in soil were developed with the aim of limiting the dependence on full scale testing. Specifically the use of the cone calorimeter for validating numerical models of heat transfer in soil and the responses of forest floor soil and laboratory created soil samples to heat input were compared. The results indicated that the laboratory created soil did a very good job of mimicking the heat response of the forest floor soil with a maximum difference in lethal heat penetration of 4%.

DEDICATION

I dedicate this thesis to my daughter Quintina, whose first steps in this world I missed seeing whilst “selfishly” seeking academic laurels.

ACKNOWLEDGMENTS

The author would like to thank the Lord God Almighty for the strength and wisdom in starting and completing this study. The author would also like to take this opportunity to thank the following people and organizations for their support, involvement, and financial assistance through which this research was made possible.

- Professor D.A. Torvi for his supervision of this research and almost fatherly guidance throughout the study especially in times of “non-academic” troubles. Thank you Sir.
- Professor J.D. Bugg, Professor O. W. Archibold and Professor Y.-H. Lin for their direction as part of the author’s supervisory committee.
- Mr. Kris Johnson of Saskatchewan Forest Center and Dr. Marty Alexander of FERIC for technical advice on various aspects of this study .
- Mr. Chris James and Mr. Dave Deutscher of the Mechanical Engineering Department for technical assistance in experiments.
- The College of Graduate Studies and Research, the Division of Environmental Engineering and the Natural Sciences and Engineering Research Council of Canada for their funding of this research.
- Mr. John Olusegun for his assistance with experiments.
- Mr. Franklin Krampa-Morlu for his assistance with aspects of the computer code development.

TABLE OF CONTENTS

LIST OF TABLES

LIST OF FIGURES

NOMENCLATURE

Notation

T_f = average fluid temperature [K^{-1}]

k = thermal conductivity [W/m·K]

c = specific heat [J/kg·K]

t = time [s]

$t_{exposure}$ = period of exposure of incident heat flux [s]

q''_o = incident heat flux from cone calorimeter [kW/m^2]

$q''_{convection}$ = convective heat flux losses [kW/m^2]

q''_{rad} = radiative heat flux losses [kW/m^2]

q''_k = heat flux conducted into soil [kW/m^2]

x = depth in soil from surface of soil [m]

Ta = ambient temperature [K]

T_o= initial temperature of soil [K]

T = temperature [K]

g = acceleration due to gravity [m/s^2]

L = thickness of soil [m]

$P = \frac{\Delta t}{\Delta x^2}$ = stability criteria of the form of the Fourier number[s/m^2]

MC = moisture content

IC = inorganic content

$\hat{P}$ = statistical probability of burning

R_M = the moisture ratio (volume of water to volume of soil), and

R_I = the inorganic ratio (volume of inorganics to volume of soil).

w = load loss rate [$g/cm^2 \cdot hr$]

w_{max} = maximum load loss [$g/cm^2 \cdot hr$]

R = smoldering spread rate [cm/hr]

k_w = the thermal conductivity at the surface, [W/m·K]

Nu_L = Nusselt number

Ra_L = Raleigh number

P_r = Prandtl's number

h = convective heat transfer coefficient [W/m^2·K]

Greek Symbols

σ = Stephan Boltzmann's constant [W/m^2·K^4]

α = thermal diffusivity [m^2/s]

ρ = density [kg/m^3]

v = kinematic viscosity of air [m^2/s]

$\beta = 1/T_f$ = expansion coefficient of air [K^{-1}]

δ = penetration depth [m]

Δx = mesh size [m]

Δt = time step [s]

ϕ = view factor

Abbreviations

TDTP = temperature dependent thermal properties

CTP = constant thermal properties

DLHP = depth of lethal heat penetration [m]

Subscripts

1 = first layer

2 = second layer

max = maximum

i = initial

∞ = ambient

CHAPTER ONE: INTRODUCTION

1.1 Forest/Wildland Fires

Fire is one of the most important factors affecting the extent, composition, and character of forest and other plants in wildlands [1]. A forest/wildland fire is an uncontained and freely spreading combustion which consumes the natural fuels of a forest. These fuels are duff (partially decomposed organic material of the forest floor beneath the litter of freshly fallen twigs, needles, and leaves), litter, grass, dead branch wood, snags, logs, stumps, weeds, brush, foliage, and to a certain degree, green trees. Thus any fire not prescribed for an area by an authorized plan can be referred to as a forest/wildland fire. There are three types of forest/wildland fires based on where combustion takes place. These are described as follows.

- Surface fire: A surface fire burns surface litter, loose debris on the forest floor and small vegetation at or near the soil surface, mostly in flaming combustion [1]. The typical spread rate of a surface fire is 8.3 to 50 m/min [2].
- Ground fires: A ground fire typically burns without flames and consumes organic material beneath the surface litter of the forest floor which lies on top of the mineral soil. The typical spread rate in a ground fire is 3.3×10^{-4} to 1.62×10^{-2} m/min [2].
- Crown fire: A crown fire evolves from surface fires and in this type of fire the upper layers or canopies of vegetation undergo flaming combustion [1]. The typical spread rate in a crown fire is 15 to 200 m/min [2].

1.2 Severity of forest/wildland fires

The term fire severity is used by several authors to describe the ecological impacts of fire [3]. Generally the severity of a fire on soil is governed by the litter and soil organic material consumed by fire. There are three levels of fire severity: low, moderate and high. In low-severity fires, temperatures do not normally exceed 100^{o}C at the surface and 50^{o}C at about 5 cm depth in the soil [4]. Moderate-severity fires have surface

temperatures in the range of 250 – 500^{o}C and consume most of the organic matter at the soil surface, leaving mineral soil exposed but not visibly altered [4]. Temperatures over 50^{o}C can be reached as deep as 5 cm into soil [5]. In high-severity fires, surface temperatures exceed 500^{o}C. In such fires temperatures in excess of 250^{o}C can be achieved at a depth of 10 cm and in excess of 100^{o}C at a depth of 22 cm [6].

1.3 Importance of forest/wildland fires

Forest/wildland fires can constitute an environmental risk especially in areas and periods of high temperatures and low precipitation. On the other hand, forest/wildland fires play a vital role in removing excess fuels and maintaining normal plant composition and density in forests. This section provides a basic review of the effects of forest/wildland fires in terms of financial impacts and effects on seeds, soil, plants and nutrients in the soil. More details on the effects of forest fires on ecosystems can be found in [7].

1.3.1 Financial impacts of wildland/forest fires

Statistics from Natural Resources Canada indicate that the average forest area burned is 2.5 million ha/year, the average fire occurrence rate is 8000 fires/year, and the average suppression cost is $500 million annually [8]. In 2003, British Columbia recorded severe forest fires during the forest fire season and it is estimated that in that year, the British Columbia Government spent $545 million in managing forest fires [9].

1.3.2 Effect of fire on soil and nutrients

In most forest types, a mantle of organic material accumulates on top of the mineral soil; this is identified as duff, muck, or peat. This organic material reduces soil erosion, increases water infiltration, stabilizes soil surface temperature and controls moisture evaporation [5]. When the organic material is reduced or removed through burning in a forest/wildland fire, the mineral soil becomes more susceptible to soil erosion, and there is increased surface water runoff. When high temperatures persist in soil it can result in reduced water infiltration [10 cited by 2], reduced water absorption [11] and alteration of the clay structure [12]. Above 300^{o}C, there is substantial loss of nitrogen and sulfur in gaseous form to the atmosphere. However, the high temperatures in a forest/wildland

fire can cause important plant nutrients like phosphorous, potassium, magnesium, calcium, manganese and sulfur to be oxidized and made readily available for plant use. More information on soil, its functions in supporting plant life and effect of fire on nutrients can be found in [4, 13, 14].

1.3.3 Effect of fire on seeds and plants

Generally, experience has shown that germination of seeds becomes more rapid as the temperature of the soil rises up to a certain point beyond which the temperature becomes lethal to the seed [15]. Studies have also shown that exposure of a living part of a plant to a temperature of 60^{o}C for even a short time is lethal [16, 17, 18]. Generally the effects of fire on seeds and plant tissues vary depending on the temperature, duration of exposures and moisture content of the plant tissue. Detailed information on the effects of fire on seeds and plants can be found in [5, 7, 17, 19].

1.4 Depth of lethal heat penetration

Scientists agree generally that a temperature of 60^{o}C is a reasonable approximation of a lethal temperature required to kill shoot tissues of land plants [5, 16, 17, 18, 20, 21]. During forest/wildland fires, the depth at which a temperature of 60^{o}C is achieved is referred to as the depth of lethal heat penetration. Ryan [2] mentions that there is a relationship between the depth of reproduction organs and seeds and the depth at which lethal temperatures are achieved. These combine to determine a plant's ability to survive a fire and to regenerate. In general, however, the likelihood of plant tissue being killed is dependant on the amount of thermal energy it receives, which is described as being the combination of the temperature reached and the duration of exposure [20].

1.5 Heat Transfer in Soil

1.5.1 Combustion

All combustion require three elements: fuel, oxygen, and a source of heat. When these three elements are combined in the appropriate environment, combustion will occur. If any of the elements is removed, combustion stops. Fire and smoke are visual manifestations of the combustion process. For a wildland fire, the vegetation in the

forest serve as the fuel, oxygen is plentiful in the atmosphere, and the source of heat could be from natural causes such as lightning or from human-made sources such as a burning cigarette butt or a camp fire.

In the development of a wildland fire, the following phases have been observed: (i) pre-ignition and pyrolysis, (ii) ignition, (iii) initial growth, (iv) secondary growth, (v) flame decay, (vi) extinction and (vii) cooling. Ryan [2] states that, once ignited, wildland fires will burn until a significant change occurs in either the weather or fuels.

1.5.2 Heat transfer principles

In the discipline of heat transfer, temperature represents the amount of thermal energy available, whereas heat flow represents the movement of thermal energy from place to place. In forest/wildland fires heat is transferred from burning fuels to the organic and mineral soils through several processes, including conduction through the soil grains, liquid, and gases; evaporation-condensation; vapor and liquid diffusion; convection; and radiation in the gas-filled pores. Some of the processes of heat transfer in soil are described below.

Radiation: All materials radiate thermal energy in amounts determined by their temperature and other factors such as emissivity. Radiation becomes the dominant mode of heat transfer at high temperatures. Thus, due to high temperatures in wildland fires, radiation is the major source of heat transfer in crown fires without close proximity between fire and unburnt fuel and also at the initiation of wildland fires [7, 22]. In soil, radiation takes place through the voids in the soil.

Convection: This is the transfer of heat by currents within a fluid. It arises from temperature differences either within the fluid or between the fluid and its boundary. There are two types of convective heat transfer:

(a) natural convection in which the temperature of the solid can induce a fluid motion, and

(b) forced convection in which air blown over warm surfaces by the use of external devices such as fans and pumps to generate a fluid motion in addition to that due to temperature.

Conduction: Regions with greater molecular kinetic energy will pass their thermal energy to regions with less molecular energy through direct molecular collisions. Conduction is the dominant mode of heat transfer in soils [16, 22, 23, 24].

Vaporisation/ condensation: Water has a high heat capacity and when it is vaporised through absorption of heat it is able to move much faster in soil pores and organic layers than in the liquid form. On condensing the amount of thermal energy required to vaporize it is released into its surroundings and this raises the temperature of the soil or organic layer.

Detailed information on heat transfer principles in porous media can be found in [25].

1.5.3 Soil temperatures:

The temperature of the soil affects climate, plant growth, the timing of budburst or leaf fall, the rate of decomposition of organic wastes and other chemical, physical, and biological processes that take place in the soil. Soil organisms and their ecological processes give an indication of the thermal and hydrological regimes of the soils they inhabit [7].

Soil temperatures typically fluctuate annually and daily as a result of variations in air temperature and solar radiation. The annual variation of daily average soil temperature at different depths due to solar radiation can be estimated using a sinusoidal function to represent surface temperature variation with time [26]. In the case of wildland fires, the type, loading and size of vegetative fuel undergoing combustion and the rate at which the fire moves determines surface and ground temperatures during forest fires. Ecologists are generally interested in soil temperatures under fires because of their influence on seed germination and plant survival [24].

During forest/wildland fires, maximum surface temperatures can be in the range of 200^{o}C to 700^{o}C [27] but fires with low fuel loadings usually have ground temperatures of less than 225^{o}C [7]. Archibold et al. [28] recorded above-ground and surface temperatures in fescue, spear grass and brome community burns. At a depth of 5 cm into the soil. They measured surface temperatures of 357^{o}C in brome stands, 189^{o}C in fescue, 209^{o}C in spear grass, 692^{o}C in a snowberry stand and 589^{o}C in an aspen grove. At a depth of 5 cm, they recorded average temperatures of 17^{o}C in brome stands, 6^{o}C in fescue, 14^{o}C in spear grass, 40^{o}C in snowberry and 452^{o}C in aspen grove.

1.6 Factors affecting heat transfer in soil

The transmission of heat within soil is dependent on the physical and thermal properties of the soil particles, the degree of compaction, and the moisture content of the soil. Typically the temperature reached by a material in a fire depends not only on the fire's behaviour but also heat transfer mechanism and the thermal properties of the material [2]. In this research, the focus is on the heat transfer mechanism within the soil and therefore the behaviour of fire will not be discussed in detail. However, data from the literature on surface temperatures and durations of such fires will aid in the choices of boundary conditions and inputs for a numerical model for heat transfer in soil that will be developed in Chapter Two.

Heat transfer in a soil, neglecting the effects of moisture, can be modeled using the Fourier field equation for the case of variable thermal properties:

$$\rho c \frac{\partial T}{\partial t} = \frac{\partial}{\partial x}\left(k \frac{\partial T}{\partial x} \right) + \frac{\partial}{\partial y}\left(k \frac{\partial T}{\partial y} \right) + \frac{\partial}{\partial z}\left(k \frac{\partial T}{\partial z} \right) \qquad (1.1)$$

where: T = temperature

t = time

k = thermal conductivity of soil

c = specific heat of soil

ρ = density

x, y, z = cartesian coordinates

For one-dimensional heat transfer with variable thermal properties, Equation (1.1) becomes:

$$\rho c \frac{\partial T}{\partial t} = \frac{\partial}{\partial x}\left(k \frac{\partial T}{\partial x} \right) \tag{1.2}$$

In the case of constant thermal properties, the Fourier field equation (Equation (1.1))is of the form:

$$\rho c \frac{\partial T}{\partial t} = k\left(\frac{\partial^2 T}{\partial x^2} + \frac{\partial^2 T}{\partial y^2} + \frac{\partial^2 T}{\partial z^2} \right) \tag{1.3}$$

For the case of constant thermal properties, one-dimensional heat transfer in the *x*-direction, Equation (1.3) reduces to:

$$\frac{\partial T}{\partial t} = \alpha \frac{\partial^2 T}{\partial x^2} \tag{1.4}$$

where $\alpha = \frac{k}{\rho c}$ is the thermal diffusivity.

Because of the porosity and the variability of the amounts of air and water contained in soil, the analysis of heat flow through soil is much more complicated than for a homogeneous solid, for which thermal conductivity and heat capacity are stable, well-defined parameters. Soil is a composite of mineral particles, organic matter, and pores which may contain either water or air. All these materials differ widely in their thermal characteristics. For example, the thermal conductivity of the mineral particles is typically five times that of water, 10 times that of organic matter, and 100 times that of air [29]. Hence thermal conductivities of soil samples can vary considerably, depending on the relative amounts of mineral particles, organic matter, and pores containing water or air.

1.6.1 Thermal properties

The thermal properties of the soil (thermal conductivity, volumetric heat capacity, and thermal diffusivity) determine the rate at which heat is transmitted within the soil. The thermal conductivity relates the heat that will flow through the material for a particular temperature gradient in the material. The volumetric heat capacity measures the soil's ability to store thermal energy. The thermal diffusivity is a ratio of the thermal conductivity to the volumetric heat capacity and is a measure of the ability of the soil to transmit a thermal disturbance. For any soil, the larger the value of thermal diffusivity,

the greater the rate of heat transfer in the soil hence the greater the depth of lethal heat penetration.

1.6.2 Moisture

The thermal properties of soil are affected by water content and the resultant effect of moisture on the heat transfer mechanism in soil has been catalogued by numerous authors [22, 30, 31, 32]. Water has a high volumetric heat capacity, about four times that of air [32], and the overall volumetric heat capacity of a soil is a linear function of water content. Water has a higher thermal conductivity than air hence there is a rapid increase in thermal conductivity of soil with just a small addition of water due to water replacing air at the contact points of soil particles [33].

The phase change associated with moisture in soil depresses the temperatures at the soil interface, in comparison to dry soils, by requiring the absorption of the heat of vaporisation [33]. This is similar to moisture's effect on reducing the rate of heat release in fuels when burning [34]. Simmerman [35] conducted a study to compare dry and moist underburns in ponderosa pine shelterwoods with the objective of reducing fuel loadings. In the study, Simmerman found that fuel reduction was as much as 70% in dry burns whereas in moist burns fuel reduction was only about 30%. Frandsen and Ryan [33], in comparing burns in wet and moist sands covered with peat moss found residual uncharred peat moss in burns on wet sand whereas there was complete charring of the peat moss in burns on dry sand. Wet soils typically do not exceed 100^{o}C at the surface until the moisture has been dried out [22, 36, 37]. The effect of moisture can literally be taken as an increase in soil thermal diffusivity due to an increased thermal conductivity and volumetric heat capacity but with a larger increase in the volumetric heat capacity than in thermal conductivity.

1.7 Challenges of prescribed fire management

Pyne et al. [38] mentions that forests in many parts of the world have suffered health losses due to prevention of fires. Fire suppression over long periods of time has resulted, in certain cases, in insect and disease damage and an increase in crown fire potential and

increased stand densities. In recent years this has resulted in severe forest fires which have accelerated forest mortality, threatened people, property and natural resources, and emitted large amounts of particulate matter [39].

Prescribed fire is widely used as a means of reducing unwanted fuels, preparing sites for seeding, and for managing vegetation. Prescribed fire involves setting fires under controlled conditions to eliminate excess fuels within the forest in order to avoid catastrophic uncontrollable fires. This is very important especially considering the economical and ecological impacts of forest fires. Prescribed fire can also be used for selective regeneration since vegetative species have depth-specific underground parts [5] and can also be used to improve wildlife habitat. Forest managers want to accomplish these objectives while minimizing adverse impacts of heat on the soil.

Much as prescribed fire can be a good tool, improper or incorrect use could lead to undesired consequences. For example, repeated prescribed fire every two to 10 years is essential to perpetuate longleaf pine ecosystems and is a valuable stand-management tool in Southeast America [40]. However, using prescribed fire on an annual basis as a tool to maintain an effective fire break may not allow enough time for the soils to fully recover [41].

In the use of prescribed fire, some of the challenges are minimizing excessive consumption of organic matter and excessive soil sterilization, and ensuring that the fire does not get out of control. Generally a duff/organic layer covering is expected to suppress mineral soil temperatures initially from persistent and abundant flames of surface fires by acting as an insulator. However, this causes drying of the duff which may burn after the passage of the fire. Due to the intimate contact between duff and the mineral soil and the long period of burn of smoldering fires, burning of duff after a prescribed fire or any other fire for that matter can have severe consequences for the mineral soil. Smoldering organic matter can transfer heat and cause temperature rises in excess of 300^{o}C to persist in the mineral soil for long periods of time. The ability to predict heating of the soil during a fire will aid in relating fire behaviour to the totality of

fire effects and is very important in determining the efficacy of a prescribed fire and ultimately its management.

1.8 Literature review

Studies on heat transfer in soil as well as smoldering combustion of organic matter have been catalogued by many authors. Some of the studies have been purely experimental in which temperatures of soil are measured during a fire (e.g., [17, 26, 32]) and in others analytical and numerical models have been developed to predict heat transfer in the soil under various surface boundary conditions with or without experimental verification (e.g., [15, 16, 29, 42]). The surface boundary conditions for most of these works are different from that which will be used in this study. Most of the works have used temperature of the source of heat as an input for the model whilst for this study the heat flux from the source of heat will be used. Some of the relevant works concerning heat transfer in soil during a fire are described below.

1.8.1 Feddes

Feddes [24] gave a general review of some of the aspects of heat transfer in soil based on experiments on a groundwater level experimental field at Oudkarspel in the Netherlands. Feddes calculated heat transfer in soils by considering heat transfer as a periodic phenomenon in an isotropic soil. The quantitative description of the heat fluxes and temperatures were based on analytical solutions of the one-dimensional Fourier equation of heat conduction (Equation (1.4)) using heat flux from the sun as surface boundary condition. He assumed that the period and amplitude of the heat flux from the sun were constant sinusoidal functions of time for periods without cloud cover and for cloudy periods a Fourier series replaced the sinusoidal function. For this study clay and light sandy loam soil of a groundwater experimental field at Oudkarspel were analysed. The thermal capacities of the soils were determined using the volume fraction formula of deVries [43] and data obtained indicated that wet soils had a larger thermal capacity than dry soils. Similar methods were used for the soil thermal conductivity and observed data indicated that wet soils had a larger thermal conductivity.

The analytical solution indicated that the temperature amplitude at the surface of the soil was proportional to the heat flux and the phase of the heat flux was in advance of that of the surface temperature. Feddes also investigated experimentally, the effect of moisture on the amplitude and phase displacement of the heat flux in soil. Data obtained from experiments indicated that dry soils showed larger heat flux amplitudes than wet soils. Results from the experiments also indicated that evaporation produced large amplitudes of heat flux and temperature. This implies that soils undergoing evaporation had higher risk of night frost.

1.8.2 Scotter

Scotter [23] presented a simplified analytical model for describing soil temperatures under grass fires. Scotter assumed that for grass fires, which are normally short-lived in any one spot, the soil temperature just beneath the surface does not rise above 100^{o}C. This assumption was based on experimental work of other researchers who had found that the temperature in partly saturated soils cannot rise above 100^{o}C until the water had been removed. The objective of Scotter's study was to provide an insight for ecologists who would be interested in soil temperatures under wildland fires due to their influence on seed germination and plant survival. The model assumed conduction to be the dominant mode of heat transfer in the soil.

Two experiments were conducted in this work for validation of the model. The first was an in situ measurement of temperatures in and beneath a grass fire in which diode thermometers were used at 2 cm and 4 cm depth to measure temperatures. The second experiment involved an artificial grass fire on an artificial soil. This latter experiment used a wooden tray measuring 60 cm by 60 cm which had been filled with sand to a depth of 4 cm. Chromel-constantan thermocouples of 0.1 mm diameter were used to measure temperatures at depths of 0.3 cm and 1.0 cm. Results for both experiments showed good agreement between model and experiment with difference between predicted and measured maximum temperatures of about 33%. In both experiments, the temperature above the soil stayed above 100^{o}C for approximately 80 seconds. For validation of the model with the first experiment, assumed values of thermal diffusivity

were used whilst for the second experiment, measured mean values of thermal diffusivity of the sand were used. However because the surface boundary condition had been assumed to be 100^{o}C, the predicted soil temperatures were independent of the actual maximum temperature in the fire just above the surface.

1.8.3 Steward et al.

Steward et al. [16] presented a solution of the one-dimensional Fourier equation (Equation (1.4)) for conduction heat transfer for six heat flux boundary conditions at the soil surface in graphical terms using dimensionless groups. These diagrams can be used to predict the depth of lethal heat penetration based on the 60^{o}C criterion. Three heat flux histories were used: a constant heat flux for a specific time, a Gaussian heat flux distribution with a specified variance in time and a triangular heat flux distribution. These three heat flux distributions, with and without convective cooling at the surface generated six heat flux boundary conditions which all had the same total heat transfer. These heat flux distributions were compared to measured heat flux distributions in experimental test fires and the triangular heat flux distribution was observed to give the closest representation of the heat flux from the experimental surface fires.

Numerical solutions of the heat conduction equation with the six boundary conditions were obtained using a finite-difference approximation. Results were presented in graphical form. For all three heat flux histories, convective cooling at the surface during and after exposure decreased the depth of lethal heat penetration from when convective cooling occurred only after heating was terminated. The heat flux distribution at the soil surface did not significantly affect the depth of lethal heat penetration within the soil. In their experimental work a radiometer was used to measure the heat flux from a fuel bed of birch dowels which was on top of Ottawa sand type C-190. Thermocouples were also used to measure temperatures up to 12 cm depth within the soil at intervals of 2 cm. The data from their experiments indicated that as the fuel loading density of the fuel bed increases, the time of heating increases and the total amount of heat transferred to the soil increases, which combine to increase the depth of lethal heat penetration.

In comparing the experimental data with the numerical solutions, boundary conditions using convective cooling at all times predicted values of depth of lethal heat penetration that were generally closer to the experimental values compared to using convective cooling only after the passage of the fire. Variations between experimental and predicted values were quite high in certain cases, sometimes as much as 100%. As fuel loading density increases, the model first under-predicts and then over-predicts the depth of lethal heat penetration. The cause was attributed to the value of the convective heat transfer coefficient used in the computation.

1.8.4 Pafford et al.

Pafford et al. [31] studied ground surface heating during a prescribed burn both analytically and experimentally. The author proposed, for a source of heat, a moving flame front model in order to determine the soil surface temperature distribution. An energy balance equation was employed in which the sum of the heat fluxes conducted and convected from the soil surface was equal to that radiated from the flame to the soil. Some of the assumptions of the heat transfer model were that the flame front moves at a constant rate, preheating of the soil ahead of the flame was negligible, thermal properties of soil remained constant and that the effect of moisture was negligible.

Starting from the three-dimensional Fourier field equation (Equation (1.3)) for a fixed origin, an equation for a moving reference frame was obtained. Further assuming a quasi-steady state and a dominant temperature gradient normal to the soil surface, the equations were reduced to one-dimensional form (Equation (1.4)). Analytical solutions of the resultant equations were then obtained. A solution for the surface temperature distribution was also determined using an iterative procedure after setting the convective heat flux at the surface to zero. A sensitivity analysis of the surface temperature distribution was carried out for various soil and flame parameters.

For their experimental work, soil surface heating was conducted by igniting a mixture of chamise and manzinata loaded on a table. The table was covered with brush and a trough of ethanol was used for ignition at one end of the table. Flame and surface temperatures

were measured using thermocouples whilst photographic means were used to determine flame height, tilt and depth. Measured and predicted temperature distributions were generally similar up to the time just past when maximum temperatures were reached and temperatures started dropping. Variations between the predicted and measured temperature profiles were then very large. The model was further modified by accounting for ash deposited after the flame front had passed which causes a reduction in the emissive power of the soil. This modification was done by reducing the emissivity of the soil from 0.9 to 0.3. Predicted temperature profiles were significantly closer to experimental values for the case of emissivity value of 0.3 than the previous value of 0.9.

1.8.5 Preisler et. al.

Preisler, et al. [17] used large prescribed fires to investigate the effects of fire in natural fuel conditions and to determine the extent of heating in the soil and also to estimate the probability of soil temperatures exceeding critical values for plant tissues and soil organism survival. Data from seven prescribed fires conducted during the summer and fall between 1988 and 1995 were analysed. Temperature measurements were taken at depths of 10, 20, 30 and 46 cm beneath the soil surface at three different locations. The thermal conductivity and volumetric heat capacity of the soils were determined as a function of the volume fractions of their various components.

Using the one-dimensional Fourier field equation (Equation (1.4)), a parametric model for heat profiles was developed assuming a one-dimensional homogenous material based on a derived source solution. Data from the seven prescribed fires were used to assess the goodness of fit to this conceptual model of soil temperature profiles. A random effects model was used to estimate temperatures in various depths of soil based on observed site characteristics such as depth, fuel loading and moisture level. These were taken from samples of temperature profiles from different fires. These temperature estimates were used to estimate probabilities associated with the risk of temperatures exceeding the critical value of 60^{o}C in the soil. In their analyses, the authors found that there were significant reductions in mean temperatures for every 10 cm drop in depth

especially for the first day of the fire. These mean temperature reductions however, reduced significantly as number of days after fire increases.

1.9 Smoldering combustion in organic soils

Organic layers in the forest are formed when low temperature, high acidity, low nutrient supply, excessive water or oxygen deficiency slow the decomposition of dead plant matter [44]. In terms of heat transfer in soil, the organic layer plays the role of an insulator and protects the mineral soil from the direct temperatures of flames. However, when the organic layers are dried out they can ignite during or after a fire and undergo smoldering combustion.

Smoldering is a slow, low-temperature, flameless form of combustion, sustained by the heat evolved when oxygen directly attacks the surface of a condensed–phase fuel [45]. Smoldering typically occurs in the interior of porous, combustible materials and is the primary mechanism in ground fires which are the most destructive of all forest fire types. This is because detection of smoldering combustion is difficult due to the fact that the reaction temperatures are relatively low, compared to flaming combustions, and occur within porous material or the organic layer. For this reason, smoldering combustion can progress for long periods of time undetected, and then could undergo a sudden transition to flaming combustion by heating up surface fuels to point of ignition. Smoldering ground fires, because of their intimate contact with the mineral soil, have the potential for making a large impact on forest regeneration [46].

Smoldering combustion in the forest normally follows a surface fire and can burn for several days to years [47]. Frandsen [48] cites Wein [49] as observing smoldering spread rates of 3 to 12 cm/hr. Frandsen [48] again cites Sheshukov [50] that in Australia the rule of thumb for smoldering spread rate is 4 cm/hr and Shearer [51] as having observed smoldering spread rates of 0.5 to 10 cm/hr.

Several factors are said to influence the ignition, sustaining and consumption of organic matter in smoldering combustion, the most important of which are moisture content and

inorganic content. As cited by Shearer [51] and Norum [52], Hungerford, et al. [44] state that average duff moisture content is thought to be the most important predictor of duff consumption. Frandsen [46, 53, 54] has conducted a series of studies on smoldering consumption in peat moss and determined that the ignition limit of organic soil does not depend only on the moisture content, but also on the inorganic content [53]. Reinhardt, et al. [55] from the data of their studies concluded that at moisture contents of greater than 175%, less than 15% of the total duff will be consumed in a smoldering fire. Reinhardt, et al. [55] describe smoldering ground fire as spreading downward and laterally, forming a balloon shaped cavity. When downward spread eventually runs out of fuel or encounters conditions that do not support combustion, lateral spread then becomes the only type of spread. Some important research on smoldering combustion is described below.

1.9.1 Hartford

Motivated by the fact that limits of smoldering combustion of peat moss are not limited by moisture alone but also by the amount and type of mineral soil and the compaction of the fuel, Hartford [56] conducted experiments in a laboratory to predict whether organic matter, conditioned with different types of mineral soils at different moisture contents, will support smoldering combustion following ignition.

Peat moss was used in this study to represent the organic layer of the forest and tests were conducted in two phases. In the first phase peat was conditioned to targeted moisture contents and three types of soil were used as inorganic material: silica (obtained as a pure chemical), an allitic clay (from lacustrine (lake) deposits) and an allophone clay of an andept or ash soil. Three levels of inorganic densities were used: 0.07, 0.11 and 0.17 g/cm^3. These levels represented the minimum, maximum and mean values of inorganic densities on file at the Intermountain Fire Sciences Laboratory (Missoula, MT). In the second phase, only silica was used. The objective of this second phase was to determine the influence of the physical and chemical characteristics of the soil on smoldering. Fuel beds were made from moisture-conditioned peat moss to which mineral soil had been added to obtain a targeted inorganic content. The fuel bed was

then packed to a depth of 4 cm in an open topped insulated box. Ignition was by means of a glowing resistance coil on one side of the box.

The results of the tests were analysed on a burn or no-burn basis. Logistic regression analysis was used to develop predictive equations of the probability that a fuel bed would burn based on the values of the independent variables being tested. The logistic equations developed were:

$$\hat{P} = 1/\left(1 + e^{-21.470+(21.114)R_M+(4.5701)R_I}\right) \quad (1.5)$$

for fuel beds including silica or clay soils, and

$$\hat{P} = 1/\left(1 + e^{-16.671+(15.407)R_M+(3.9981)R_I}\right) \quad (1.6)$$

for fuel beds including ash soils

where: $\hat{P}$ = probability of burning

R_M = the moisture ratio (volume of water to volume of soil), and

R_I = the inorganic ratio (volume of inorganics to volume of soil).

Data from tests indicated that silica and clay soil inorganics did not cause significantly different results whilst ash soil did appear to be significantly variable. By using peat moss of different particle size distribution and shape, Hartford found that there were indications that differences exist in the likelihood of burning due to some characteristics of the peat moss itself.

1.9.2 Frandsen

Frandsen [48] developed a model for a smoldering spread rate in organic soils in terms of the organic bulk density, the moisture content and the inorganic content of the fuel bed. Smoldering spread rates were derived from the results of an experimental evaluation of the burning rate per unit area of smoldering material. The smoldering spread rate was expressed as the ratio of load loss rate to the organic bulk density. Frandsen cited an expression for load loss rate from an earlier research as:

$$w = 0.27 - 0.097R_M - 0.033(R_I - D) \quad (1.7)$$

where: w = load loss rate, g/cm^2·hr

$D = R_I$ if $R_I < 1.0$

$= 1.0$ if $R_I \geq 1.0$

R_M = moisture ratio (0 to 0.8) (volume of water to volume of soil),
R_I = Inorganic ratio (0 to 4) (volume of inorganic to volume of organic in soil).

Data used for the evaluation of the burn rate suggested a ratio of maximum to average load loss rate of 2.3. Thus the load loss equation was modified using a factor of 2.3 for an approximation of the maximum load loss rate with an estimated error of 33%. The resulting maximum load loss rate was

$$w_{max} = 0.62 - 0.22R_M - 0.076(R_I - D) \quad (1.8)$$

and the smoldering spread rate was expressed as

$$R = w_{max}/\rho \quad (1.9)$$

where: w_{max} = maximum load loss, g/cm^{2}hr
R = smoldering spread rate, cm/hr,
ρ = organic bulk density, g/cm^3.

In the analysis of results, it was observed that the smoldering spread rate increased with a decrease in organic bulk density and decreased with an increase in moisture and inorganic content. From the data used in their analysis, Frandsen [48] found that the results which were for an organic content of 0.2 g/cm^3, showed a spread rate that was not less than 2 cm/hr. This agreed with the results of Wein [49].

Frandsen [46] in a different study, conducted experiments to determine the ignition limit of organic soils. This study was similar to previous studies by Frandsen [53] and Hartford [56], but whereas these previous studies were limited to one fuel type, this particular study covered fuels over a wide geographical area range and ignition was attempted over a range of moisture contents.

Samples were collected from 17 locations over the Northern and South-eastern United States. Field samples were obtained by gridding an area of 40 x 100 cm from which smaller samples of 10 x 10 x 5 cm were cut. Using the samples measuring 10 x 10 x 5 cm Frandsen tested the transition from burn to no burn whilst traversing a moisture content

range. Various moisture contents were obtained by oven drying samples and adding moisture to obtain targeted values. The inorganic contents were obtained from sub-samples that were collected by determining the mass of samples remaining after combustion. In the tests, an ignition box measuring 10 x 10 x 5 cm was used to house soil samples. Samples were ignited on the 5 x 10 cm side using an electrically powered ignition coil located inside the box to simulate lateral smoldering. An ignition was labelled as being successful if it was followed by sustained combustion that consumed the sample.

Logistic regression was applied to analyse the results by setting the burn response (burn or no burn) as the dependent variable and moisture content, inorganic content and bulk density as the independent variables. In their analysis of the data, the inorganic content and organic bulk density were fixed at their average values and all sample groups showed a reversed sigmoid curve (curve shaped like the letter S) moving from high probability of ignition at low moisture contents to low probability of ignition at high moisture contents.

1.9.3 Frandsen and Ryan

Frandsen and Ryan [33] made direct comparison of temperatures and heat loads between duff covered and uncovered mineral soils that had been placed beneath a burning fuel pile. In this work, four different duff mineral soil profiles were positioned under the same fuel pile measuring 2.5 x 2.5 x 0.75 m. A fuel load of 560 tons/ha with moisture content of 11% was placed above an artificial soil made up of 8 cm of sand and 2 cm of peat moss. The peat moss was used to represent duff whilst the sand represented mineral soil. Temperatures were recorded with 30-gauge Chromel-alumel thermocouples in the duff, 1 cm above the duff-mineral soil interface, at the surface and 1 cm intervals downward to a depth of 4 cm. One of the profiles had no duff covering so that the dry sand could receive the full impact of the downward heat flux and serve as a standard for comparison with other soil profiles. Two of the covered profiles were dry sand covered with dry peat moss and dry sand covered with wet peat moss and the third profile had a wet sand covered by wet peat moss.

In the experiment, the maximum flame height from the fuel was 6 m and flaming combustion lasted for 45 minutes with glowing lasting for another 2 – 3 hours. Results indicated that covering the sand with 2 cm of dry peat moss lowered the peak temperatures from 680 to 360^{o}C, adding water to the peat moss lowered peak temperatures from 680^{o}C to 430^{o}C, adding water to both the peat moss and sand reduced peak temperatures to about 80^{o}C.

Using the temperature difference between two points in the soil, heat fluxes were computed. The uncovered dry sand recorded peak heat flux of about 10 kW/m^2 whilst that of the covered dry sand covered with dry peat moss was 3.3 kW/m^2. For dry sand covered with wet peat moss the peak heat flux was about 2.1 kW/m^2 whilst that of wet sand covered with wet peat moss as about 2.5 kW/m^2.

1.9.4 Anderson

Anderson [57] tabulated data from the literature to create equations for the probability of fire survival for Canadian forest fuel types. Anderson used equations developed by Hartford [56] and Frandsen [46] on the probability of ignition and probability of survival of ignition of organic materials. Using data on duff characteristics from Fire Behaviour Prediction models, Anderson determined the probability of survival for each of the fuels and plotted curves against duff moisture code (a numerical rating of the average moisture content of loosely compacted organic layers of moderate depth). The probability of survival equation (such as Equations (1.5) and (1.6)) was then introduced into a simple fire growth model. The fire growth model calculated fire spread in terms of ignition of cells. Inputs of fuel type and current duff moisture code within each cell were employed to compute the probability of survival for each burned cell. This was done in order to denote areas likely to have smoldering conditions after passage of a fire.

Inference from their curves suggested inorganic content had a more significant effect than bulk density. An instantaneous probability of survival of ignition map for a primary protection zone within Saskatchewan on a particular day was simulated to show areas that could maintain holdover fires (fires that remain dormant for a considerable time).

Similarly a probability of survival map was simulated for a hypothetical fire in Wood Buffalo National Park in the North-West Territories, Canada, to show areas within a burned region that were likely to undergo smoldering. The results of such simulations could be used to decide where to emphasize mop up effects (extinguishing or removing burning and hazardous material).

1.9.5 Other reviews

Albini, et al. [47] provided a comprehensive review of all models of heat transfer for which the source of heat was fire-driven. They looked at models with soil science ancestry as well as those from engineering and geophysics and described the differences between these approaches. Albini, et al. noted the inconsistencies and inaccuracies in some of these models and found the model of Campbell et al. [37] to be performing well in predicting temperature histories. The work of Campbell et al. was not reviewed in detail in this study because the work of Campbell et al. treats the presence of moisture extensively and incorporates latent heat transport by vapour flux which is outside the scope of this study. Cromer et al. [58] measured soil temperatures under a burning windrow of eucalypt logs. The soil was sand with initial moisture content of 12.5% and burning and smoldering all together lasted for over 12 hours. A maximum temperature of 330^{o}C was recorded 2.5 cm below the surface and 56^{o}C at a depth of 30 cm.

1.10 Cone calorimeter

In this study, one equipment that will be used widely in all experiments is the cone calorimeter (Fire Testing Technology Ltd, West Sussex, UK). This is a small-scale instrument that measures rate of heat release of materials under a wide range of conditions, using the oxygen consumption technique based on the fact that majority of plastics, rubbers and natural organic materials produce 13.1 MJ/kg of oxygen consumed with an accuracy of ±5% [59]. A square sample of 10 x 10 cm is exposed to the radiant flux from an electric heater. The heater has the shape of a truncated cone (hence the name of the instrument) and is capable of providing heat fluxes to the specimen in the range of 10-100 kW/m^2. This essentially covers the range of heat fluxes available from early burning to fully developed fires. The fire effluent passes through a duct containing

sensors which permit the rate of heat release, effective heat of combustion, carbon monoxide and carbon dioxide to be determined. By means of a load cell, the mass loss rate of the specimen as it burns is given and a laser instrument also gives the extinction coefficient that gives a measure of the amount of smoke that is produced. Tests can be conducted with the sample being in either the horizontal or vertical orientation [60]. For the purpose of this study only the heater of the cone calorimeter will be utilised. Figure 1.1 shows a picture of the cone calorimeter.

Figure 1.1: Cone Calorimeter

The cone calorimeter has been used widely and successfully in structural fire research but has not been used extensively for wildland/forest fire research. The cone calorimeter will be used for the source of heating in all experiments in this study.

1.11 Objectives of this research

The ability to predict the heating of soil during a forest fire is an effective tool that can be used to predict below-ground effects of such fires. The ability to predict

belowground-effects of fire can aid forest managers in effectively quantifying the total effects of a fire before conducting prescribed burning in order to achieve desired results. This can become very important especially where selective regeneration of species in forest settings is desired. Many of the models for predicting below-ground temperatures are complex and do not include dependence of thermal properties on temperature, and predictions from such models in some cases vary from experimental measurements by as much as 100%. As mentioned by Albini et. al. [47], the simplest model that can be used to predict below-ground effects of a fire is one that neglects the presence of moisture. Such a model could have good predictive ability. In addition to depth of lethal heat penetration arising from direct temperatures of forest fires, combustion of organic matter in the forest during or after a forest fire is another important below-ground effect due to high heat residence times of such combustion process and the effect on the organic and mineral soil. In all cases, validation of models of heat transfer in the soil could be costly especially in the use of large scale fires in forest settings or the use of small scale fires. For both of these methods there is lack of repeatability and control over parameters and these are always problematic in the experimental validation of models.

With the above mentioned, the objectives of this research are:

- to develop and increase the predictive power of a simple model of heat transfer in soil that neglects the presence of moisture. This is done through the inclusion of temperature dependent thermal properties,
- to determine the effect of inorganics present in organic materials on the rate of smoldering combustion of such organic materials,
- to develop methods of creating forest floor soil in the laboratory using commercially available materials like peat and sand for small scale tests with greater control over parameters and greater assurance of repeatability,
- to develop laboratory scale tests and methods to use the cone calorimeter for wildland fire research.

The model will help forest managers to predict temperature profiles in forest floors and also the depth of lethal heat penetration for any prescribed or unprescribed fire. Knowledge of the effect of inorganics on smoldering combustion of organic material in

the forest will help extensively in predicting spread rates of ground fires and expected maximum temperatures which can be used in determining depth of lethal heat penetration. The ability to construct forest floor soils in the laboratory with commercially available material and to conduct small scale tests of heat transfer in soil will go a great length in aiding the understanding of the principles of heat transfer in forest soil and in the prediction of depth of lethal heat penetration. The ability to develop small scale laboratory tests incorporating the use of equipment that can provide controlled heat inputs will be a great tool in wildland fire research.

1.11 Scope of thesis

In this thesis, a background to forest/wildland fires and their types, heat transfer in soil and effects of high temperatures on plants and nutrients within the soil are described in Chapter One. Some of the works involving heat transfer in soil relevant to this work are catalogued in this Chapter. In Chapter Two, a finite-difference formulation of constant and temperature dependent thermal properties models of heat transfer in dry soil are detailed and extended to cover a two-layer soil. Methods of determining thermal properties for the model and numerical results are discussed along with sensitivity study of properties of the soil on heat transfer in Chapter Three. The procedure for collection of sand and soil samples and construction of soil in the laboratory, a description of the equipment and procedure for conducting the experiments as well as the experimental results are given in Chapter Four. Experimental and numerical results are compared in Chapter Five, and implications of the results to fire research are discussed. Conclusions are drawn and recommendations for future work are given in Chapter Six.

CHAPTER TWO: DEVELOPMENT OF NUMERICAL MODEL

This chapter will describe the development of a numerical model for heat transfer in dry soil. The following will be discussed in this Chapter:

- assumptions of semi-infinite behaviour and one-dimensional heat transfer,
- the use of constant and temperature dependent thermal properties in the formulation of a model for a homogenous dry soil,
- the extension of the model to two-layer dry soil,
- the implementation of these models in a computer program, and
- validation of the models using analytical solutions.

2.1 One-dimensional approach to heat transfer in soil

Most heat transfer models in soil have treated soil as a one-dimensional semi-infinite medium (e.g. [5, 16, 61]). Richon [5] considered both one- and two-dimensional modes of heat transfer in soil and found that the difference between model results for the one- and two-dimensional approaches were less than 3%. This implies that assuming heat flow in the soil to occur only in the vertical direction is appropriate.

Heat transfer in soil can be computed using the Fourier field equation (Equation (1.1)). For the one dimensional case, the time rate of change of soil temperature, *T*, is a function of the divergence of soil heat flux, q'':

$$\rho c \frac{\partial T}{\partial t} = \frac{\partial}{\partial x}\left(k \frac{\partial T}{\partial x} \right) \tag{2.1}$$

where: x is depth from surface of soil,

t is time,

k is the thermal conductivity,

c is the specific heat,

ρ is density, and

$$q'' = -k\frac{\partial T}{\partial x}, \tag{2.2}$$

In the case where thermal properties (k, c, ρ) are independent of temperature, a special case of Equation (2.1) arises as:

$$\frac{\partial T}{\partial t} = \alpha \frac{\partial^2 T}{\partial x^2} \tag{2.3}$$

where $\alpha = \frac{k}{\rho c}$ is thermal diffusivity. (2.4)

In this formulation of the heat transfer equation, energy exchanges associated with the presence of moisture (latent heat of evaporation or phase changes due to condensation) are ignored. Recall that in Chapter One, the effects of moisture as literally reducing the thermal diffusivity by requiring drying out of the water was mentioned. The effects of moisture have been neglected because the focus in this study is to develop a simple model that neglects the complexities that arise from the phase changes. Also, heat transfer will be assumed to be one-dimensional and this assumption of one-dimensional heat transfer will be verified with an experiment in Chapter Four.

2.2 Thermal properties

The most influential factors governing heat transfer in soil are the thermal properties, in this case the thermal conductivity, k, specific heat, c and the density ρ. Due to their complexity, cases of temperature dependent thermal properties have rarely been treated. Richon [5] indicated that thermal properties were not supposed to affect results in any significant way since thermal properties were weak functions of temperature. However, Pourhashemi et al. [61] suggest that thermal conductivity and specific heat are strong functions of temperature especially at high temperatures. In this study, the dependence of thermal properties on temperature will be determined through experimental correlations and from the literature. These will be discussed in Chapter Three.

2.3 Boundary conditions

Figure 2.1 shows the cone calorimeter heater and a soil sample in a sample holder. Figure 2.2 is a schematic representation depicting the energy exchange at the surface of the soil exposed to a radiative incident heat flux. Recall that in Chapter One it was

mentioned that the cone calorimeter will be used as a radiant heat source in this study. The energy exchange at the surface in addition to that at the bottom of the soil will be used to generate the boundary conditions for the model.

Figure 2.1: Soil sample beneath cone calorimeter's heater

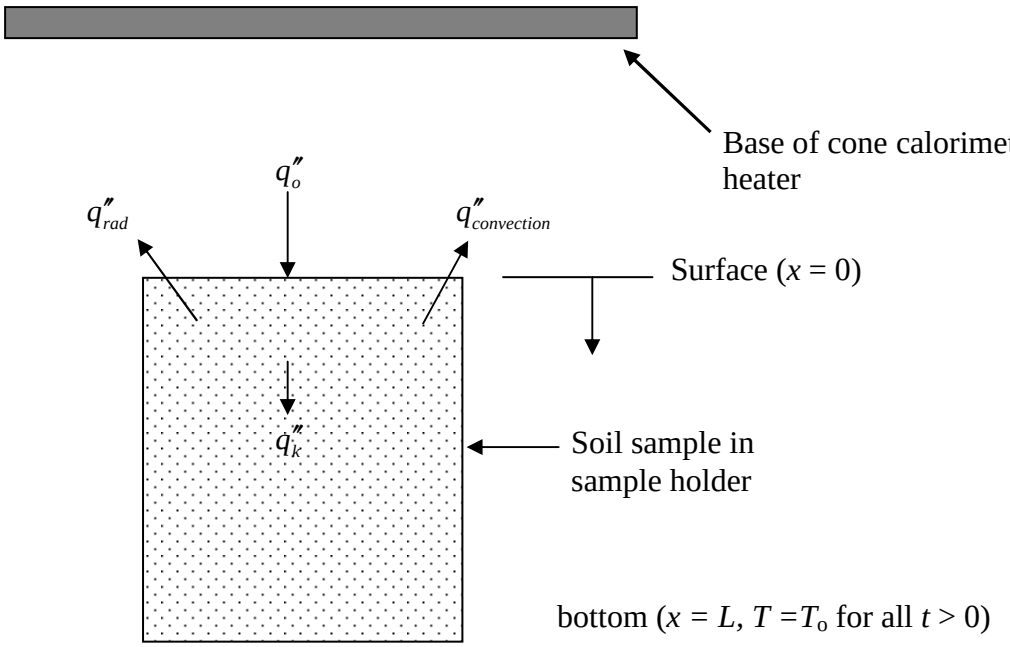

Figure 2.2: Schematic Representation of Soil Sample and Cone Heater Showing Energy Exchange at the Surface of the Soil

where:

q''_o = incident heat flux from cone calorimeter

$q''_{convection}$ = convective heat flux losses

q''_{rad} = radiative heat flux losses

q''_k = heat flux conducted into soil

The incident heat flux has been idealised in this study as it has been chosen to be constant over space and time. However, this is not the case in reality, where a fire passes over the soil surface.

2.3.1 Bottom boundary condition - Semi-infinite assumption

The bottom boundary condition will be obtained by considering the soil as a semi-infinite solid. A semi-infinite solid is one in which the temperature does not change as the depth within the solid tends to infinity. In reality, temperature gradients deep within soil are not very high and all models of heat transfer in soil known to author (e.g., [5, 16, 23]) have treated soil as a semi-infinite solid. For soil in the forest, when the surface is

subjected to a source of heat input, the temperature deep down in the soil remains constant and equal to the initial temperature. Many researchers (e.g., [31, 62]) have also found that irrespective of the temperature at the surface of the soil, depth in soil at which appreciable heating is achieved is not to a large extent. However, if a finite depth of soil is heated, like in a laboratory, the semi-infinite assumption will be valid for a limited period of time depending on the thermal properties of the soil. The criterion in such a case for the semi-infinite assumption to be valid is:

$$\frac{L}{2\sqrt{\alpha t}} > 2 \qquad (2.5)$$

where: L = depth of soil, m,

α = thermal diffusivity, m^2/s,

t = time within which semi-infinite assumption is valid, s.

In this study the semi-infinite assumption will be used. Thus the boundary condition at the bottom of the soil is:

$$T_{(x=L)} = T_o \qquad \text{for all } t \geq 0; \qquad (2.6)$$

where: T_o= initial temperature of soil.

2.3.2 Surface boundary condition

At the surface of the soil, the temperature could be constant or changing with respect to time depending on the presence or absence of a source of heat, the intensity of the source of heat and convective cooling. Since there will be a source of heat at the surface for this study, there will be conduction of heat into soil at the surface and then there will be convective cooling at the surface as well (Figure 2.2).

For the source of heat for the surface boundary condition, a heat flux boundary condition was chosen in favour of a temperature boundary condition primarily because of the following reasons:

- the cone calorimeter which will be used in the experiments for validation of the model subjects samples to a purely radiative heat flux, a description of the cone calorimeter has been given in Chapter One,

- a soil surface is not clearly defined and large temperature gradients can exist across it making it difficult to measure accurately temperatures at the surface [63].
- fire behaviour models (e.g., [2]) exist that are able to estimate amount of heat a fire transmits to the soil and it is easier to obtain data of heat input into the soil than obtaining surface temperature data.

With reference to Figure 2.2, at the surface of the soil, the energy exchange can be reduced to the net incident heat flux and convective heat flux losses.

2.3.3 Radiative heat flux

The cone calorimeter imposes a purely radiative heat flux on samples through resistive heating of the cone's coils with the sample located at 25 cm beneath the lowest point of the heating cone. Janssens [65] determined that the view factor from the cone heater to a 10 cm x 10 cm surface located at 2.5 cm beneath the cone heater is 0.9678, it is thus assumed that during the period in which the soil surface is exposed to the heat flux from the cone calorimeter, the cone heater and the soil surface exchange radiation only with each other. The radiative heat flux at the surface of the sample, $q''_{radiative}$, will be:

$$q''_{radiative} = \varepsilon\sigma(T^4_{cone} - T^4_{x=0}) \tag{2.7}$$

where: ε = Emissivity of the soil surface,

σ = Stefan-Boltzmann constant,

$T_{x=0}$ = Temperature at surface of soil, and

T_{cone} = Temperature of cone calorimeter's heating coil.

As $T^4_{cone} >> T^4_{x=0}$ at time $t=t_0$, The boundary condition given by Equation (2.7) can be expressed in terms of the nominal incident heat flux, q''_o, such that,

$$q''_{radiative} = \varepsilon\sigma T^4_{cone} \approx q''_o \tag{2.8}$$

where q''_o = incident heat flux from cone calorimeter.

Therefore:

$$q''_{radiativet} = q''_o - \varepsilon\sigma T^4_{x=0}, \; t \leq t_{texposure} \tag{2.9}$$

After heating of soil surface ceases, it is anticipated that the soil will be moved away from underneath the heater to a different area in the laboratory such that the soil surface will be exposed entirely to the ambient. The radiative exchange in this case is between the soil surface and the walls which are assumed to have the same temperature as the ambient. The net radiative heat loss thus becomes:

$$q''_{radiative} = -\varepsilon\sigma(T_{x=0}^4 - T_a^4) \ , \ t > t_{exposure} \tag{2.10}$$

where T_a is the ambient temperature.

2.3.4 Convective heat flux

Once the temperature at the surface of the soil sample exceeds the ambient temperature, convective cooling will commence. Richon [5] considered six surface boundary conditions arising from three surface convective cooling scenarios:

- no convective cooling at the surface at all times of test,
- convective cooling at the surface after passage of fire, and
- convective cooling at surface at all times.

For this study, convective cooling at the surface at all times will be the focus, however, convective cooling only after the exposure to the heat flux will also be considered in a sensitivity study in Chapter Three. The convective heat flux is given by:

$$q''_{convective} = -h(T_{x=0} - T_a) \tag{2.11}$$

where: h = convective heat transfer coefficient

The approach of convective cooling at all times may overestimate the convective heat losses during exposure to the nominal incident heat flux as the temperature of air next to the surface of the soil will likely be greater than the ambient.

2.3.5 Net heat flux

The net radiative heat flux and the convective heat flux provide the net heat flux at the surface of the soil. The net heat flux, q''_{net}, is given by:

$q''_{net} = \varepsilon\sigma(T_{cone}^4 - T_{x=0}^4) - h(T_{x=0} - T_a)$, which in terms of the nominal incident heat flux is:

$$q''_{net} = q''_o - \varepsilon\sigma T_{x=0}^4 - h(T_{x=0} - T_a) \ , \ t \le t_{exposure} \tag{2.12}$$

After the exposure period, the net heat flux becomes:

$$q''_{net} = -\varepsilon\sigma(T^4_{x=0} - T^4_a) - h(T_{x=0} - T_a)\,,\ t > t_{exposure} \tag{2.13}$$

2.3.6 Net energy exchange

From the net heat flux and the convective heat flux losses at the surface, the energy exchange at the surface gives the surface boundary conditions as:

$$q''_{conduction} + E_{sm} = q''_{net} \tag{2.14}$$

Recalling the definition for q'' from Equation (2.2), Equation (2.14) becomes:

$$k\frac{dT}{dx} + E_{sm} = q''_{net}$$

where E_{sm} is the internal energy storage.

Substituting q''_{net} from Equations (2.12) and (2.13) yields:

$$k\frac{dT}{dx} = q''_o - \varepsilon\sigma T^4_{x=0} - h(T_{x=0} - T_a) - E_{sm}\,,\ t \le t_{exposure} \tag{2.15}$$

$$k\frac{\partial T}{\partial x} = -\varepsilon\sigma(T^4_{x=0} - T^4_a) - h(T_{x=0} - T_a) - E_{sm}\,,\ t > t_{exposure} \tag{2.16}$$

The net energy exchange as it stands in Equations (2.15) and (2.16) are highly non-linear as a result of the radiative heat loss terms. The non-linearity associated with the radiative heat losses will be linearised in the finite-difference model using temperatures at the previous time steps. For the purpose of this study, a step input type of heat flux exposure was chosen for simplicity, both experimentally and analytically. The period of exposure of the heat flux is referred to as $t_{exposure}$, this is the period from the heat flux at surface of soil being a non-zero value to the time it again becomes a zero value.

2.4 Conduction in soil

Between the surface and the bottom of the soil, the heat transfer mechanism in the soil will be treated as one-dimensional heat conduction in a plane wall, specifically as an inert slab, which for temperature dependent thermal properties takes the form of Equation (2.1):

$$\rho c\frac{\partial T}{\partial t} = \frac{\partial}{\partial x}\left(k\frac{\partial T}{\partial t}\right)$$

and for constant thermal properties takes the form of Equation (2.3):

$$\frac{\partial T}{\partial t} = \alpha \frac{\partial^2 T}{\partial x^2}$$

The equations of interest thus become:

$$\begin{cases} k\dfrac{\partial T}{\partial x} = q_o^{"} - \varepsilon\sigma T_{x=0}^4 - h(T_{x=0} - T_a) & \text{at } x = 0 \text{ for } 0 < t \le t_{exposure} \\ k\dfrac{\partial T}{\partial x} = -\varepsilon\sigma(T_{x=0}^4 - T_a^4) - h(T_{x=0} - T_a) & \text{at } x = 0 \text{ for } t > t_{exposure} \\ \rho c\dfrac{\partial T}{\partial t} = \dfrac{\partial}{\partial x}\left(k\dfrac{\partial T}{\partial t}\right) & \text{at } x > 0 \text{ and } t \ge 0 \text{ (temperature dependent properties)} \\ \dfrac{\partial T}{\partial t} = \alpha\dfrac{\partial^2 T}{\partial x^2} & \text{at } x > 0 \text{ and } t \ge 0 \quad \text{(constant properties)} \\ T_{x=L} = T_a & \text{for } \quad 0 < t \le \infty \end{cases} \tag{2.17}$$

2.5 Solution methods

All the differential equations and associated boundary conditions given by Equation (2.17) form the basis for the numerical model for both constant and variable thermal properties. A finite difference method was chosen to solve the differential equations and an explicit (or Euler) time-marching scheme was used in formulating the descritized equations [66]. This method of moving ahead in time is very simple to use especially when variable thermal properties are involved [66]. It can generate very accurate results when small time and spatial steps are used. For the Euler method of moving ahead in time, the finite difference equation (Equation (2.3)) for an interior node m, becomes:

$$\frac{1}{\alpha}\frac{T_m^{\,i+1} - T_m^i}{\Delta t} = \frac{T_{m+1}^i + T_{m-1}^i - 2T_m^i}{(\Delta x)^2} \tag{2.18}$$

where: *i+1* is the current time step,

i is the previous time step and

Δx is the mesh size

Δt is the time step

m-1 is the preceding node

m+1 is the succeeding node

In developing the descritized equations for the model, the methods described in Myers [66] were followed especially for the case of variable thermal properties.

2.5.1 Thermal properties

For the case of constant thermal properties, values of the thermal conductivity, *k*, and specific heat *c*, computed at room temperature were used. For the case of variable thermal properties, linear equations of thermal conductivity and specific heat (which will be discussed in Chapter Three) were used. The equations were of the form:

$$k(T) = a + bT \tag{2.19}$$

$$c(T) = e + fT \tag{2.20}$$

where a, b, e and f are constants and *T* is the temperature. To avoid complications due to non-linearity, *k(T)* and *c(T)* were evaluated using temperatures at the previous time steps.

Details on the use of finite differences to arrive at the descritized equations are given in Appendix A. A summary of the system of equations for the case of constant thermal properties are given by:

$$[T]^{i+1} = [A]\,[T]^{\,i} + [C] \tag{2.21}$$

where

$$[T]^{\,i+1} = \begin{bmatrix} T_o \\ T_1 \\ - \\ - \\ T_{last-1} \\ T_{last} \end{bmatrix}^{i+1}$$

$$[A] = \begin{bmatrix} 1-2\alpha P(1+h\Delta x/k) & 2\alpha P & & & & \\ \alpha P & 1-2\alpha P & \alpha P & & & \\ & - & & & & \\ & & - & & & \\ & & \alpha P & 1-2\alpha P & \alpha P & \\ & & & & & 1 \end{bmatrix}$$

$$[T]^{i} = \begin{bmatrix} T_o \\ T_1 \\ - \\ - \\ T_{last-1} \\ T_{last} \end{bmatrix}^{i}$$

$$[C] = \begin{bmatrix} 2\alpha P\Delta x(q''_{net} + hT_a)/k \\ 0 \\ - \\ - \\ 0 \\ 0 \end{bmatrix}$$

where the superscript *i* refers to previous time step, *i+1* refers to current time step and $P = \frac{\Delta t}{(\Delta x)^2}$ is a stability parameter.

The model for the case of temperature dependent thermal properties was formulated by replacing the thermal conductivity and specific heat with linear equations, Equations (2.19) and (2.20). For the case of temperature dependent thermal properties the matrix obtained is:

$$[T]^{i+1} = [A][T]^{i} + [C] \qquad (2.22)$$

$$[T]^{i+1} = \begin{bmatrix} T_o \\ T_1 \\ - \\ - \\ T_{last-1} \\ T_{last} \end{bmatrix}^{i+1}$$

$$[A] = \begin{bmatrix} 1-\frac{k_o+k_1}{(\rho c)_o}P-\frac{h\Delta x}{(\rho c)_o}2P & P\frac{k_o+k_1}{(\rho c)_o} & & & \\ \frac{k_{m-1}+k_m}{2(\rho c)_m}P & 1-\frac{k_{m-1}+2k_m+k_{m+1}}{2(\rho c)_m}P & \frac{k_m+k_{m+1}}{2(\rho c)_m}P & & \\ & - & & & \\ & & - & & \\ & & & - & \\ & & & & 1 \end{bmatrix}$$

$$[T]^{i} = \begin{bmatrix} T_o \\ T_1 \\ - \\ - \\ T_{last-1} \\ T_{last} \end{bmatrix}^{i} \text{ and}$$

$$[C] = \begin{bmatrix} \frac{2P\Delta x}{(\rho c)_o}(q''_{net}+hT_a) \\ 0 \\ - \\ - \\ 0 \\ 0 \end{bmatrix}$$

The definitions of the various symbols are given in Appendix A.

Analytical solution of Equation (2.17) for the case of soil exposed to a given heat flux with convective cooling and constant thermal properties was obtained by adapting and combining methods from [5] and [67]. Microsoft® Excel was used to generate the analytical solution and a Fortran computer code was developed for implementing the numerical model. Appendix B gives the analytical solution for the case of constant thermal properties.

The nodes for the numerical model were numbered in order from the surface of the soil to the bottom and were of constant size. The stability criterion [68] requires that the

coefficient of T_m^{i+1} for the surface node be greater than zero. From the discretization, the coefficient of T_m^{i+1} at the surface was $1-2\alpha P(1+h\Delta x/k)$. Hence it is required for the stability of the solution that:

$$1-2\alpha P(1+h\Delta x/k) \geq 0 \tag{2.23}$$

With a thermal diffusivity, α, of 2.2 x 10^{-7} m^2/s [68], which is an average for soil, a node size, Δx, of 0.5 mm and a time step, Δt, of 0.1 seconds were found to give a robust code and satisfy the stability criterion described in Equation (2.23). There was no benefit to further decreasing the time step and node size and an increase in these quantities showed some amount of variation from the analytical solution.

Figure 2.3 shows the effect of varying the nodal size on the results of the model in comparison with the analytical solution. From Figure 2.3, the results using node sizes of 1.0 and 1.5 mm varied from the analytical solution by 45% and 63% at the early stages of heating. The variations of their values from the analytical were consistently greater than for 0.5 mm at all times. Using a node size of 0.25 mm gave values that were higher than the analytical solution. Figure 2.4 gives the effect of varying the time step on the model results. Time steps of 0.5, 0.1 and 0.05 s are shown and compared with the analytical solution. There is practically no variation between 0.05 and 0.1 s time steps and they both give very good results in comparison with the analytical solution. The 0.5 s time step gives a larger variation from the analytical solution compared to 0.1 s time step especially at the initial stages of heating. Since no further benefits are obtained with 0.05 s time step, the 0.1 s time step was chosen for the model.

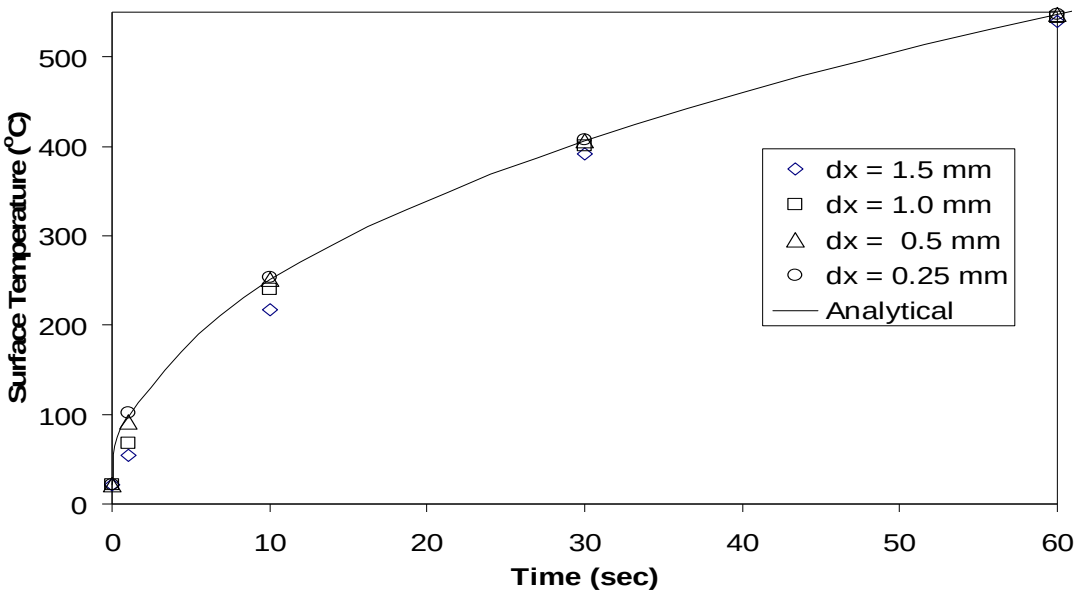

Figure 2.3: Comparison of Numerical Results and Analytical Solution for Prediction of Surface Temperature Showing Effect of Different Nodal Sizes (Exposed to Heat Flux of 50 kW/m^2)

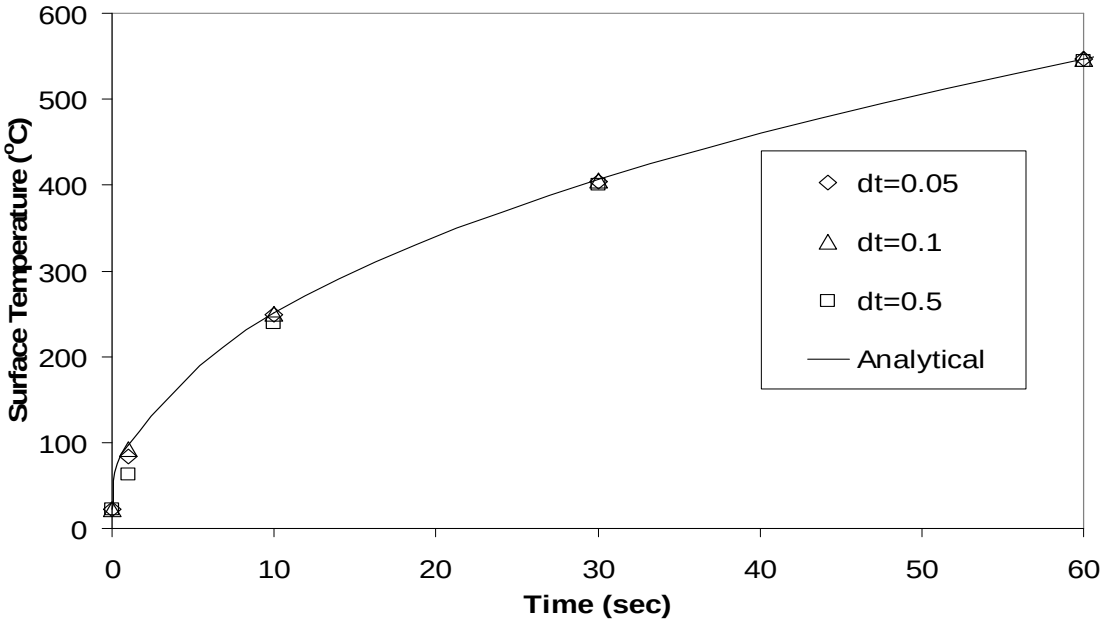

Figure 2.4: Comparison of Numerical Results and Analytical Solution for Prediction of Surface Temperature Showing Effect of Different Time Steps (Exposed to Heat Flux of 50 kW/m^2)

2.6 Validation of model.

Validation of the model was necessary to ensure that the differential equations were properly formulated, the discretization of the differential equations and the coding of the resulting matrix using Fortran were properly implemented.

2.6.1 Constant thermal properties single layer model

An analytical solution of the heating period was obtained and compared with numerical results. The following properties were used based on average taken from various literature (e.g., [5, 68]):

k = 0.2345 W/m·K

c = 1550 J/kg·K, and

ρ = 1513 kg/m^3.

Figures 2.5 and 2.6 show the numerical and analytical profiles at the surface and at a depth of 1 cm for exposure to a heat flux of 50 kW/m^2 for an exposure time ($t_{exposure}$) of 5 minutes. Figure 2.5 shows excellent agreement between the numerical model and the analytical solution. The maximum variation between the numerical and analytical solution was 4.8% at 1 second. After this the variation drops to less than 1% throughout the simulation period. Figure 2.5 also shows excellent agreement between the numerical and analytical results at a depth of 1 cm. A comparison was also made for an exposure to 120 kW/m^2 for an exposure period of 5 minutes and the variation between the analytical and model results were less than 1% at all depths.

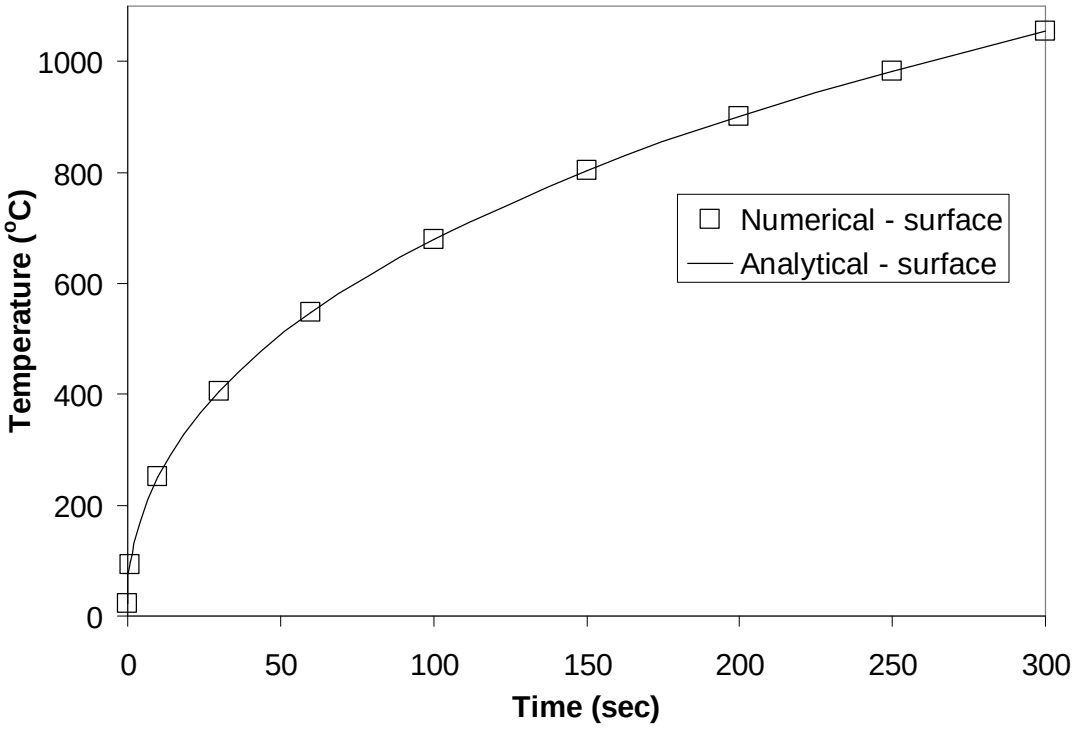

Figure 2.5: Comparison of Model and Analytical Results for Heating Period of Soil Surface (Exposed to 50 kW/m^2 for Exposure of 5 Minutes)

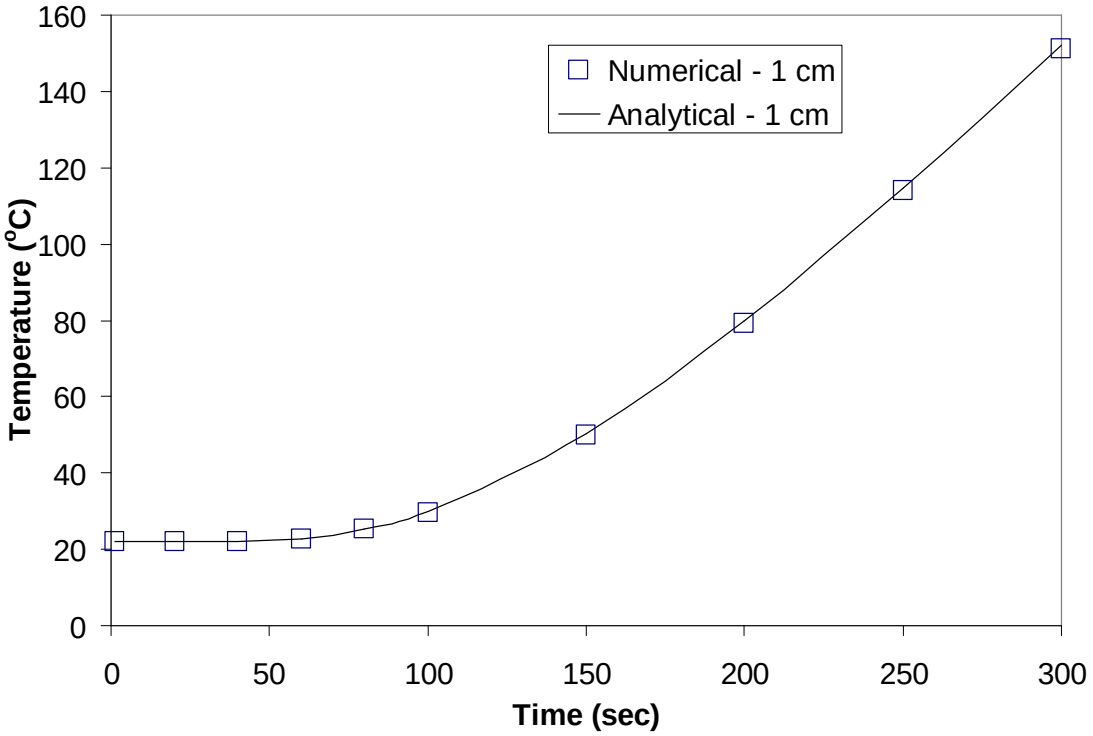

Figure 2.6: Comparison of Numerical and Analytical Results at Depth of 1 cm for Exposure of Five Minutes (Heat Flux of 50 kW/m^2)

The model results were also compared to a special case of a semi-infinite medium subjected to a constant heat flux without convective cooling for which analytical solutions are available in many heat transfer texts (e.g [66, 67, 68]). This was done by setting the convective heat transfer coefficient, *h*, in the numerical solution to zero. Table 2.1 gives a comparison of temperatures obtained from the numerical and analytical methods with two different constant heat flux boundary values.

Table 2.1: Temperatures Obtained From Model and Analytical Results Without Convective Cooling at the Surface

Depth (cm)	q'' = 75 kW/m^2, duration of exposure = 300 seconds		q'' = 50 kW/m^2, duration of exposure= 500 seconds	
	Temperature at 300 seconds in ^{o}C		Temperature at 500 seconds in ^{o}C	
	Numerical	Analytical	Numerical	Analytical
Surface	2717.9	2721.2	2343.5	2345.1
1	605.8	607.4	772.7	773.8
2	85.8	85.9	185.4	185.6
3	25.2	25.2	44.8	44.8
4	22.1	22.1	24.0	24.1

As can be seen from the data in the table, the results of the numerical model are very close to that of the analytical with variations of less than 1% in all cases. Hence it is concluded that the numerical model is implemented correctly.

The cooling portion of the model (after $t_{exposure}$) was validated by setting the model to have an initial temperature distribution of 300^{o}C throughout the soil, selecting an ambient temperature of 22^{o}C and then setting the incident heat flux to zero. Since the initial temperature is greater than the ambient temperature, this reduces to a convective cooling heat flux boundary case for which analytical solutions are available in many heat transfer texts (e.g., [66, 67, 68]). Figure 2.7 gives a comparison of the surface temperatures as they cooled using the numerical model and analytical solution. The graph shows very good agreement between the analytical and numerical solution. The maximum variation between the numerical and analytical solutions was less than 1%

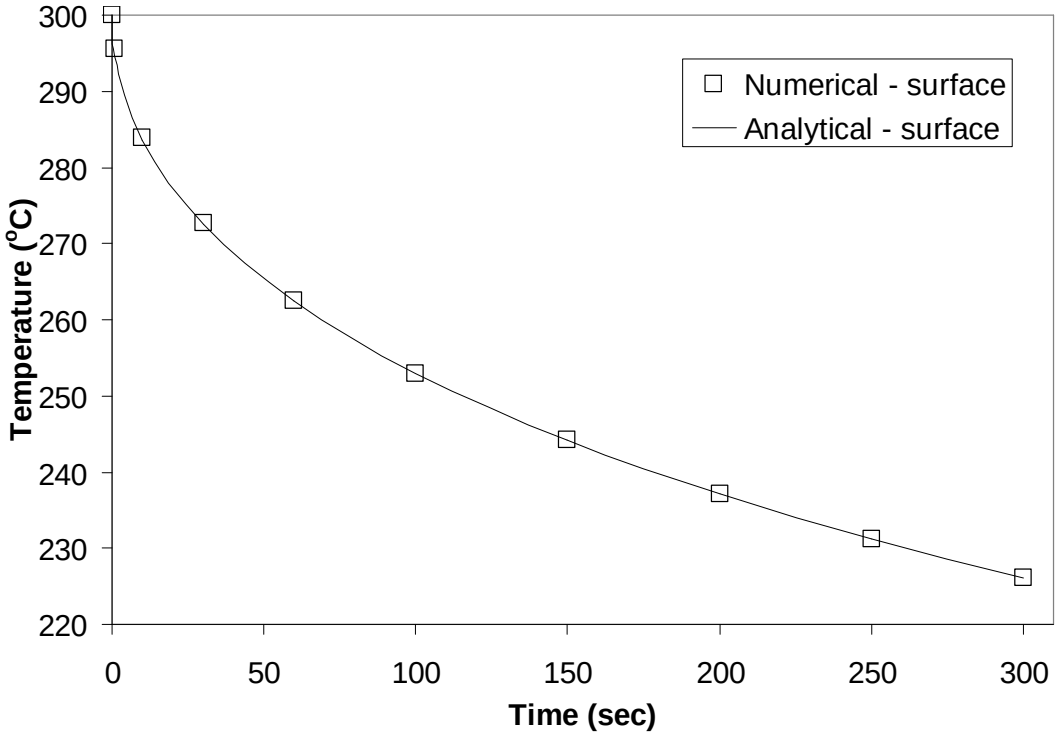

Figure 2.7: Comparison of Numerical and Analytical Results of Surface Temperature During Convective Cooling

2.6.2 Temperature dependent thermal properties single layer model.

Having verified the accuracy of the constant thermal property numerical model with various analytical solutions, it was necessary to verify that the inclusion of temperature dependent thermal properties in the formulation of the model had not affected the accuracy of the model. This was done in three ways.

The first was by replacing the temperature dependent thermal properties with constant values in Equation (2.22). Thus in Equation (2.22), the temperature dependent thermal conductivities, k_n, k_{n+1} were replaced with a constant value k, and the temperature dependent specific heats, c_n, c_{n+1} were replaced with a constant value c. This generated the same matrix equation as was obtained for formulating with constant thermal properties, k and c (Equations (2.21)).

Second, the linear equations of the temperature dependent heat capacity and thermal conductivity used in the computer code (Equations (2.19) and (2.20)) were replaced with the constant values used for the constant thermal properties model. The results obtained from this modification were then compared to that from the constant thermal properties model. The results obtained were identical, implying that the inclusion of temperature dependent thermal properties in the discretization and formulation had not affected the accuracy of the model.

Third, the results of the model were compared to an analytical solution for a semi-infinite medium whose thermal conductivity was an average for the material and dependent on the surface temperature. The solution is given by:

$$k(T) = k(T_i)(1 - \kappa(T - T_i)) \tag{2.23}$$

$$T(x,t) = T_i + \frac{q\delta}{3k_w}\left(1 - \frac{x}{\delta}\right)^3 \tag{2.24}$$

where δ is the penetration depth, calculated using

$$\delta = \sqrt{\frac{12k_w t}{\rho c}}, \tag{2.25}$$

k_w is the thermal conductivity at the surface calculated using

$$k_w(k_w - k_i)^2 = \frac{4}{3}\frac{(k_i \kappa q)^2}{\rho c} t, \tag{2.26}$$

k(T) is the thermal conductivity at the surface of the material

k_i is the thermal conductivity at the initial temperature and κ is a constant.

A computer code of the analytical solution developed in Q-Basic 4.5 was adapted from Torvi [69].

Figure 2.8 gives a comparison of the numerical solution and the results of the computer code of the analytical solution adapted from Torvi [69] at the surface and depths of 0.5 mm and 2 mm. The properties used in this case were:

- ρ = 400 kg/m^3
- c = 1100 J/kg.K
- k = 0.001T-0.2057

As can be seen from the figure, excellent agreement is achieved between the numerical and analytical results.

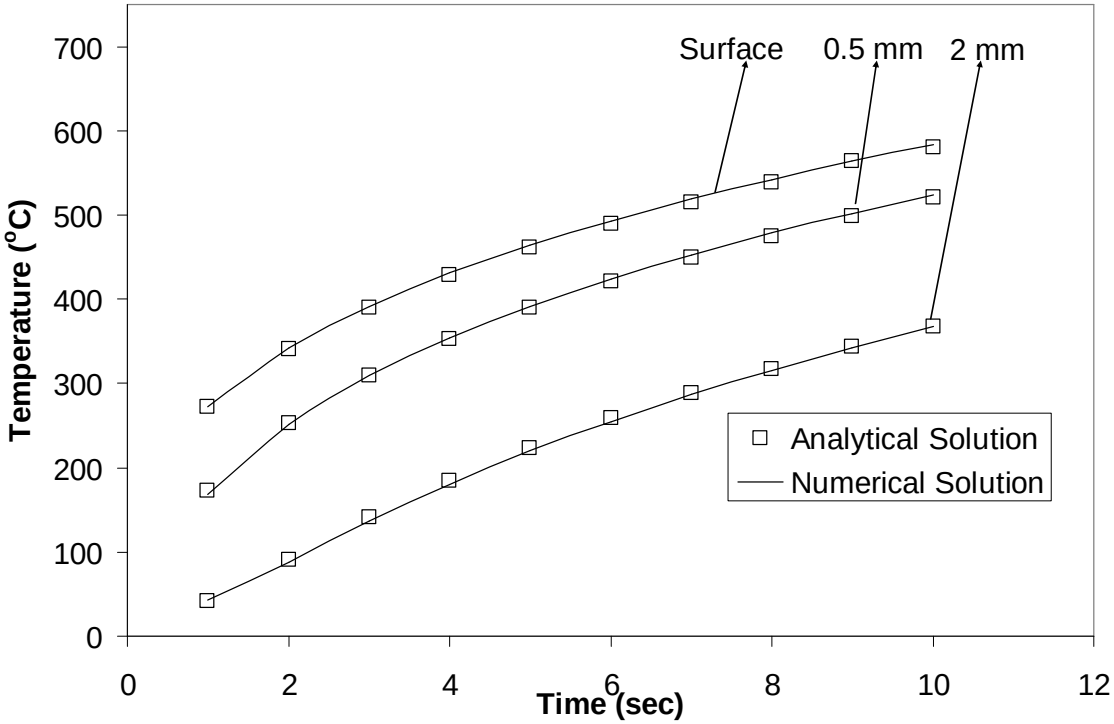

Figure 2.8: Comparison of Numerical Results and Analytical Results Adapted from Torvi [69] Variable Thermal Conductivity at Surface, 0.5 mm and 2 mm

2.7 Constant thermal properties two-layer model

The approach used in formulating the one layer model can be extended to cover for multiple layers of soil column. In this case, a two-layer model was considered.

2.7.1 Formulation of model

The soil column in this case consisted of a first layer with thermal and physical properties having subscript “1” and a second layer having thermal and physical properties with subscript “2”. The surface boundary conditions for the first layer will be similar to the surface boundary conditions of the single-layer model, hence the surface temperature will be of the same form as that given by the matrix in Equation (2.16). The bottom boundary condition of the first layer is a temperature boundary condition in which the temperature at the bottom of the first layer is equal to the temperature at the top of the second layer.

Figure 2.9 gives a representation of the node at the interface of the two layers. In the figure:

$M_{1,L}$ represents the node at the bottom of the first layer,

$M_{1,L-1}$ represents the last but one node of the first layer,

$M_{2},_{1}$ represents the first inner node of the second layer.

A typical node is surrounded by a mesh of size Δx.

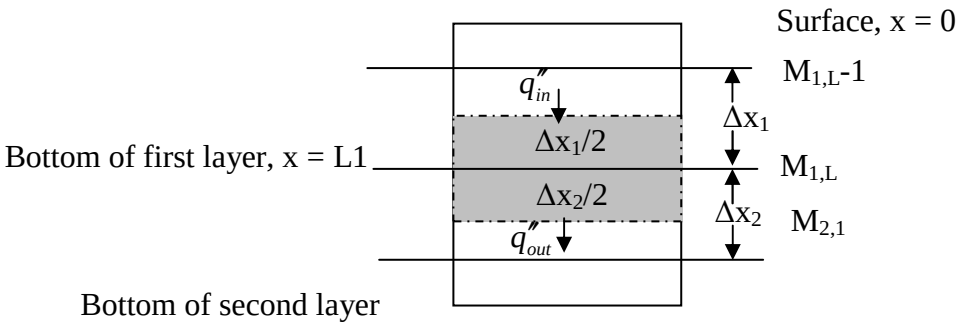

Figure 2.9: Depiction of Mesh and Nodes for Bottom Boundary of First Layer in Two-Layer Model Formulation.

At the last node for the first layer, heat flux is into a mesh of size Δx/2 and the energy transfers are given by:

$$q''_{in} = k_1 \frac{T_{M1,L-1} - T_{M1,L}}{\Delta x_1}$$

$$q''_{out} = k_2 \frac{T_{M1,L-1} - T_{M2,1}}{\Delta x_2} \qquad (2.27)$$

$$E_{sML,1} = (\rho c)\frac{\Delta x_1}{2}\frac{dT_{ML,1}}{dt}$$

Formulating with the explicit method of moving ahead in time yields:

$$T^{i+1}_{ML,1} = 2\alpha_1 P_1 T^{i}_{M1,L-1} + T^{i}_{ML,1}\left(1 - 2\alpha_1 P_1 - 2\frac{k_2}{(\rho c)_1}\frac{\Delta t}{\Delta x_1 \Delta x_2}\right) + 2\frac{k_2}{(\rho c)_1}\frac{\Delta t}{\Delta x_1 \Delta x_2} T^{i}_{M2,1} \qquad (2.28)$$

This gives the descritized equation for the temperature at the last node of the first layer. Since the surface node of the second layer will have the same temperature as given above, then the first and interior nodes of the second layer will have similar formulation as that for the first layer with subscript “2”. The bottom node of the second layer will

have the same formulation as the bottom node of the single layer model. Details of these derivations are given in Appendix A. The Fortran code used for outputting the results as well as its flowchart are given in Appendix C

2.7.2 Verification of two-layer model

The two-layer model was compared to an analytical solution of heat transfer in fabrics in close contact with the human skin. The analytical solution for the temperature of the top layer is given by:

$$\begin{aligned} T_1(x,t)-T_1(x,0) &= \frac{q}{k_1}\left[\left(2\sqrt{\frac{\alpha_1 t}{\pi}}\exp\left(-\frac{x^2}{4\alpha_1 t}\right)-x\left(1-erf\left(\frac{x}{2\sqrt{\alpha_1 t}}\right)\right)\right)\right. \\ &-\frac{1}{\gamma}\sum_{n=0}^{\infty}\left(-\frac{1}{\gamma}\right)^n\left[2\sqrt{\frac{\alpha_1 t}{\pi}}\left(\exp\left(-\frac{(x+2L_1(n+1))^2}{4\alpha_1 t}\right)+\exp\left(-\frac{(x-2L_1(n+1))^2}{4\alpha_1 t}\right)\right)\right] \\ &-(x+2L_1(n+1)\left(1-erf\left(\frac{x+2L_1(n+1)}{2\sqrt{\alpha_1 t}}\right)\right) \\ &\left.+(x-2L_1(n+1)\left(1-erf\left(\frac{x-2L_1(n+1)}{2\sqrt{\alpha_1 t}}\right)\right)\right] \end{aligned} \tag{2.29}$$

For the bottom layer, the temperature T_2 is given by:

$$\begin{aligned} T_2(x,t)-T_2(x,0) &= \frac{2q''\lambda}{\gamma}\sum_{n=0}^{\infty}\left(-\frac{1}{\gamma}\right)^2\left[2\sqrt{\frac{\alpha_2 t}{\pi}}\exp\left(\frac{-\left(x-L_1\left(1-\sqrt{\frac{\alpha_2}{\alpha_1}}(2n+1)\right)\right)^2}{4\alpha_2 t}\right)\right. \\ &\left.-\left(x-L_1\left(1-\sqrt{\frac{\alpha_2}{\alpha_1}}(2n+1)\right)\right)\left(1-erf\left(\frac{x-L_1\left(1-\sqrt{\frac{\alpha_2}{\alpha_1}}(2n+1)\right)}{\sqrt{2\alpha_2 t}}\right)\right)\right] \end{aligned} \tag{2.30}$$

where $\gamma = \dfrac{k\rho c_2 + \sqrt{(k\rho c)_1 (k\rho c)_2}}{k\rho c_1 - \sqrt{(k\rho c)_1 (k\rho c)_2}}$ (2.31)

$$\lambda = \left(k_2\sqrt{\alpha_1} - k_1\sqrt{\alpha_2}\right)^{-1} \tag{2.32}$$

α_1 and α_2 are the thermal diffusivities are the thermal diffusivities of the top and bottom layers

A computer code in Q-Basic 4.5 developed by Torvi [70] for the analytical solution given by Equations (2.25) and (2.26) was adapted for comparison with the two-layer model developed in this study. Two cases were compared here:

1. an exposure period of 30 seconds with no convective cooling at the surface, and
2. an exposure period of 30 seconds with convective cooling at the surface.

Figure 2.10 compares the numerical and analytical results for the two cases described above. The figure shows excellent agreement between the numerical and analytical results as variation between them was less than 1% for the two cases considered.

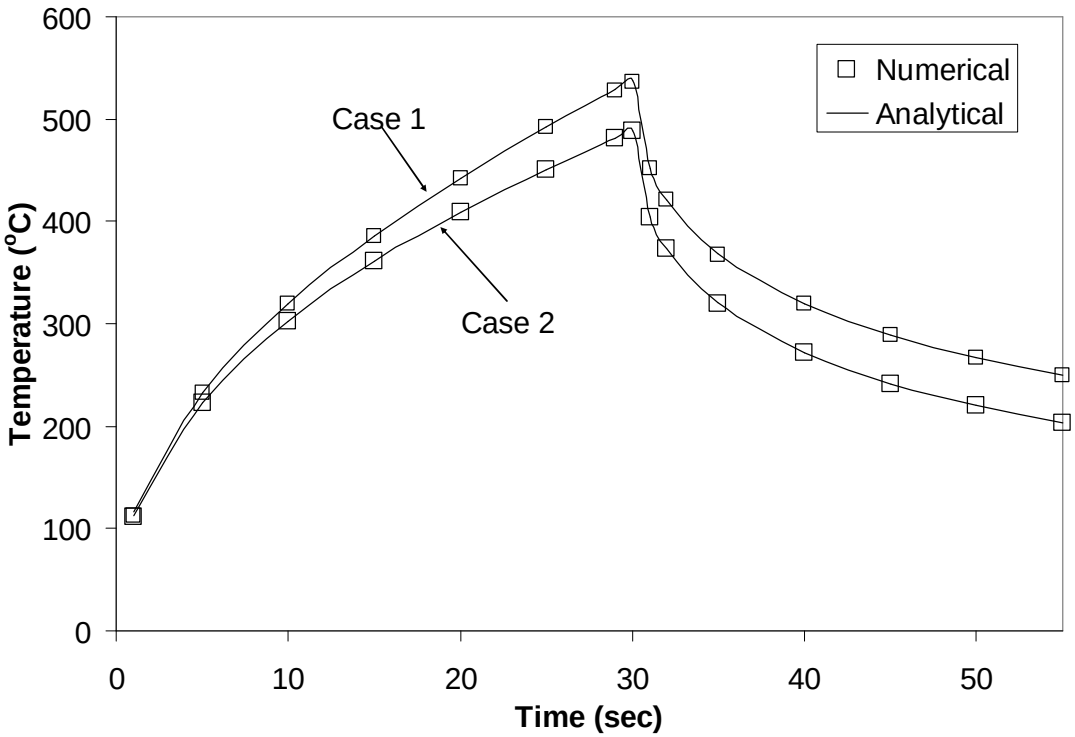

Figure 2.10: Comparison of Analytical and Numerical Results for Predicted Surface Temperatures of Case 1 (No Convective Cooling at all Times) and Case 2 (Convective Cooling at all Times) from the Two-layer Model

2.8 Summary of Chapter

In this chapter a model of heat transfer in soil with convective cooling has been developed. Numerical models to address cases of constant and temperature dependent thermal properties have been formulated. The model for the case of constant thermal properties has been extended to the case of two different layers having constant thermal properties. Methods of treating the boundary conditions such as the net incident heat flux have also been described. Solution of the differential equations governing the transfer of heat in dry soil was done using a finite difference approach and employing an explicit time-stepping method. The results of the constant thermal property models, both single and two-layer, were compared to analytical solutions and very good agreement was obtained. The varying thermal property model was then validated against the constant thermal properties and a simple analytical solution of varying thermal conductivity, and results were found to be very good. In general the results from the numerical model have agreed well with analytical solutions during both transient and steady state periods.

CHAPTER THREE: NUMERICAL RESULTS

In this chapter, predictions from the numerical models formulated in Chapter Two will be presented. Methods used to obtain thermal properties used in the model will be discussed. The following predictions will be made with the model.

- Heat transfer in dry sand: the temperature profiles, maximum temperatures and depth of lethal heat penetration will be predicted for exposure to heat fluxes of 25, 50 and 75 kW/m^2 for 5 minutes with convective cooling at all times.
- Heat transfer in dry sand: the temperature profiles, maximum temperatures at various depths and depth of lethal heat penetration will be predicted for exposure to a heat flux of 50 kW/m^2 for 5, 7 and 10 minutes.
- Heat transfer in dry two-layer soil: temperature profiles, maximum temperatures and depth of lethal heat penetration will be predicted for exposure to a heat flux of 50 kW/m^2 for 5 minutes and exposure to a heat flux of 25 kW/m^2 for 10 minutes.

In addition to the above, a sensitivity analysis will be conducted to determine the effect of the thermal properties on the models predictions.

3.1 Thermal properties used in model

In Chapter Two, numerical models were formulated from the Fourier field equation in one dimension with all relevant equations and boundary conditions given by Equation (2.12). The numerical models developed are:

- a constant thermal properties single-layer model
- a temperature dependent thermal properties single-layer model, and
- a constant thermal properties two-layer model.

The boundary conditions used in developing these models include:

- an assumption of a semi-infinite medium (for which the temperature at the bottom of soil is constant throughout the period),
- a constant incident heat flux surface boundary condition with convective cooling and radiative losses during and after exposure to heat.

Based on the governing equations, Equation (2.12) and the boundary conditions, the input parameters required for the models are:

q_o = incident heat flux (kW/m^2),

h = convective heat transfer coefficient (W/m^2·K),

c = specific heat (J/kg·K),

k = thermal conductivity (W/m·K),

$t_{exposure}$ = time of exposure of the source of heat flux (s), and

ρ = density (kg/m^3).

For the temperature dependent thermal properties model, linear relationships depicting the dependence of the specific heat and the thermal conductivity on temperature will be used whilst for the constant temperature properties model, room temperature values of the specific heat and thermal conductivity will be used. The methods used in determining the specific heat, thermal conductivity and the convective heat transfer coefficient will be presented in the next two sections.

3.1.1 Treatment of thermal conductivity

Generally, the thermal conductivity of soil depends on the relative fractions of water, gas, mineral and organic matter as well as temperature. The most popular model for soil thermal conductivity is that of de Vries [43]. deVries model of 1962 [43] considered soil as a continuous element of water for moist soil and air for dry soil in which granules of soil particles, air or water are dispersed. deVries computed the thermal conductivity as a weighted average of the conductivities of various components of the soil. For sand, which is being used in this study, the thermal conductivity ranges from 0.2 when dry to about 2.5 W/m.^{o}C when moist [62]. Pourhashemi, et al. [61] cites Flynn, et al. [72] as noting that between 300 K and 1500 K, there is a polynomial dependence of thermal conductivity on temperature. Pourhashemi, et al. [61] determined that the temperature

dependence of thermal conductivity for their study was a third-order polynomial given as:

$$k = -0.25 + 1.92\times10^{-3}T - 3.54\times10^{-6}T^2 + 2.6\times10^{-9}T^3 \text{, cal/(cm·min·K)} \qquad (3.1)$$

for quartz sand and

$$k = -0.13 + 1.3\times10^{-3}T - 2.5\times10^{-6}T^2 + 1.9\times10^{-9}T^3 \text{, cal/(cm·min·K)} \qquad (3.2)$$

for sea sand.

In their model, smaller temperature ranges were used and the polynomial dependence of thermal conductivity was converted to linear functions, the parameters of these linear relationships were determined experimentally.

For the present study a FOX heat flow meter was used to obtain the experimental variation of thermal conductivity with average temperature over a range of 17.5 to 37.5^{o}C, which was the maximum average temperature that could be used with the equipment. Figure 3.1 is a picture of the Fox 314 heat flow meter. The FOX heat flow meter measures the thermal conductivity of materials based on the general principle of heat transfer using the one-dimensional Fourier equation, Equation (1.2):

$$q'' = -k\frac{dT}{dx} \qquad (3.3)$$

where: q'' is heat flux flowing through the sample, W/m^2,

k is its thermal conductivity, W/m.^{o}C, and

dT/dx is temperature gradient on the isothermal flat surface, ^{o}C/m.

If a flat sample is placed between two flat isothermal plates maintained at two different temperatures, and a uniform one-dimensional temperature field has been stabilized, the temperature field in the sample should be uniform within the entire sample's volume. The temperature gradient can be determined by measurements of the difference between temperatures of the hot and cold plates and thickness of the sample, this is given by:

$$\frac{\partial T}{\partial t} \approx \frac{\Delta T}{\Delta x} = \frac{T_{hot} - T_{cold}}{\Delta x} \qquad (3.4)$$

where T_{hot} is the temperature of the hot plate surface

T_{cold} is the temperature of the cold plate surface and

Δx, is the sample thickness.

In this case average temperature gradient *dT/dx* is assumed equal to $\Delta T/\Delta x$.
The instrument produces conductivity results accurate to within 1% [73]. Both instrument plates utilize solid state heating/cooling and operate between 0°C and 80°C

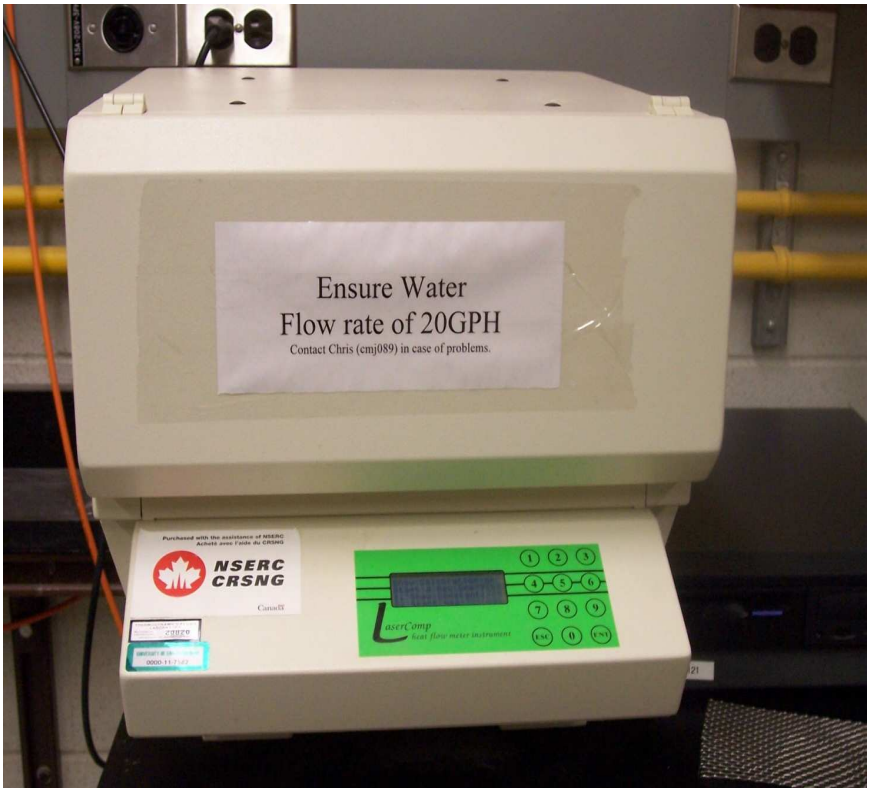

Figure 3.1: Laser Comp FOX 314 Heat Flow Meter

For the thermal conductivity tests conducted with the Laser Comp FOX 314 heat flow meter (Saugus, MA), a rectangular holder with internal dimensions of 20 cm x 20 cm and a depth of 2 cm was constructed from polystyrene to hold the sand sample. Sand of mass 1271 g was used to fill the rectangular polystyrene element to the brim such that the bulk density of the sand was approximately 1588 kg/m^3. This value of bulk density is same as that which will be used for the heat transfer experiments of the sand that will be described in Chapter Four. The heat flow meter was set to determine conductivity values at average temperatures of 37.5^{o}C, 32.5^{o}C, 22.5^{o}C and 17.5^{o}C. 37.5^{o}C was the maximum average temperature setting for the equipment. The test was set to run five times. Table 3.1 gives the mean and standard deviations of the five tests.

Table 3.1: Mean Heat Flux Values Obtained for Various Average Temperatures Using the Fox Heat Flow Meter

Average Temperature (^oC)	Thermal Conductivity of Fine Sand(W/m^oC)	
	Mean	Standard Deviation
17.5	0.2376	0.00404
22.5	0.2402	0.00356
32.5	0.2465	0.00263
37.5	0.2492	0.00318

The data obtained from the tests were correlated and a linear relationship was established between temperature and thermal conductivity. It is assumed for simplicity that this linear relationship is valid throughout the range of temperatures in this study. The obtained relationship between temperature and conductivity is:

$$k(T) = 0.0006\mathrm{T} + 0.0661 \tag{3.5}$$

where k is the temperature dependent thermal conductivity in W/m·K and T is the temperature in Kelvin.

Figure 3.2 shows a comparison of the dependence of thermal conductivity of the sand used in this study on temperature with that of different sands obtained from Pourhashemi [53]. As can be seen from the temperature dependence of thermal conductivity given by Figure 3.2, there is an increase in thermal conductivity with increase in temperature. Data from other literature (e.g. Hiraiwa, et al. [74]) also suggest that for dry soils, there is an increase in thermal conductivity for increasing temperature of soil. From the experimental correlated data, considering the range of interest from 300K up to a temperature of about 700K, the thermal conductivity values range from 0.2413 to 0.4861 W/m·K. This shows an increase of close to 100%. For a 100% increase in thermal conductivity over a temperature range of 400K, it can be said that thermal conductivity is a strong function of temperature.

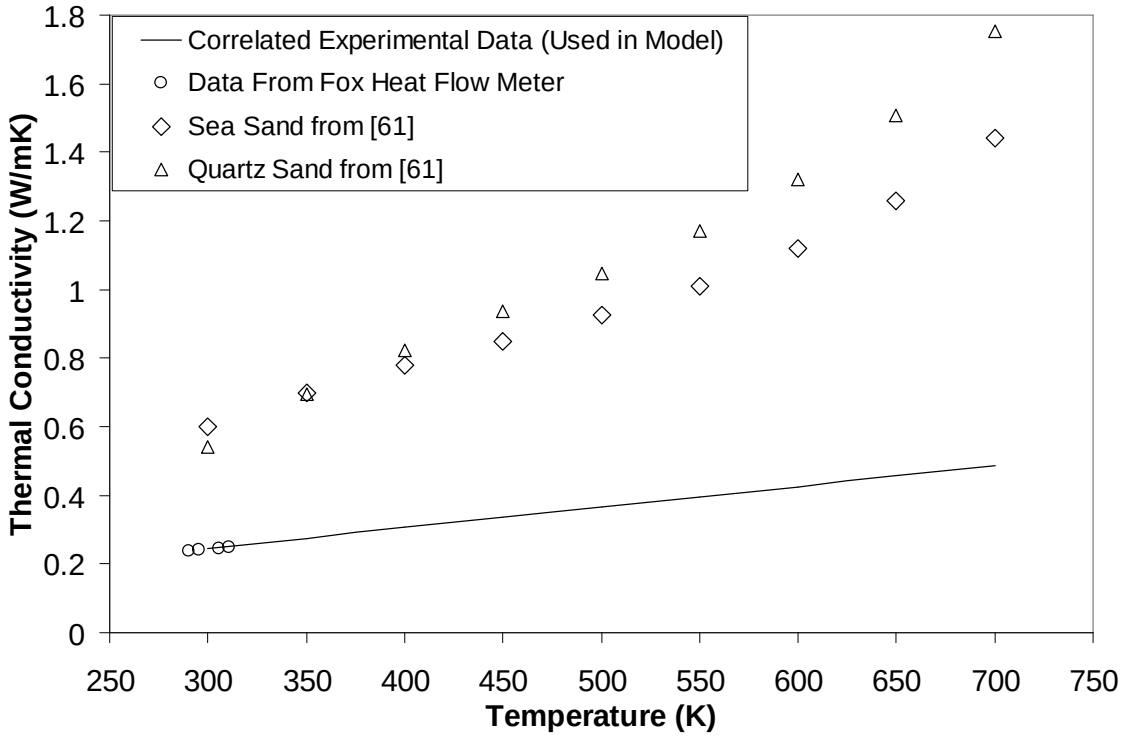

Figure 3.2: Comparison of Temperature Dependence of Thermal Conductivity from Experimental Data for this Study and the Literature

As can be seen from Figure 3.2, the experimental correlated data used in this study shows a linear variation throughout the temperature range of interest. However, data from Pourhashemi et. al. [61] on quartz and sea sand depict a rather rapid increase especially at high temperatures (from 500K) where the polynomial variation of thermal conductivity with temperature causes rapid increase in thermal conductivity values. From 500K to 650K, quartz sand shows an increase in thermal conductivity of 0.46 W/m·K, sea sand shows an increase of 0.33 W/m·K whilst the experimental correlated data shows an increase of only 0.09 W/m·K. This implies that the experimental correlated thermal conductivity relation used in this study is likely to be deficient at high temperatures since the correlation was determined at low temperatures. Pourhashemi et al. [61] cites Flynn et al. [72] that for soil undergoing a temperature change of more than 500K, the temperature dependence of thermal conductivity cannot be ignored due to the polynomial dependence given in Equations (3.1) and (3.2).

Between 300K and 600K, there is a 73% increase in the experimentally correlated thermal conductivity. At 300K, the quartz sand has a thermal conductivity of 0.5411 W/m·K, the sea sand has a thermal conductivity of 0.6018 W/m·K. whilst the experimentally correlated thermal conductivity is 0.2461 W/m·K. Compared to the literature (e.g., [5, 22, 68]), the experimentally correlated thermal conductivity of 0.2461 W/m·K at 300 K is a better approximation of the thermal conductivity of sand compared to the values obtained for the sea and quartz sands from Pourhashemi et al. [61].

3.1.2 Treatment of variable specific heat

Pourhashemi et al. [61] cites [75] as giving a power relationship between specific heat c and temperature for dry quartz and sea sand for a temperature range of 300 K to 1000 K as:

$$c(T) = 0.0097T^{0.52} \tag{3.6}$$

where $c(T)$ is the specific heat as a function of temperature, cal/g·K

T is temperature in K.

Equation (3.6) can be written to have S.I. units as:

$$c(T) = 40.612T^{0.52}\text{ , J/kg·K} \tag{3.7}$$

In the absence of reliable data on the variation of specific heat with temperature for the sand to be used in the validation of the model in this study, this relationship will be adapted. To avoid complications with the non-linearity in Equation (3.7), the values of $c(T)$ will be computed at previous time steps. Figure 3.3 shows the dependence of specific heat with temperature as given by Pourhashemi et al. [61]. There is an increase in specific heat with temperature and between 300K and 600K, there is a 43% increase in specific heat.

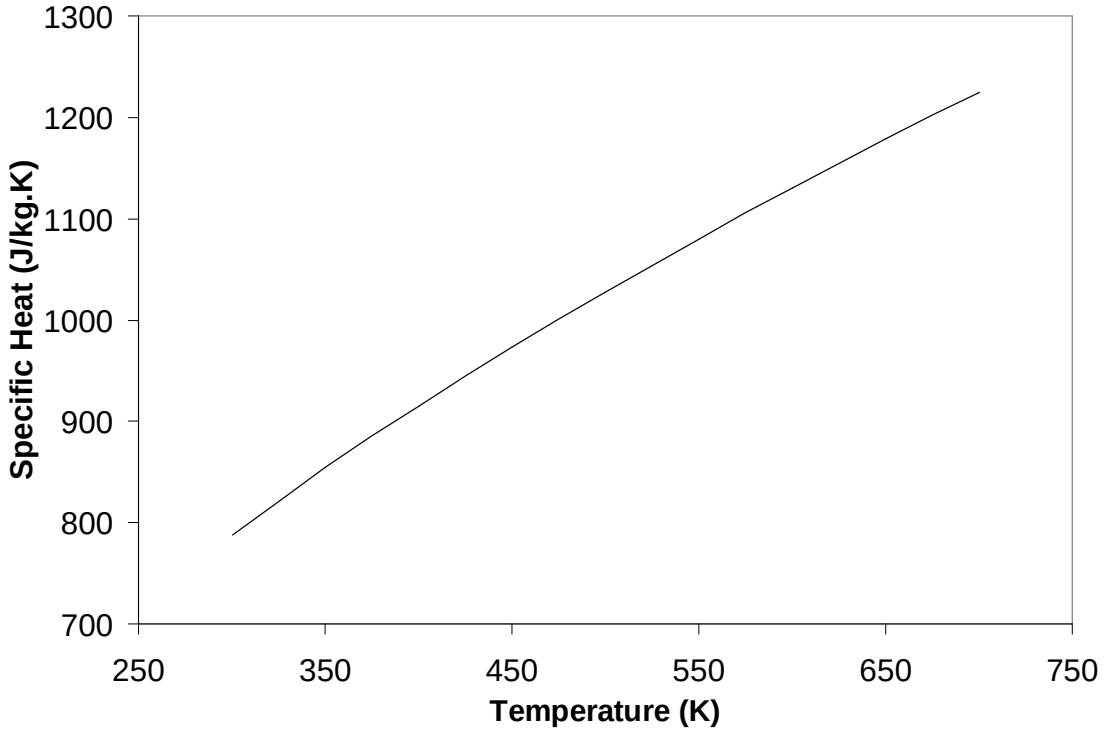

Figure 3.3: Dependence of Specific Heat on Temperature Adapted from Pourhashemi et al. [61]

3.1.3 Convective heat transfer coefficient.

The convective heat transfer coefficient, *h*, governs the heat transfer due to convection. Buoyancy forces due to temperature gradients between two surfaces, such as will exist between a heated soil surface and the surroundings, creates convective heat transfer [68]. Incropera and DeWitt [68] give detailed analysis on correlations used in determining the value of *h* for certain cases based on the average temperatures of the heated surface and the ambient. For this study the value for convective heat transfer coefficient, *h*, will be obtained by using one such correlation by considering the soil as a horizontal plate with hot surface up. For such a plate, the recommended correlation for the average Nusselt number is given as [68] :

$$\overline{Nu_L} = 0.54 Ra_L^{1/4} \quad (10^4 \le Ra_L \le 10^7) \tag{3.8}$$

$$\overline{Nu_L} = 0.15 Ra_L^{1/3} \quad (10^7 \le Ra_L \le 10^{11})$$

where Ra_L is the Raleigh number and is given by:

$$Ra_L = \frac{g\beta(T_s - T_\infty)L^3}{\alpha\nu} \tag{3.9}$$

where g = acceleration due to gravity, 9.81 m/s^2

$\beta = 1/T_f$ = expansion coefficient of air K^{-1},

T_f = average fluid temperature K,

T_s = surface temperature of soil K,

T_∞ = ambient temperature K,

α = thermal diffusivity of air m^2/s,

ν = kinematic viscosity of air m^2/s,

L = ratio of surface area to perimeter of plate.

From the experiments that will be conducted, it is estimated that an average surface temperature of 255^{o}C and ambient temperature of 22^{o}C will prevail. The average temperature for T_f is (255+22)/2 = 146^{o}C which corresponds to 419 K. From Table A.4 of Incopera and DeWitt [68] and using Equations (3.9) and (3.10), the value of h obtained is 13 W/m^2·K. Details of determining the value of the convective heat transfer coefficient is given in Appendix D. Selving [22] used an h value of 20 W/m^2·K whilst Richon [5] used a value of 10 W/m^2·K. The value of h chosen is closer to that of Richon [5] whose work dealt with medium intensity fire and obtained heat fluxes of approximately 54 kW/m^2.

3.2 Comparison of predictions by constant and temperature dependent thermal property models

As mentioned in the introduction to this chapter, predictions of temperature profiles and depths of lethal heat penetration will be made with both the temperature dependent and constant thermal properties models and comparisons will be made between the results from both models. Predictions of temperature profiles and depths of lethal heat penetration will also be made for a two-layer soil. Table 3.2 gives the values of the input parameters used in the models. The values of specific heat, c, and thermal conductivity, k, used for the constant thermal properties model are based on room temperature of 22^{o}C using Equations (3.5) and (3.7). The value of density used was obtained from the density of the fine sand that was used in experimental work in detailed in Chapter Four

Table 3.2: Input Parameters for Prediction of Temperature Profiles and Depth of Lethal Heat Penetration in Soil Using Various Models

Input Parameters	Type of Model		
	CTP Single-layer Model	TDTP Single-layer Model	CTP Two-layer Model 1 = Top Layer 2 = Bottom Layer
Incident Heat Flux, q'' (kW/m^2)	25, 50 and 75	25, 50 and 75	25, 50
Thermal Conductivity, k (W/mK)	0.2431	Equation 3.6	k_1=0.42, k_2=0.2431
Specific Heat, c (J/kg.K)	781.6	Equation 3.8	c_1= 908.6, c_2=781.6
Exposure Time, $t_{exposure}$ (s)	300	300	600, 300
Density, ρ (kg/m^3)	1588	1588	ρ_1= 662.2, ρ_2 =1588
Convective Heat Transfer Coefficient, h (W/m^{2}K)	13	13	13
Thickness of Soil, L(cm)	17.0	17.0	L_1= 5.0, L_2 = 12.0
Ambient Temperature, T_a (K)	295	295	295

to validate the model. For the two-layer model, the subscript "1" refers to the top layer and "2" refers to the bottom layer. For simplicity in labelling, the Constant Thermal Properties Model will be referred to as CTP model whilst the Temperature Dependent Thermal Properties Model will be referred to as TDTP model. For this study, heat flux values of 25, 50 and 75 kW/m^2 will be used with exposure times ranging from 5 minutes to 10 minutes. These values of heat flux and times are based on the literature. For example, Richon [5] measured heat flux values equivalent to 54 kW/m^2 whilst Archibold [28] recorded fire temperature durations of between 1 and 9 minutes. For the values of thermal properties and the depth of sand used in the predictions, the semi-infinite assumption was valid for a

period of 9215 seconds, which is equivalent to $2^1/_2$ hours. This was done by setting the time, *t*, as the subject in Equation (2.5) to obtain:

$$t < \frac{L^2}{16\alpha}, \text{ s.} \tag{3.10}$$

Additionally, it is assumed that the sand surface will behave like a black body and hence have emissivity, ε, of unity.

3.2.1 Single-layer model exposed to heat flux of 50 kW/m^2

Predictions of temperature profiles using the CTP and TDPT models for exposure to heat fluxes of 25, 50 and 75 kW/m^2 for 5 minutes (300 seconds) are shown in Figures 3.4, 3.5 and 3.6 respectively. The maximum temperatures reduce with increasing depth of the soil as expected. Tables 3.3, 3.4 and 3.5 give more information on the maximum temperatures obtained at various depths. The maximum temperatures at each depth in soil will be used to determine the depth of lethal heat penetration based on the 60^{o}C criterion.

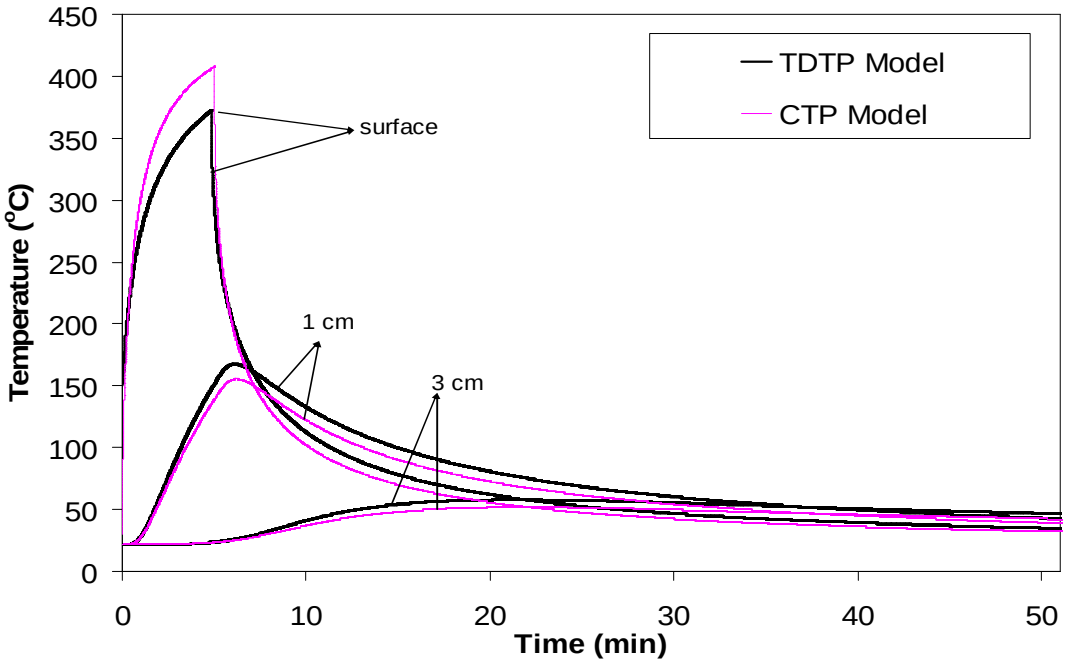

Figure 3.4: Predicted Temperature Profiles at Surface and Depths of 1 and 3 cm from the CTP and TDTP Models During and After 5 Minutes Exposure to Heat Flux of 25 kW/m^2

Table 3.3: Predicted Maximum Temperatures From TDTP and CTP Models for 5 Minutes Exposure to Heat Flux of 25 kW/m^2

Depth (cm)	Temperature in ^{o}C	
	TDTP Model	CTP Model
surface	368.6	403.9
1	165.5	153.8
2	84.7	75.3
3	56.4	50.4
4	43.5	39.5
5	36.6	33.8
10	24.6	24.1

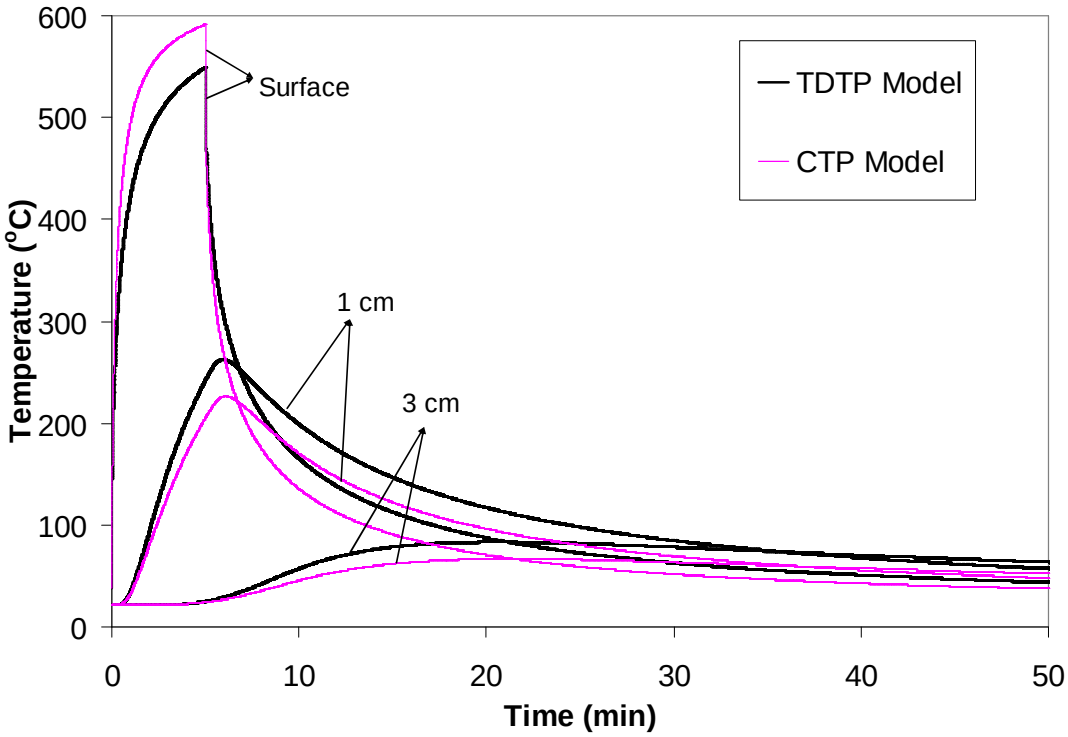

Figure 3.5: Predicted Temperature Profiles from TDTP and CTP Models at the Surface and Depths of 1 cm and 3 cm During and After 5 Minutes Exposure to a Heat Flux of 50 kW/m^2.

Table 3.4: Predicted Maximum Temperatures from TDTP and CTP Models at Various Depths For 5 Minutes Exposure to Heat Flux of 50 kW/m^2

Depth (cm)	Temperature in ^{o}C	
	TDTP Model	CTP Model
Surface	546.8	589.1
1	260.7	225.2
2	129.6	103.6
3	81.9	65.6
4	60.1	49.0
5	48.2	40.3
10	28.4	26.3

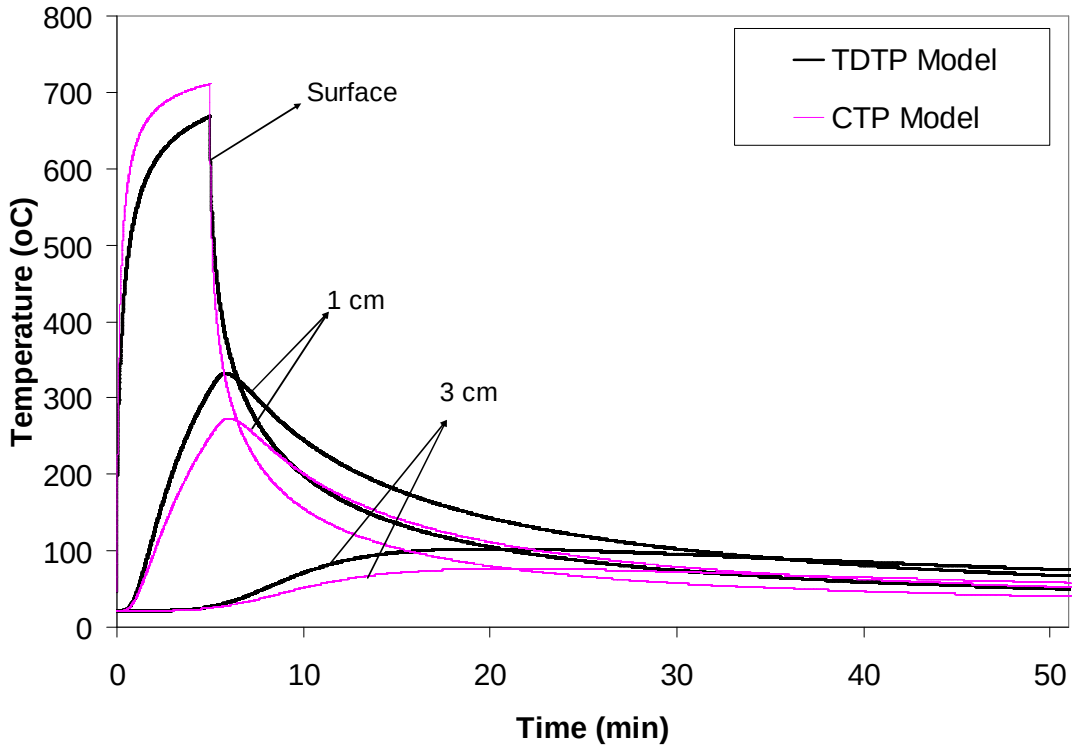

Figure 3.6: Predicted Temperature Profiles From the TDTP and CTP Models at Surface and Depths of 1 and 3 cm During and After 5 Minutes Exposure to Heat Flux of 75 kW/m^2

Table 3.5: Predicted Maximum Temperatures from TDTP and CTP Models For 5 Minutes Exposure to Heat Flux of 75 kW/m^2

Depth (cm)	Temperature in ^oC	
	TDTP Model	CTP Model
Surface	666.7	709.2
1	331.0	272.5
2	163.7	122.1
3	101.5	75.4
4	72.8	55.2
5	57.2	44.5
10	30.8	27.4

As can be seen from the Figures 3.4 to 3.6 and from Tables 3.3 to 3.5, the CTP model predicted higher maximum temperature at the surface than the TDTP model but then predicted lower values of temperature at the other depths within the soil than the TDTP model. Recall that earlier on, it was mentioned that over a temperature range from 300K to 600K, there was approximately 73% increase in thermal conductivity values whilst there was about 43% increase in specific heat values. From this it implies that for the TDTP model, as temperature increases, the change in thermal properties (being more in thermal conductivity than in specific heat) results in an increase in the thermal diffusivity. Hence heat is transmitted through the soil faster for the TDTP model than for the CTP model since for the CTP model the unchanging value of thermal diffusivity (thermal property values were computed at room temperatures of 22^o) becomes smaller than that of the TDTP at temperatures larger than the room temperature. The smaller value of thermal diffusivity inhibits the flow of heat into the soil from the surface and results in higher temperatures at the surface and lower temperatures within the soil.

The depth of lethal heat penetration is obtained by plotting the maximum temperatures at every depth versus the depth and tracing a line from 60^oC on the maximum temperature

axis to the curve and then to the depth axis. Selving [22], in determining the depth of lethal heat penetration used a curve fitting method of the maximum temperatures at various depths. In between any two depths, it can be assumed that the maximum temperatures vary linearly and hence a simple linear interpolation method can also be used to obtain the depth of lethal heat penetration. In this study the method of assuming linear relationship (linear interpolation) or curve fitting the temperature data points were both analysed. Figure 3.7 shows the curve fitting and linear interpolation methods that can be used in estimating the depth of lethal heat penetration for the case of exposure to a heat flux of 50 kW/m^2 for 5 minutes exposure. The curve fitting was done using a second-order polynomial curve fitting features of Microsoft® Excel.

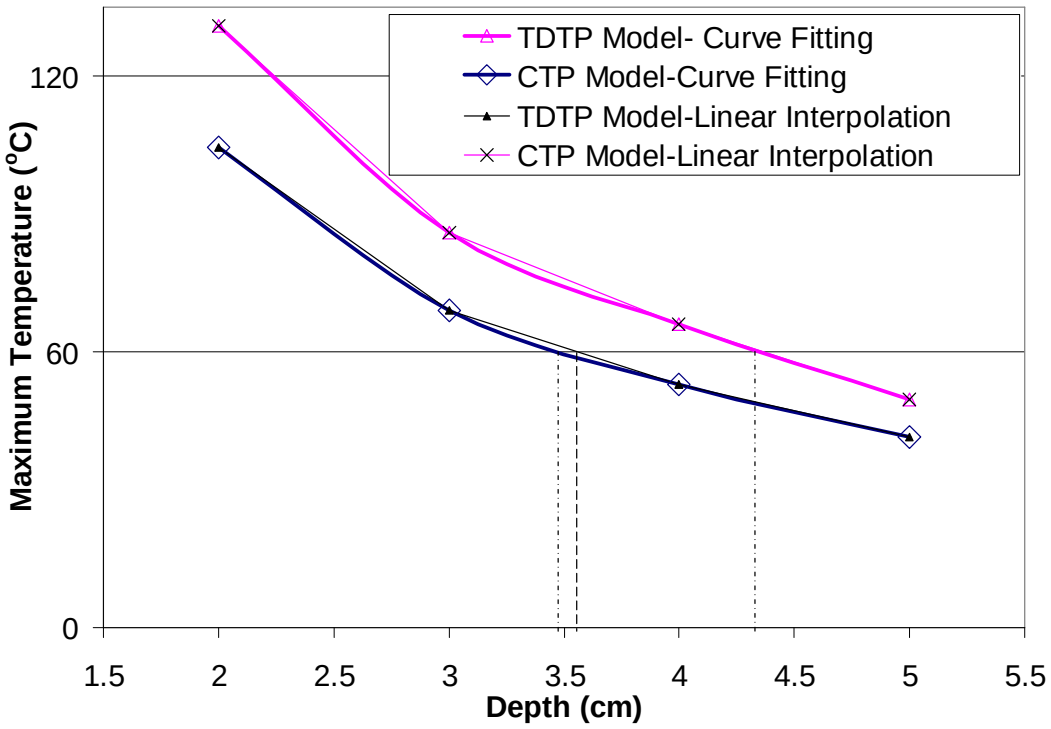

Figure 3.7: Plot of Maximum Temperatures Versus Depth Used in Estimating Depth of Lethal Heat Penetration for Exposure to Heat Flux of 50 kW/m^2 (5 Minutes Exposure)

The depth of lethal heat penetration estimated with the curve fitting method is 3.5 cm for CTP model and 3.6 cm using the linear interpolation method. For the TDTP model the

estimated depth of lethal heat penetration was 4.3 cm from both the curve fitting and linear interpolation methods. Since the maximum temperature at 4 cm was close to 60^{o}C, both the curve fitting and linear interpolation methods gave approximately the same depth of lethal heat penetration.

Typically, for the numerical model, the depth of lethal heat penetration can be obtained directly by using a high grid resolution as against using a curve fitting method, however, in the experimental work it will not be possible to obtain a high grid resolution since temperature measurements cannot be done at high grid resolutions. This makes it more appropriate to use the curve-fitting method. Hence for this study, to ensure consistency in the method of determining the depth of lethal heat penetration for both model and experimental works, the curve-fitting method will be used. Table 3.6 gives the predicted values of depth of lethal heat penetration from TDTP and CTP models for exposure to heat fluxes of 25, 50 and 75 kW/m^2 for 5 minutes exposure.

Table 3.6: Depths of Lethal Heat Penetrations Predicted by the Temperature Dependent and Constant Thermal Properties Models

Incident Heat Flux (kW/m^2)	Depth of lethal heat penetration (cm)	
	TDTP Model	CTP Model
25	3.0	2.6
50	4.3	3.5
75	5.1	4.0

As can be seen from Table 3.6, the depth of lethal heat penetration predicted by the constant thermal properties model is less than that predicted by the temperature dependent thermal properties model. This is due to the inhibition of heat inflow due to the smaller value of thermal diffusivity compared to that of the temperature dependent thermal properties model as described previously. For the same quantity of thermal energy input, the temperature dependent model, with a varying thermal diffusivity which tends to decrease with increase in temperature, permits faster heat flow which produces a larger value of depth of lethal heat penetration whilst the constant thermal properties

model with a smaller value of thermal diffusivity tends to inhibit heat flow produces a smaller value of depth of lethal heat penetration. Thus for the two models the TDTP model predicts a larger value of depth of lethal heat penetration than the CTP model as depicted in Table 3.6. The TDTP model is thus conservative.

Table 3.7 gives the predicted maximum temperature at various depths for an exposure to heat flux of 50 kW/m^2 for 5, 7 and 10 minutes exposure. The depth of lethal heat penetration (DLHP) is also given in the Table. The data from the Table indicates an increase in maximum temperatures at all depths for increase in time of exposure. There was a corresponding increase in depth of lethal heat penetration for increase in exposure time.

Table 3.7: Predicted Maximum Temperatures for Exposure to Heat Flux of 50 kW/m^2 and Various Exposure Times.

Depth (cm)	Maximum Temperature (^{o}C)					
	TDTP Model			CTP Model		
	5 min	7 min	10 min	5 min	7 min	10 min
Surface	546.8	564.2	579.6	589.1	600.0	609.4
1	260.7	309.7	360.0	225.2	269.8	317.8
3	81.9	101.7	128.9	65.6	79.3	98.5
5	48.2	57.4	70.3	40.3	46.3	54.8
10	28.4	30.8	34.2	26.3	27.8	29.8
DLHP (cm)	4.3	5.3	6.2	3.5	4.2	5.0

3.2.2 Two-layer constant thermal properties model

Predictions of temperature profiles and depths of lethal heat penetration using the CTP two-layer model are given below. It is assumed that the top layer is a black earth top soil and the bottom layer is fine sand having properties similar to those used in the one-layer predictions. The thermal properties of the top soil were obtained from Usowicz [76]. Two predictions are made here; the first is for an exposure to a heat flux of 25 kW/m^2 for a period of 10 minutes and the second is for exposure to heat flux of 50 kW/m^2 for a

period of 5 minutes. Figure 3.8 gives the temperature profiles for depths of 1 cm, 5 cm (interface) and 7 cm obtained for the case of exposure to heat flux of 25 kW/m^2 for 10 minutes. Table 3.8 gives the maximum temperatures obtained at various depths for both predictions. The depth of lethal heat penetration obtained was 6.0 cm for the case of exposure to heat flux of 25 kW/m^2 for 10 minutes and 5.6 cm for the case of exposure to heat flux of 50 kW/m^2 for period of 5 minutes.

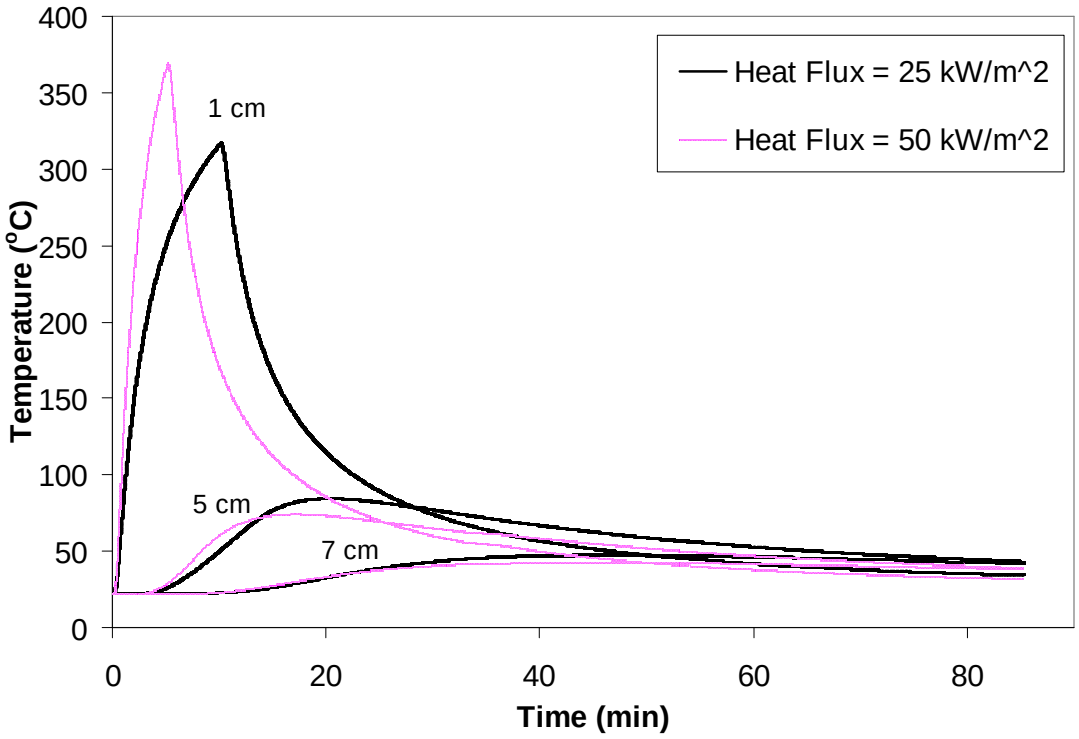

Figure 3.8: Predicted Temperature Profiles at Depths of 1 cm, 5 cm and 7 cm During and After 10 Minutes Exposure to a Heat Flux of 25 kW/m^2 and 5 Minutes Exposure to a Heat Flux of 50 kW/m^2 (Two-layer model)

Table 3.8: Predicted Maximum Temperatures at Various Depths for Two-Layer Model

Depth	Temperatures in ^{o}C	
	q'' = 50 kW/m^2 for 5 minutes	q'' = 25 kW/m^2 for 10 minutes
Surface	595.2	437.6
1	368.1	315.1
3	136.4	151.3
5	72.9	82.6
7	41.9	46.0
10	27.8	29.2

3.3 Sensitivity analyses

Methods used to measure the physical and thermal properties of the soil are not 100% accurate. Moreover, the thermal conductivity relation used in the model was correlated from a limited temperature range whilst the specific heat was adapted from the literature. Since variations in these properties can affect the results of the model, a sensitivity analysis was carried out to determine the effects of changes in the thermal and physical properties on the predictions of the model, typically the maximum temperatures. These changes are transformed into the depth of lethal heat penetration. The sensitivity analysis is considered for the case of exposure to a heat flux of 50 kW/m^2 for an exposure period of 5 minutes. The TDTP model is used in the sensitivity analyses whilst that for the CTP model is given in Appendix E. The CTP model predicted results similar to that of the TDTP model but to different degrees.

In these analyses, the thermal conductivity and specific heat were varied by 10 and 20% above and below their nominal values given by Equations (3.5) and (3.7). The density, convective heat transfer coefficient and the incident heat flux were also varied by 10% and 20% above and below their nominal values used in predictions. The effect of the change in properties on the results predicted by the models were analysed in terms of percentage change of the maximum temperatures from the nominal values at each depth.

The effect of the convective heat transfer coefficient during heating was also analysed. The symbol "↑" denotes an increase and "↓" denotes a decrease. It should be noted that the sensitivity analyses do not include the effect of interactions between density and thermal conductivity.

3.3.1 Effect of thermal conductivity on predicted maximum temperatures and depth of lethal heat penetration

Table 3.9 shows the effect of thermal conductivity on predicted maximum temperatures from the TDTP model. From the Table, the effect of thermal conductivity varies with depth but is smaller near and at the surface. At the surface, an increase in thermal conductivity causes a decrease in the surface temperatures whilst at the inner depths, an increase in thermal conductivity causes an increase in maximum temperatures. This is due to the fact that as thermal conductivity increases, heat is conducted faster into the soil and results in lower temperatures at the surface and higher temperatures within the soil.

Table 3.9: Effect of Thermal Conductivity on Predicted Maximum Temperatures at Various Depths from the TDTP Model.

Depth (cm)	Temperature (^{o}C) at Nominal value of Thermal Conductivity K (Equation (3.5))	Percentage Change in Maximum Temperatures			
		10% Increase in k	20% Increase in k value	10 % Decrease in k	20% Decrease in k value
0	546.8	↓1%	↓2%	↑1%	↑2%
1	260.7	↑2%	↑4%	↓3%	↓6%
3	81.9	↑5%	↑9%	↓5%	↓10%
5	48.2	↑4%	↑8%	↓4%	↓9%
10	28.4	↑4%	↑9%	↓4%	↓8%

The increase in thermal conductivity results in larger value of thermal diffusivity. The opposite occurs when there is a decrease in thermal conductivity. The surface temperature increases whilst the internal temperatures decrease. Also, this literally results in a smaller value of thermal diffusivity. Increase in depth of lethal heat penetration with increase in k value is consistent with results obtained by Selving [22] who found that for different soils with different thermal conductivities, the depth of lethal heat penetration was larger in soils with larger thermal conductivities. This is because the thermal conductivity increases significantly than either the density or specific heat [22]. Figure 3.9 shows the effects of change in thermal conductivity on the temperature at depth of 1 cm.

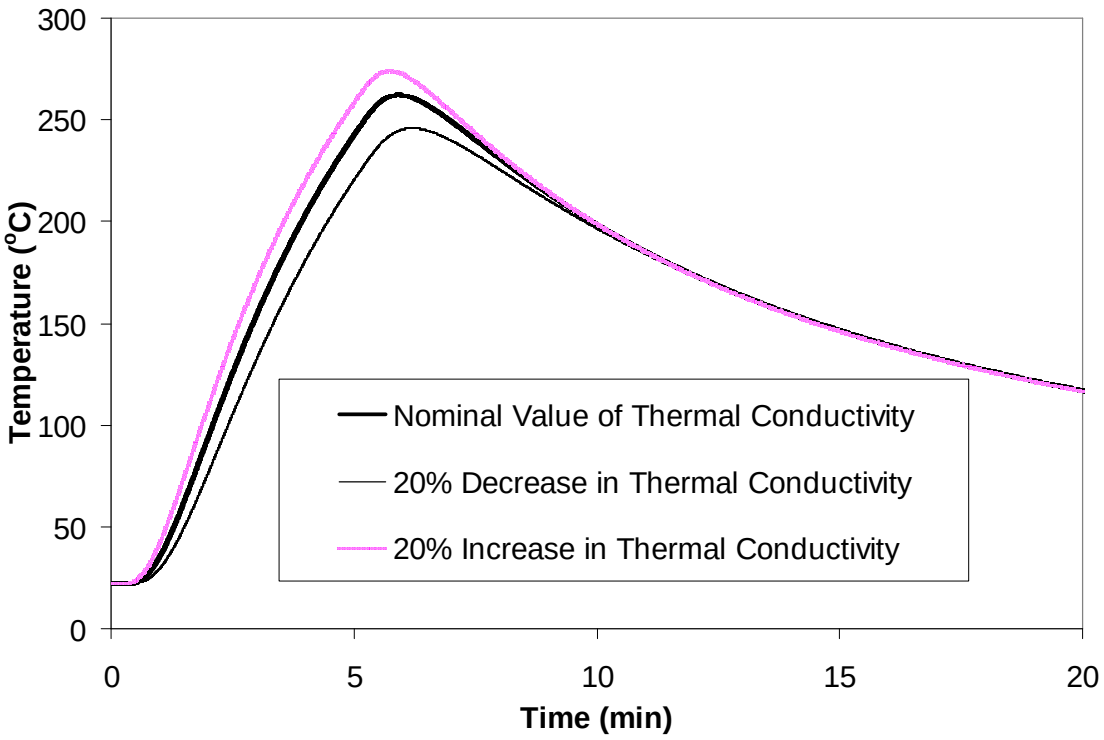

Figure 3.9 : Effect of Change in Thermal Conductivity on Predicted Temperatures at Depth of 1 cm.

Table 3.10 shows the effect of change in thermal conductivity on the predicted depth of lethal heat penetration (DLHP) from the TDTP model. The data from Table 3.10

indicates that there is a 5% increase in depth of lethal heat penetration for a 10% increase in the value of the thermal conductivity.

Table 3.10 Effect of Thermal Conductivity on Predicted Depth of Lethal Heat Penetration (DLHP) from TDTP Model

Change in Input Value	Depth of Lethal Heat Penetration (DLHP)	
	Nominal Value of DLHP (cm)	Percentage change
Nominal values	4.1	-
10% increase	4.3	↑5%
20% increase	4.5	↑10%
10% decrease	3.9	↓5%
20% decrease	3.7	↓10%

Recall that in Table 3.9 the effect of thermal conductivity on predicted maximum temperatures showed an increase in thermal conductivity resulting in an increase in predicted maximum temperatures. The increase in predicted maximum temperatures will result in a higher value of depth of lethal heat penetration as seen in Table 3.10. A decrease in the value of thermal conductivity results in a decrease in the depth of lethal heat penetration similar to the effect on maximum temperatures.

3.3.2 Effect of specific heat on predicted maximum temperatures and depth of lethal heat penetration

Table 3.11 gives the effect of a change in specific heat on the predicted maximum temperatures from the TDTP model. From Table 3.11, an increase in specific heat causes a decrease in maximum temperatures. This is also evident from definition of specific heat as with increase in the value of specific heat, more thermal energy is required to raise a unit mass of sand by $1^{o}C$ which results in a reduction in the maximum temperatures obtained. On the average a 10% change in the specific heat value causes about 5% change in internal maximum temperatures.

Table 3.11: Effect of Specific Heat on Predicted Maximum Temperatures at Various Depths from the Temperature Dependent Thermal Properties Model.

Depth (cm)	Maximum Temperature (°C) at Nominal Value of Specific Heat (Equation (3.7))	Percentage Change in Maximum Temperatures			
		10% Increase in c Value	20% Increase in c Value	10 % Decrease in c Value	20% Decrease in c Value
0	546.8	↓1%	↓2%	↑1%	↑2%
1	260.7	↓5%	↓10%	↑6%	↑12%
3	81.9	↓6%	↓10%	↑7%	↑15%
5	48.2	↓4%	↓8%	↑5%	↑12%
10	29.2	↓5%	↓8%	↑4%	↑9%

Figure 3.10 shows the effect of a 20% change in specific heat on temperatures at a depth of 1cm. As can be seen from Figure 3.10, with an increase in specific heat, there is a

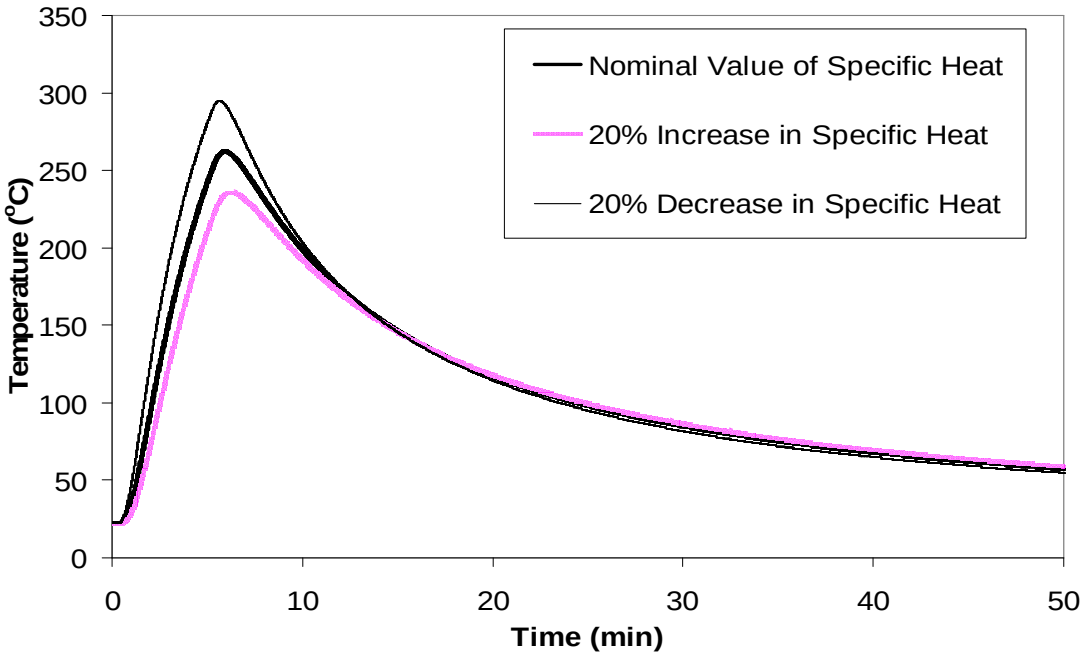

Figure 3.10 : Effect of 20% Change in Specific Heat on Predicted Temperatures at Depth of 1 cm

reduction in the rate of heating compared to the nominal value, and during cooling, there is also a reduction in rate of cooling compared to the nominal value. The converse is true for a decrease in the value of specific heat.

Table 3.12 gives the effect of specific heat on lethal heat penetration. From the data in Table 3.12, there is a decrease in depth of lethal heat penetration for an increase in specific heat. This follows from basic principles of heat transfer and also from Table 3.11 where the effects of specific heat on predicted maximum temperatures were presented. From Table 3.11 it was observed that an increase in specific heat caused a decrease in predicted maximum temperatures, this decease in maximum temperatures will cause a decrease in the depth of lethal heat penetration.

Table 3.12: Effect of Specific Heat on Predicted Depth of Lethal Heat Penetration

Change in Input Value	Depth of Lethal Heat Penetration (DLHP) from the TDTP Model	
	Nominal Value of DLHP (cm)	Percentage change
Nominal values	4.1	-
10% increase	3.9	↓5%
20% increase	3.7	↓10%
10% decrease	4.4	↑7%
20% decrease	4.6	↑12%

3.3.3 Effect of density on predicted maximum temperatures

Table 3.13 gives the effect of density on the predicted maximum temperatures from the TDTP model. Similar to the effect of specific heat, an increase in density results in a decrease in maximum temperatures. A 10% change in density results in about 5% change in maximum temperatures. This is obvious from basic heat transfer principles since both specific heat and density are in the denominator in thermal diffusivity.

Table 3.13: Effect of Density on Predicted Maximum Temperatures at Various Depths from the TDTP Model.

Depth (cm)	Maximum Temperature (^oC) at Nominal Value of ρ = 1588 kg/m^3	Percentage Change in Maximum Temperature			
		10% Increase in ρ Value	20% Increase in ρ Value	10 % Decrease in ρ Value	20% Decrease in ρ Value
0	546.8	↓1%	↓2%	↑1%	↑2%
1	260.7	↓5%	↓10%	↑6%	↑12%
3	81.9	↓7%	↓10%	↑7%	↑15%
5	48.2	↓4%	↓8%	↑5%	↑12%
10	28.4	↓4%	↓8%	↑4%	↑9%

Table 3.14 shows the effect of density on the depth of lethal heat penetration. The effect of density on the depth of lethal heat penetration is similar to the effect of specific heat stemming from basic heat transfer principles and also from Table 3.13 where the effects of density on the predicted maximum temperatures were presented. As can be seen from

Table 3.14: Effect of Density on Predicted Depth of Lethal Heat Penetration from TDTP Model

Change in Input Value	Depth of Lethal Heat Penetration (DLHP)	
	Nominal Value of DLHP (cm)	Percentage change
Nominal values	4.1	0
10% increase	3.9	↓5
20% increase	3.7	↓10
10% decrease	4.3	↑6
20% decrease	4.6	↑12

data in the Table 3.14, a 10% increase in density causes approximately a 5% decrease in the depth of lethal heat penetration.

3.4 Effect of boundary conditions

The effect of the boundary conditions (convective heat transfer coefficient and incident heat flux) on the predicted maximum temperatures and the depth of lethal heat penetration are presented in this section.

3.4.1 Effect of convective heat transfer coefficient on predicted maximum temperatures

Table 3.15 shows the effect of the heat transfer coefficient on predicted maximum temperatures using the TDTP model. Table 3.16 also shows the effect of ignoring convective cooling during heating of soil on predicted maximum temperatures. As can be seen from Table 3.15, the changes in the maximum temperatures are minimal, on the average there is about 1% decrease in maximum temperatures for a 10% increase in the value of the convective heat transfer coefficient. Though the effect on the maximum temperatures is not significant, changes in the convective heat transfer coefficient will affect the shape of the temperature profiles during the heating and cooling periods.

Table 3.15: Effect of Convective Heat Transfer Coefficient on Predicted Maximum Temperatures at Various Depths from the TDTP.

Depth (cm)	Maximum Temperature (^{o}C) at Nominal Value of h = 13 W/m^{2}K	Percentage Change in Maximum Temperatures			
		10% Decrease in h Value	20% Decrease in h Value	10 % Increase in h Value	20% Increase in h Value
0	546.8	↓0.6%	↓1%	↑0.6%	↑1%
1	260.7	↓0.8%	↓2%	↑0.7%	↑2%
3	81.9	↓1%	↓2%	↑1%	↑3%
5	48.2	↓1%	↓2%	↑1%	↑3%
10	28.4	↓1%	↓2%	↑0%	↑1%

Table 3.16: Effect of no Convective Cooling During Heating of Soil on Predicted Maximum Temperatures from the TDTP Model

Depth (cm)	Maximum Temperature (^{o}C) at Nominal Value of h	Maximum Temperature (^{o}C) with no Convective Cooling During Heating	Percentage Difference
0	546.8	586.5	↑7%
1	260.7	282.7	↑8%
3	81.9	95.1	↑14%
5	48.2	58.3	↑18%
10	28.4	31.6	↑8%

An increase in the value of the convective heat transfer coefficient causes a decrease in the maximum temperatures. This is due to the fact that with an increase in the value of *h*, there is an increase in the convective heat losses at the surface of the soil and hence faster cooling, resulting in lower temperatures both at the surface and within the soil. A decrease in the value of *h* results in an increase in the maximum temperatures as the convective heat losses are reduced. From Table 3.16 the effect of ignoring convective heat transfer coefficient during heating can be seen to be significant showing a consistent increase in maximum temperatures at all depths. This is a special case of reduction in the value of *h* as explained. The increase in maximum temperatures varies from 7% at the surface to about 18% at a depth of 5 cm.

3.4.2 Effect of incident heat flux on predicted maximum temperatures

Table 3.17 shows the effect of varying the incident heat flux on the predicted maximum temperatures. An increase in the value of the incident heat flux causes an increase in the maximum temperatures at all depths within the soil. This is also evident since an increase in the source of heat implies an increased total thermal energy in a given period.

Table 3.17: Effect of Incident Heat Flux on Predicted Maximum Temperatures at Various Depths from TDTP Model.

Depth (cm)	Temperature at Nominal Value of q'' = 50 kW/m^2	Percentage Change in Maximum Temperatures			
		10% increase in q'' Value	20% increase in q'' Value	10 % decrease in q'' Value	20% decrease in q'' Value
0	546.8	↑5%	↑9%	↓5%	↓11%
1	260.7	↑6%	↑11%	↓6%	↓13%
3	81.9	↑5%	↑10%	↓5%	↓11%
5	48.2	↑4%	↑8%	↓4%	↓8%
10	28.4	↑1%	↑3%	↓2%	↓4%

3.4.3 Effect of convective heat transfer coefficient on the depth of lethal heat penetration

Table 3.18 gives the effect of the convective heat transfer coefficient on the predicted depth of lethal heat penetration. Recall that from Table 3.15 the effect of convective heat transfer coefficient was seen to be marginal on the predicted maximum temperatures. This marginal effect in predicted maximum temperatures will transcend to the depth of lethal heat penetration. As can be seen from Table 3.18, there are marginal increases in the depth of lethal heat penetration with change in the convective heat transfer coefficient. An increase in the value of the convective heat transfer coefficient causes a decrease in the depth of lethal heat penetration, similar to the effect on maximum temperatures. A decrease in the value of the convective heat transfer coefficient causes an increase in the depth of lethal heat penetration. In the case of no convective cooling during heating, the depth of lethal heat penetration is 4.9 cm, representing a 20% increase.

Table 3.18: Effect of Convective Heat Transfer Coefficient on Depth of Lethal Heat Penetration

Change in Input Value (h)	Depth of Lethal Heat Penetration (DLHP)	
	Nominal Value of DLHP (cm)	Percentage Change
Nominal values	4.1	-
10% increase	4.1	0
20% increase	4.0	↓2
10% decrease	4.2	↑2
20% decrease	4.2	↑2

3.4.4 Effect of incident heat flux on depth of lethal heat penetration

Table 3.19 gives the effect of incident heat flux on the predicted depth of lethal heat penetration from the TDTP model. Similar to the effect of incident heat flux on the maximum temperatures, there is an increase in the depth of lethal heat penetration for an increase in the incident heat flux. There is 5% change in the depth of lethal heat penetration for a 10% change in the value of the incident heat flux.

Table 3.19: Effect of Incident Heat Flux on Predicted Depth of Lethal Heat Penetration

Change in Input Value	Depth of Lethal Heat Penetration (DLHP)	
	Nominal Value of DLHP (cm)	Percentage Change
Nominal values	4.1	-
10% increase	4.3	↑5%
20% increase	4.5	↑10%
10% decrease	3.9	↓5%
20% decrease	3.7	↓10%

3.5 Summary of sensitivity studies.

The following gives a summary of the sensitivity analyses made in this section:

- An increase in the thermal conductivity will decrease the predicted surface temperature but increase the predicted internal temperatures and depth of lethal heat penetration. For example, a 10% increase in the thermal conductivity decreased the surface temperature by 1% , the temperature at a depth of 3 cm increased by 5% and the depth of lethal heat penetration increased by 5%. A decrease in the thermal conductivity will increase the predicted surface temperature, decrease the predicted internal temperatures and depth of lethal heat penetration. For example, a 10% decrease in the thermal conductivity increased the surface temperature by 1%, the temperature at a depth of 3 cm decreased by 5% and the depth of lethal heat penetration decreased by 5%.
- An increase in the specific heat will cause a decrease in the predicted maximum temperatures and depth of lethal heat penetration. For example a 10% increase in specific heat decreased the surface temperature by 1%, the temperature at depth of 3 cm decreased by 6% and the depth of lethal heat penetration decreased by 5%. A decrease in specific heat will cause an increase in the predicted maximum temperatures and depth of lethal heat penetration. For example, a 10% decrease in specific heat caused a 1% increase in surface temperature, the temperature at depth of 3 cm increased by 7% and the depth of lethal heat penetration increased by 7%.
- An increase in density will decrease the predicted maximum temperatures and depth of lethal heat penetration. For example a 10% increase in density decreased the surface temperature by 1%, the temperature at a depth of 3 cm decreased by 7% and the depth of lethal heat penetration decreased by 5%. A decrease in the density will increase the predicted maximum temperatures and depth of lethal heat penetration. For example a 10% decrease in the specific heat caused the surface temperature to increase by 1%, the temperature at a depth of 3 cm increased by 7% and the depth of lethal heat penetration increased by 6%.

- Changes in the thermal properties (thermal conductivity, specific heat and density) give the same magnitude of change on the predicted maximum temperatures and depth of lethal heat penetration.
- An increase in the convective heat transfer coefficient will decrease the predicted maximum temperatures but not significantly as there was generally less than 1% change in temperatures for a 10% change in convective heat transfer coefficient value. The absence of convective cooling during heating will increase the maximum temperatures and depths of lethal heat penetration significantly. For example there was a 7% increase in surface temperature, 18% increase in temperature at a depth of 5 cm and a 20% increase in depth of lethal heat penetration for no convective cooling during heating.
- An increase in the incident heat flux will increase the predicted maximum temperatures and depth of lethal heat penetration. For example a 10% increase in the value of the incident heat flux caused a 5% increase in the surface temperature, a 5% increase in temperature at depth of 3 cm and a 5% increase in the depth of lethal heat penetration.

3.6 Summary of Chapter

Predictions from the models developed in Chapter Two have been presented in this Chapter. Determination of thermal properties used in the models has been presented. The effects of various parameters as well as the thermal properties on the results of the model have been presented for the case of exposure to a heat flux of 50 kW/m^2 and with an exposure time of 5 minutes. A summary of the effects has been presented. In the next Chapter, experiments that were performed to validate the predictions of the model made in this chapter will be given.

CHAPTER FOUR: EXPERIMENTAL RESULTS

In this chapter the experimental apparatus used in this study is briefly described. The experiments are mainly on heat transfer in sand and smoldering combustion. Methods of collecting and conditioning of soil and sand samples as well as procedures for conducting the experiments are described. Experiments conducted include the following.

- Heat transfer in dry homogenous sand exposed to various heat fluxes: temperature profiles and depths of lethal heat penetration were measured for comparison with predictions made using the numerical models detailed in Chapter Three.
- Heat transfer in moist homogenous sand: temperature profiles and depth of lethal heat penetration were measured and used to demonstrate the effects of moisture on temperature profiles and depth of lethal heat penetration.
- Heat transfer in dry two-layer soil: temperature profiles and depths of lethal heat penetration were measured for comparison with predictions made using the numerical models detailed in Chapter Three.
- Heat transfer in peat moss of various moisture contents: temperature profiles and maximum temperatures measured were used to demonstrate the effect of moisture on spread rate of smoldering combustion,
- Smoldering spread rate in peat moss with different inorganic contents: maximum temperatures were measured to determine effect of inorganics on maximum temperatures and spread rate of smoldering combustion in organic soil.
- The experimental values of time to reach ignition temperature in dry peat moss with various inorganic contents will be used to obtain a correlation to account for the effect of inorganic content on smoldering spread rate of peat moss. Results from this correlation will be compared to the results from a model developed by Frandsen [48].

- Heat transfer in forest floor soil and laboratory constructed soil: temperature profiles and depths of lethal heat penetration were measured for comparison to verify how closely the laboratory created soil from mixtures of sand and peat moss mimicked the temperature response of the forest soil.

The results obtained from each of these experiments are also discussed in this chapter.

4.1 Experimental apparatus

In this study, four major experimental apparatus were used:

- cone calorimeter,
- differential scanning calorimeter,
- Agilent data acquisition unit,
- sample holder.

Recall that the functions of the cone calorimeter have already been described in Chapter One. A brief description of the functions of the other three is given below.

4.1.1 Differential Scanning Calorimeter

The operation of a Differential Scanning Calorimeter (DSC) is based on a thermal technique that involves measurement of the thermal response of an unknown specimen as compared with a standard when the two are heated uniformly at a constant rate. The DSC is used to measure specific heat capacity (between 100 to 1200^{o}C) and heats of transition as well as to detect the temperature of phase changes and melting points in the range of 20 to 1500^{o}C. To determine specific heat capacity, a baseline is established by measuring the temperature difference of the two empty crucibles as the temperature is changed at a constant rate over the temperature range of interest. Thermal response records are then acquired for a standard material (usually sapphire) and an unknown material under identical conditions. The ratio of the departure of the standard and unknown from the baseline is then used to calculate the specific heat of the unknown.

4.1.2 Agilent data logger

Data loggers are used to monitor multiple signals (voltage, temperature, etc) over extended periods of time. The Agilent 34970A, manufactured by Hewlett-Packard, Palo Alto, California was used in this study to monitor and record temperature variation within the soil during experiments at a sampling rate of 1 second. Figure 4.1 is a picture of the Agilent data logger.

Figure 4.1: Agilent 34970A Data Logger

4.1.3 Sample holder

The original sample holder of the cone calorimeter consists of two separable parts, a base and a top part, both are made from steel. The base measures 10 cm by 10cm at the surface and is 2 cm deep. The top part, called the retainer frame, also measures 10 cm by 10 cm at the surface and is 5 cm deep with a covering edge of approximately 4 mm. The base is generally used alone in tests but for certain materials like wood for which the sides are capable of burning faster than the surface, the retainer frame is used in conjunction with the base to ensure uniform burn rate at the surface. The nature and dimensions of the retainer frame was not suitable for the objectives of this study considering that the 5 cm depth of the holder would not be sufficient for the purpose of semi-infinite assumption. Also being made of steel, a good conductor of heat, loss of heat from the sides would have made the assumption of one-dimensional heat transfer

inappropriate. Thus for this work, in order to be able to test soil specimens to depths of up to 17 cm and to reduce heat losses, a new specimen holder was constructed from a frame measuring 12.5 cm by 12.5 cm by 20 cm deep. Thermal Ceramics HS-45 Kaowool® insulating board (Inproheat Industries, Edmonton, AB) of thickness 1.25 cm, was used to line the frame to create a specimen holder of dimensions 10 cm by 10 cm by 20 cm deep. HS-45 Kaowool insulating board is designed for a maximum temperature rating of 1316°C with very high compressive and flexural strengths. Kaowool® HS-45 has a thermal conductivity of 0.15 W/m·K at 260^{o}C and density of 673 kg/m^{3} [76]. Six holes of about 5 mm diameter each were drilled through the Kaowool ® board to provide access for the thermocouples. The holes were drilled at depths of 1 cm, 3 cm, 5 cm, 7 cm, 10 cm and 15 cm from the surface.

The frame housing the kaowool boards was constructed from steel plate such that the dimensions were 12.5 cm x 12.5 cm with a height of 20 cm. The bottom of the frame had a small lip to hold the Kaowool ® boards in place at the bottom whilst the smaller width pieces wedged in between the bigger ones provided a natural support and balance for the whole sample holder. Cylindrical steel tubes of internal and external diameters of 3 mm and 5 mm respectively were cut to lengths of about 7 cm to help hold the thermocouples at one location in the soil at the three upper access holes in the Kaowool® board. Steel coils of 2 mm diameter were welded to the frame at 1cm, 3cm and 5cm from the tip of the holder such that the tops of these coils were flush with the bottom of the holes drilled in the Kaowool® board. These steel coils will provide additional stability for the steel tubes that will be inserted through the three upper holes, which will in turn ensure stability for the thermocouples, especially in cases where the weight of the soil sample at those depths will not be able to provide stability for the thermocouples. Figure 4.2 shows a picture of the sample holder with soil.

Figure 4.2: Sample Holder Constructed from Kaowool ® Insulating Board With Soil

4.1.4 Mass measuring device

Precise measurement of mass was very important in this work since the bulk density of the soil was going to have an impact on the rate of heat transfer. For this study a Mettler PM6100 digital scale with a precision of 0.01 g, manufactured by Fisher Scientific (Ottawa, ON) was used.

4.2 Collection and conditioning of soil samples

Four main types of samples were dealt with in this study: commercial fine sand, black earth top soil, peat moss, and forest floor soil. The following section details collection and conditioning of the various samples.

4.2.1. Forest soil sample collection

Forest soil samples from the forest were taken from the Nisbet Provincial Forest Number 1, located north of Duck Lake on Highway Number 11 in Saskatchewan. This forest is approximately 83,000 hectares in size and administered by both Federal and Provincial

governments. It is located within the Boreal Transition Region and is primarily a level, sandy glaciofluvial plain [77]. The samples were taken on 17 October 2005 and the spots sampled were within 22 – 24 km from Duck Lake. In all, five different spots were sampled with each spot having a different degree of vegetation. Generally the soil was sandy with Jack Pine and Black Spruce being the dominant vegetation. The diameter of the Jack Pine ranged from 66 cm to 78 cm and the Black Spruce averaged 70 cm in diameter. To cut the forest floor soil, a soil scoop measuring 15 cm x 15 cm with a depth of 15 cm with the cutting edge angled at about 26^{o} was constructed (Figure 4.3) An axe, a hammer and a shovel were also used to aid in soil collection. Soil samples were taken from the floor by first digging a hole big and deep enough to allow the soil scoop to be used to obtain the required depth of soil. A hammer was used to force the scoop to cut through the soil. Areas around the scooped soil were then dug to allow for easy removal of the cut soil without disturbing its compactness. The cut soil was then placed in a plastic bag to prevent loss of moisture and then into a plastic container for transport to the laboratory. Figure 4.4 shows a cut soil in the scoop.

Figure 4.3: Soil Scoop Used in Cutting Soil From Forest Floor of Nisbet Provincial Forest, Saskatchewan

Figure 4.4: The soil scoop containing freshly cut soil

4.2.2 Fine sand

The fine sand used in this study was obtained commercially from a garden centre in Saskatoon (Dutch Growers). As of the time of purchase the moisture content of the sand was approximately 14%. In order to have a more uniform and homogenous fine sand, it was decided to sieve samples through a choice of mesh size of 0.2 mm or 0.4 mm. The sand was thus first dried in an oven at a temperature of 104^{o}C for about 20 hours to get it dry enough in order to be able to pass it through the choice of sieves. Samples were passed through the two sieves and the two sieved sand samples were compared. The 0.2 mm sieved sand sample was found to be too fine, to the point of being dust-like. As this would have been difficult to work the 0.4 mm mesh size was chosen to be the required maximum size of sand grain to be used in this experiment.

4.2.3 Black soil

Black soil was obtained from the garden section of supermarket (Real Canadian Super Store, Saskatoon). The black soil was dried and the dried soil was sieved through a mesh size of 2 mm to obtain a homogenous sample.

4.2.4 Peat moss

The peat moss used in this study was obtained from the same garden centre as the fine sand. The peat moss type used was Premium, manufactured by Schultz Company, Mississauga, ON. The peat as obtained was highly non uniform for the purpose of this study with the presence of twigs of about 2.5 cm and lumps of organic matter. In order to obtain a uniform material the peat moss was also sieved through a mesh size of 2 mm. This produced a peat moss of a generally uniform and suitable size that could be easily mixed with the fine sand size chosen for this study. The moisture content of the peat at the time of purchase was approximately 160%.

4.2.5 Conditioning of samples

In order to be assured of uniform and accurate moisture content to be used in the test, all sieved peat moss, black soil, and fine sand samples were again dried in an oven at a temperature of 104^{o}C for a period of 24 hours to obtain a moisture free sample. Each batch of dried samples was sealed in a plastic container to prevent interaction with the atmosphere.

4.3 Experimental procedure

As mentioned in the introduction to this chapter, several experiments were conducted with the aim of validating the numerical model detailed in Chapter Three. The experiments conducted are described below.

4.3.1 Temperature measurement

In all the experiments, 24 gauge chromel-alumel (Type K) thermocouples were used for temperature measurements and data was processed using the Agilent 34097A data acquisition system together with a Pentium 4 desktop computer. For all soil temperature measurements, about 5 mm of thermocouple insulation was stripped at the edges of the thermocouples and the exposed parts were crossed to form an 'X', the junction of the 'X' were then spot welded such that the spot welded point was just about 1 - 2 mm from the tip of wire. The temperature data was taken at 1 second intervals.

4.3.2 Verification of one-dimensional heat transfer assumption

Recall that an assumption of one-dimensional heat transfer was made in formulating the numerical model in Chapter Two. This implies that we expect heat to travel only in the vertical direction. Thus, as part of this study experiments were conducted to verify if the assumption of one-dimensional heat transfer within the soil was valid. For this purpose, three 24-gauge chromel-alumel (type K) thermocouples were spot-welded at the centre, and at two opposite sides of the central one on a steel shim stock of thickness 1 mm and surface area 9.5 cm by 9.5 cm. The thermocouples would be referred to as 1, 2 and 3 as shown in Figure 4.5.

The sample holder was then filled up to a certain level in the sample holder with dry sand such that the when the shim stock was placed on the sand, the shim stock was at a depth of 1 cm from the top of the sample holder. The steel shim stock was placed in a horizontal position and a spirit level was used to ensure that the shim was horizontal. More sand was poured on the shim stock to fill up the holder and the cone calorimeter was then set to a heat flux of 50 kW/m^2. The sand with the shim stock was placed under the cone element and exposed to the set heat flux for a period of five minutes and then taken off and allowed to cool, temperature data was taken throughout the process. The experiment was performed two more times by varying the position of the shim stock to determine the effect of depth on the one dimensional assumption by conducting other tests at depths of 3 cm and 5 cm. For these two depths, the exposure time was increased

to 10 minutes so that there would be enough heat input to cause significant temperature rises. This will help in making a better analysis of the one-dimensional mode of heat transfer. The data was plotted for all three cases.

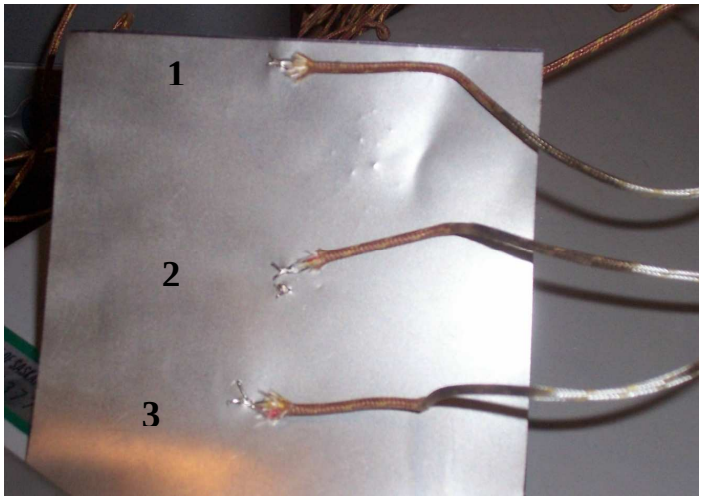

Figure 4.5: Thermocouples on Shim Stock for One-dimensional Heat Transfer Verification, Numbers Show Location of Each Thermocouple

4.3.3 Heat transfer in dry sand.

The bottom of the sample holder was sealed with wood samples and wool. Both the wood samples and wool had surface areas of 10 cm x 10 cm with a total thickness of 3 cm. The total sample holder depth available to fill with sand was 17 cm. The holder was then filled to the brim with previously sieved and dried sand and then the sand poured and weighed to determine the mass of sand required to fill the sample holder. This mass was consistently used in other experiments involving dry sand in order to ensure a consistent bulk density. The mass used for the experiment was 2650 g which for a volume of 1.7×10^{-3} m^3 yields a bulk density of 1588.8 kg/m^3. This is within the range of bulk densities reported for sand in literature.

Thermocouples were connected to the data logger and the controlling software set to take temperature readings at one second intervals. The thermocouples were inserted into the

drilled holes in the Kaowool® board such that they extended to about 5 cm into sand, approximately midpoint of the holder. The thermocouples were inserted at depths of 1, 3, 5, 10 cm and 15 cm. The tests were conducted at three different heat fluxes, 75, 50, and 25 kW/m^2 by setting the cone calorimeter's heating element to temperatures that would generate the required heat flux. The heat flux was verified using a Schmidt Boelter heat flux sensor. The heat flux sensor was placed at a distance of 25 mm from the lowest point of the cone heating element as required in ASTM E 1354-97 [78].

The sample holder containing the dry sand was then placed under the cone heating element with the shutters in closed position. The shutters were then opened at the same time as the Agilent software was set to take temperature readings. The sand was exposed to the set heat flux for a period of 5 minutes after which the shutters were closed and the sand taken away from under the shutters to a cooler place where the ambient temperature was more representative of that in the laboratory. A typical test required a total of 20,000 seconds, approximately $5^1/_2$ hours, for heating and then cooling to ambient temperatures. For each heat flux, two more replications were done. For each replication, a new batch of dry sand was used. Bulk density however, was maintained at an approximate value of 1558.8 kg/m^3. Figure 4.6 shows a picture of the sample holder placed under the cone calorimeter's heating element with the inserted thermocouples during an ongoing test.

Figure 4.6: An Ongoing Test with Sand Sample in Sample Holder Under the Cone Calorimeter's Heater

In order to determine the effect of time exposure on the maximum temperature and depth of lethal heat penetration, additional tests were conducted at 50 kW/m^2 for exposure times of 7 minutes and 10 minutes.

4.3.4 Two-layer soil

The sample holder was filled with dried fine sand such that the remaining space in the sample holder above the sand was 5 cm deep. The bulk density of the sand was approximately 1588 kg/m^3 with a depth of 12 cm. The remaining space above the fine sand was then filled with black earth top soil which had been oven-dried and sieved through a mesh size of 2 mm. The mass that filled the space yielded a bulk density of 622.2 kg/m^3. Thermocouples were then inserted at depths of 1, 3, 5, 7, 10 and 15 cm. Two sets of tests were conducted. In the first test, the two-layer sample was subjected to

a heat flux of 25 kW/m^2 for a period of 10 minutes and for the second test, the sample was subjected to a heat flux of 50 kW/m^2 for a period of 5 minutes.

4.3.5 Heat transfer in moist sand

Sand samples were conditioned to five different moisture contents: 5%, 10%, 15%, 18% and 20%. This was done by taking the mass of sand used in the dry sand experiments and determining the mass of water that would give the targeted moisture contents. The sand and water were then mixed thoroughly and kept in a plastic bag to allow for equilibration. Sample calculations of moisture content determination are given in Appendix D. A quantity of the moist sand with a mass equal to that of dry sand that would fill the sample holder was used to fill the sample holder. This was to ensure a consistent bulk density for both dry and moist sands. Filling was done whilst trying as much as possible to avoid uneven compaction of the moist sand. The moist sand was then exposed to a heat flux of 50 kW/m^2. The processes of exposure of the moist sand to heat flux, and temperature data collection were same as described for the dry sand experiments. In this case the time for cooling back to ambient temperatures was considerably shorter compared to the dry sand. In this experiment, it was assumed that the moisture content of the moist sand was uniform and constant throughout the depth of the mixture.

4.3.6 Smoldering Combustion

Tests were conducted to determine the effect of moisture on the rate of smoldering combustion, the inherent inorganic content of peat moss and the effect of inorganic content on the spread rate in peat moss.

4.3.7 Heat transfer in moist peat

Dried peat of 2 mm mesh size was conditioned to moisture contents of 30, 100, 110 and 120% using methods as described for the moist sand. The mass of dry peat required to fill the sample holder was first determined and formed the basis for determining the mass of water for conditioning to the various moisture contents. The weight of dry peat required to fill up the sample holder was 250 g. Details of computation of the mass of

water needed for conditioning the peat moss to required moisture contents are shown in Appendix D. A consistent bulk density was ensured in all tests and in all cases exposure of the sample was to a heat flux of 50 kW/m^2 for a duration of 2 minutes which was deemed sufficient to initiate sustained combustion. Initial flaming of moist peat was observed at low moisture contents. At high moisture contents, there was no flaming.

4.3.8 Inherent inorganic content of peat moss.

In order to be able to determine accurately the total inorganic content of peat moss undergoing combustion in this study, the inherent inorganic content of the peat moss had to be determined. The inherent inorganic content is the ash content of the organic material. A sample of peat moss weighing approximately 52 g was subjected to a heat flux of 50 kW/m^2 until ignition occurred. With the heat flux source removed, the sample was allowed to burn until only ash remained. This took approximately 1 hour. The ash remaining was weighed and the inorganic content was determined as the ratio of the mass of ash to the original mass of the peat sample. This procedure was repeated two more times and the average taken. This method of determining inherent inorganic content was also used by Hartford [56]. Additionally, the differential scanning calorimeter was used to determine an approximate temperature for phase change in dry peat moss. This will help in estimating the temperature at which ignition and hence smoldering combustion starts in the peat moss used in the study.

4.3.9 Effect of inorganic content on smoldering

The mass of peat moss of inherent inorganic content required to fill the sample holder, 250 g, was used as the basis for determining the total inorganic content of the peat-sand mixture. Peat without any sand (inherent inorganic content) was first tested. A measured weight of peat moss, approximately 250 g, that filled up the sample holder was subjected to a heat flux of 50 kW/m^2 with thermocouples inserted at depths of 1 cm, 3 cm, 5 cm, 10 cm and 15 cm. The sample was exposed for a period of between 1 to 2 minutes by which time smoldering combustion had developed to a stage that could be sustained. The burning sample was then taken away from the cone calorimeter to an area where

ambient temperature was what prevailed in the laboratory. The sample was allowed to burn until the last thermocouple (depth of 15 cm) had registered a temperature above ignition and then cooled back to ambient temperature. Two more repetitions were done with each test taking an average of 10 hours. Fine sand of predetermined weights was then added to measured weights of peat moss to obtain a targeted total inorganic content by weight. This mixture of peat moss and sand was exposed to heat flux of 50 kW/m^2 in the same manner as that described previously for a period of 2 minutes by which time combustion had developed to a degree that could be sustained. Combustion tests in this study were done to simulate downward smoldering combustion as against lateral spread.

4.3.10 Forest soil samples

The forest samples which had been kept in plastic bags were tested one at a time in the condition in which they were. The bulk density of the mineral soil was first determined by taking out a compact piece of the mineral soil and then determining the mass of that piece. The volume of that piece was determined by measuring the volume of water that the piece displaced as it was wrapped tightly in a plastic material, without breaking its compactness, and then dipped into a graduated beaker of water. The bulk density was then obtained by taken the measured mass per unit volume. The moisture content was also determined by weighing about 20 g of the soil sample and then drying in an oven at a temperature of 104^oC for a period of 24 hours. The moisture content was determined as the ratio of the difference in mass between the moist and dry soils to the mass of the dry soil.

The interface of the organic and mineral layers was determined visually and the thickness of the organic layer was measured using a meter rule. The inorganic content of the organic layer was determined by the same method as used to determine that of the inherent inorganic content for peat moss described in section 4.3.8. The bulk density of the organic layer was also determined in the same way as the mineral soil. The forest sample was then meticulously trimmed to a size that would fit into the sample holder, typically about 9.5 cm by 9.5 cm. In the case where the mineral soil portion had

disintegrated and separated from the organic layer, the disintegrated mineral soil was constructed to the determined bulk density and the organic layer was placed on the reconstructed mineral soil. This procedure has a possibility of introducing slight errors in the conduction of heat at the organic layer mineral layer interface as compared to one for which the organic and mineral layers were still intact. In certain cases, the organic layer had to be reduced to either 5 cm or 7 cm so that the interface temperature could be measured. Figure 4.7 shows a prepared forest floor material ready to be placed in the sample holder for testing. The physical properties as measured are given in Table 4.1.

Figure 4.7: Forest Floor Soil Sample Prepared to be Placed in Sample Holder.

The top or organic layer for the various samples had inorganic contents ranging from 57.5% to 86.7%. According to Frandsen [46], an inorganic content of 82%, marks the beginning of the transition from organic to mineral soil. Of all the samples tested, only sample one had an inorganic content greater than the 82% transition level. All the other samples had inorganic contents that placed them under organic soil.

In order to be able to determine temperatures at the interface of organic and mineral soil layers, another hole was created in the sample holder at a depth of 7 cm to accommodate one more thermocouple. The first set of samples was exposed to a heat flux of 50 kW/m^2

for five minutes. Due to the high inorganic and moisture contents, the rises in temperatures were not very significant. Since the objective was to compare responses of the forest soils with laboratory constructed soils to heat input, the subsequent samples were tested at a higher heat flux of 80 kW/m^2, with various exposure times between 5 and 10 minutes. In all, five forest floor samples with varying degrees of physical and thermal properties and layers of organic material tested.

Table 4.1: Physical Properties of Forest Floor Soil Samples

Sample #	Vegetation	Organic (Top) Layer	Mineral Soil
1	Jack Pine	Bulk density – 1024 kg/m^3 Moisture content – 32.9% Inorganic content – 86.7% Thickness – 5 cm	Bulk Density – 1545 kg/m^3 Moisture content – 5.3%
2	Jack Pine	Bulk density – 681 kg/m^3 Moisture content – 65.7% Inorganic content – 72.7% Thickness – 5 cm	Bulk Density – 1550 kg/m^3 Moisture content – 12%
3	Jack Pine	Bulk density – 632 kg/m^3 Moisture content – 74.4 Inorganic content – 78.8 % Thickness – 7 cm	Bulk Density – 1330 kg/m^3 Moisture content – 10.4%
4	Jack Pine and Black Spruce	Bulk density – 793 kg/m^3 Moisture content – 76.9% Inorganic content – 78.1% Thickness – 5 cm	Bulk Density – 1501 kg/m^3 Moisture content – 8.8%
5	Black Spruce	Bulk density- 655.5 kg/m^3 Moisture content – 81.5% Inorganic content – 57.5% Thickness – 5 cm	Bulk Density – 1504 kg/m^3 Moisture content – 8.5%

4.3.11 Laboratory constructed soils

Based on data obtained from the physical and thermal properties of the forest soil samples, soils of equivalent physical properties were constructed in the laboratory from fine sand and mixtures of fine sand and peat moss. Each soil constructed was based on the physical properties measured from a forest soil sample. The following methods were used in the construction of the laboratory soil.

- For each forest soil, a mass of fine sand was conditioned to a moisture content equivalent to that of the mineral soil of the forest soil.
- The moist fine sand was then packed into the sample holder to a depth that will give a bulk density equivalent to that of the mineral soil of the forest soil, and such that the space above the packed moist sand was equivalent to the thickness of the organic layer of the forest soil.
- Based on the inorganic content determined for organic layer of the particular forest soil sample, peat moss was mixed with fine sand to obtain an equivalent inorganic content.
- The mixture of sand and peat moss was then mixed with a measured mass of water in order to obtain a moisture content equivalent to that of the organic layer of the forest soil.
- A mass of the moist mixture of peat moss and sand which when packed within the remaining space in the sample holder will give the same bulk density as that of the organic layer of the forest floor sample, was then packed on top of the moist fine sand.

Thermocouples were then inserted at depths of 1 cm, 3 cm, 5 cm, 7 cm, 10 cm and 15 cm. The constructed soil samples were then subjected to heat fluxes and durations corresponding to what were used for its corresponding forest soil.

4.4 Experimental results

The results of all the experiments conducted will now be presented in the same order in which the experiments were conducted. Recall that a step-input type of heat flux boundary condition was chosen for this study in the development of the model and for the simplicity of the experiments. For majority of tests, a surface heat flux of 50 kW/m^2 was used with an exposure time of 5 minutes. Other tests were also conducted at 25 and 75 kW/m^2 and with other exposure times. Recall that it was mentioned in Chapter Three that these values of heat flux and times of exposure were based on the literature. The values can also be representative of low to medium-severity fires.

4.4.1 One-dimensional heat transfer verification

The results from the data obtained from the one-dimensional heat transfer verification experiments were analysed based on the maximum differences between the temperatures recorded for the three points, 1, 2 and 3 in Figure 4.6. The shim stock used in the test had a thickness of 0.7 mm, is not expected to affect the transfer of heat within the sand due to the fact that it is a thermally thin material. The averages of the measured temperatures for these three positions are as shown in Figures 4.8 to 4.10. The maximum difference always occurred between thermocouples 2 and 3. For the 1 cm test, the maximum deviation between numbers 2 and 3 thermocouples occurred at the maximum temperatures and the difference was 7.5% of the central thermocouple reading. For the 3 cm test, the maximum deviation between the 2 and 3 thermocouples was 3.4^oC and occurred during heating up and before the maximum temperatures were reached. This represents a deviation of 8.8% of the temperature difference reached by the central thermocouple at that time. At a depth of 5 cm, the maximum difference recorded between the 2 and 3 thermocouples was 1.4^oC. This represents 3.8% of the temperature rise of the central thermocouple. The maximum temperature gradient in the horizontal direction at depths of 1 and 3 cm was 48 and 41$^oC/m$ respectively. The vertical temperature gradient from depth of 1 cm to 3 cm was 4300$^oC/m$. The horizontal temperature gradient at depth of 5 cm was 92.5$^oC/m$ whilst the vertical temperature gradient from depths of 3 to 5 cm was 1935$^oC/m$.

From the data from the three different depths, it can be seen that the variation in temperatures between numbers 2 and 3 thermocouples reduces with increasing depth of location of thermocouples. The percentage difference in maximum temperatures was less than 8% in the three tested cases across a horizontal plane. Moreover, the horizontal temperature gradients at the three depths were far less than the vertical temperature gradients hence the assumption of one-dimensional heat conduction in the soil sample for this experiment is appropriate.

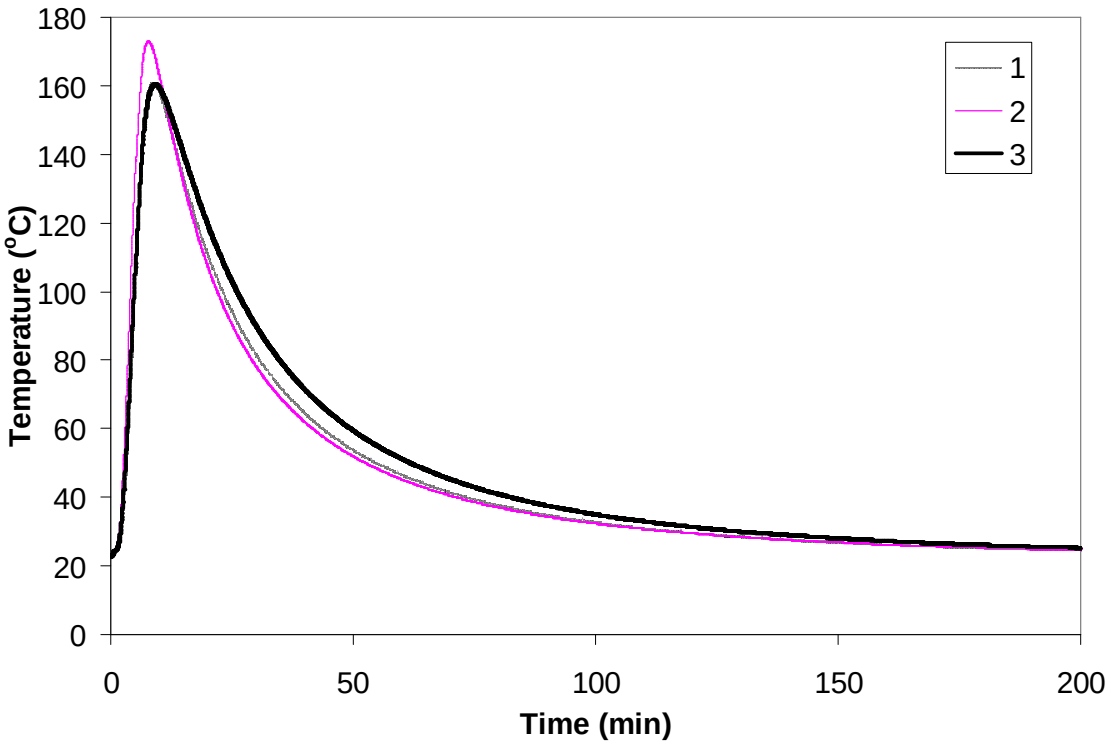

Figure 4.8: Temperature Profiles for Three Different Horizontal Positions at a Depth of 1 cm into Dry Sand

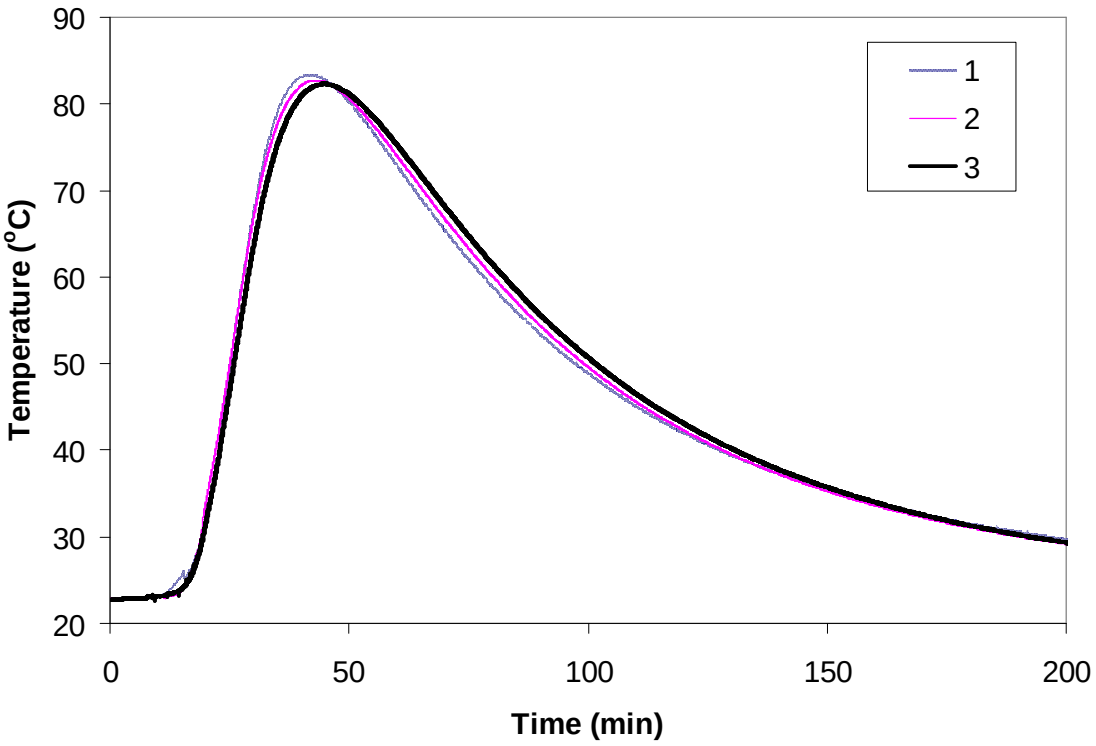

Figure 4.9: Temperature Profile for Three Different Horizontal Positions at a Depth of 3 cm into Dry Sand

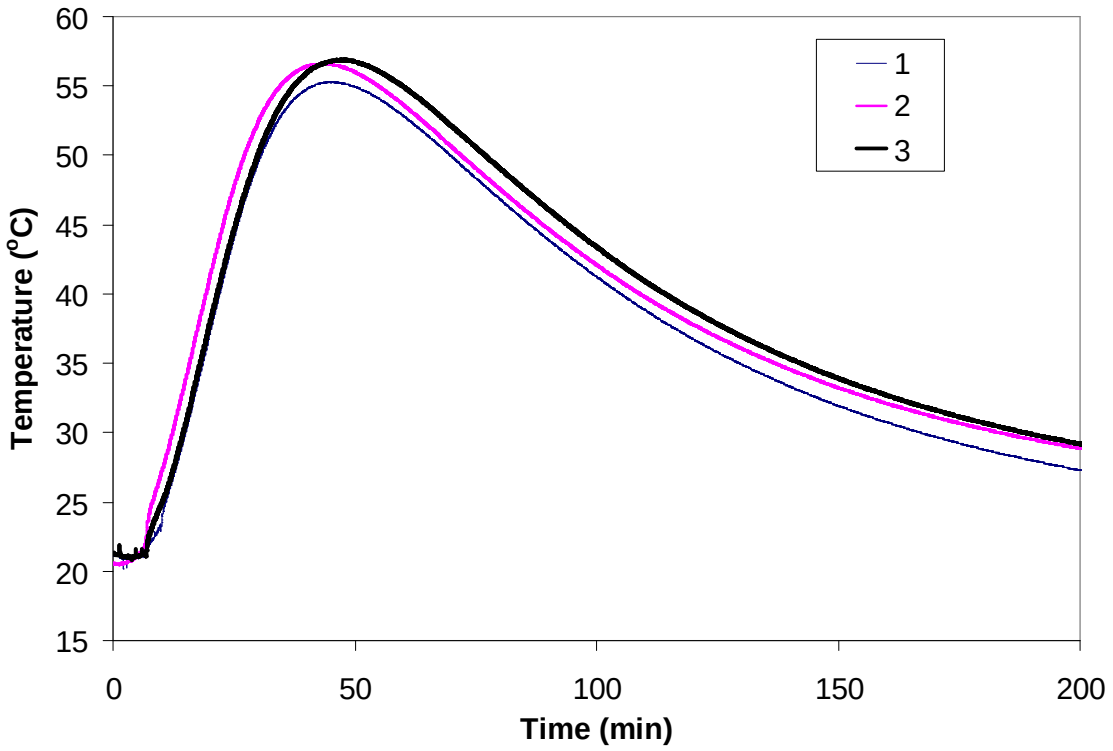

Figure 4.10: Temperature Profile for Three Different Horizontal Positions at a Depth of 5 cm into Sand

4.4.2 Dry sand

Results of the experiments on fine sand are shown in Figures 4.11 to 4.14. Figure 4.11 shows the temperatures recorded at four different depths for an incident heat flux of 50 kW/m^2. It can be seen that the temperature profiles for the four different depths and hence the maximum temperatures reduce with increasing depth. Considering the profile for 1 cm depth, there is a steady increase in temperature over the heating period until the maximum of 273^{o}C is achieved. Cooling at 1 cm depth commenced approximately 60 s after the source of heat had been taken off.

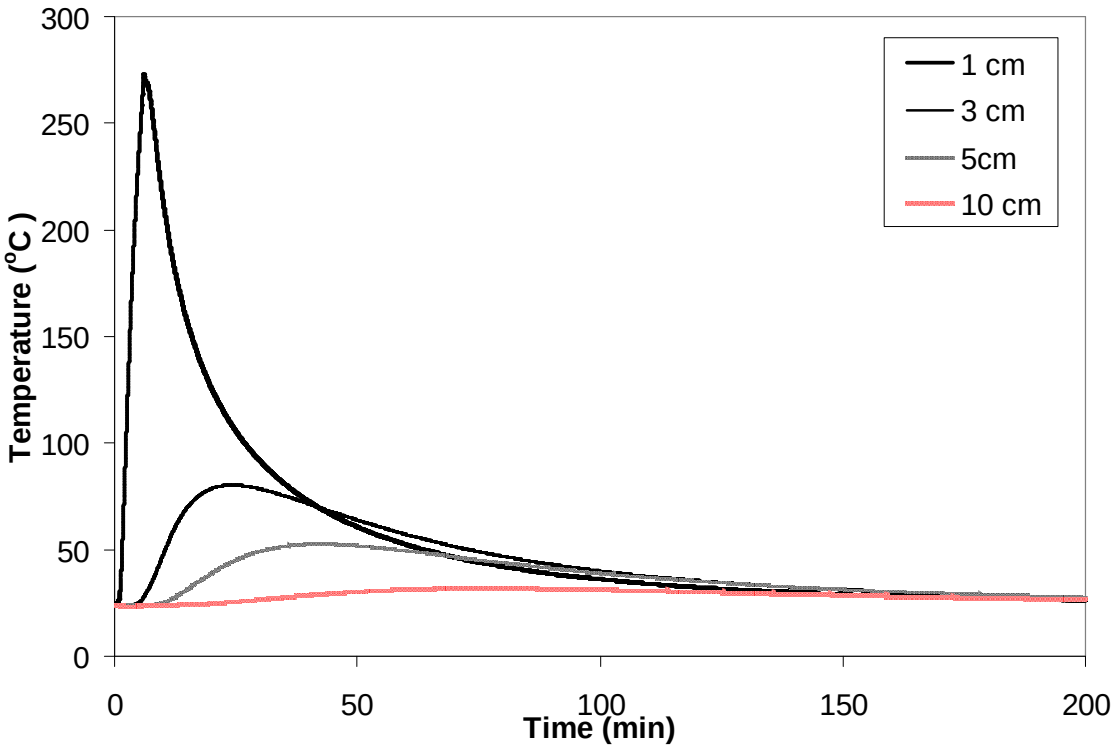

Figure 4.11: Measured Temperature Profile in Dry Sand During and After 5 Minutes Exposure to Heat Flux of 50 kW/m^2

Recall that in Chapter Three, the depth of lethal heat penetration was obtained by curve fitting the temperature data points for each depth using the curve fitting features of Microsoft® Excel. A horizontal line is then traced from 60^{o}C to meet the curve and then traced vertically to the depth axis. Figure 4.12 is a graph of maximum temperature versus depth for 50 kW/m^2. The depth of lethal heat penetration is estimated as 4.2 cm for 50 kW/m^2 heat flux for exposure time of 5 minutes.

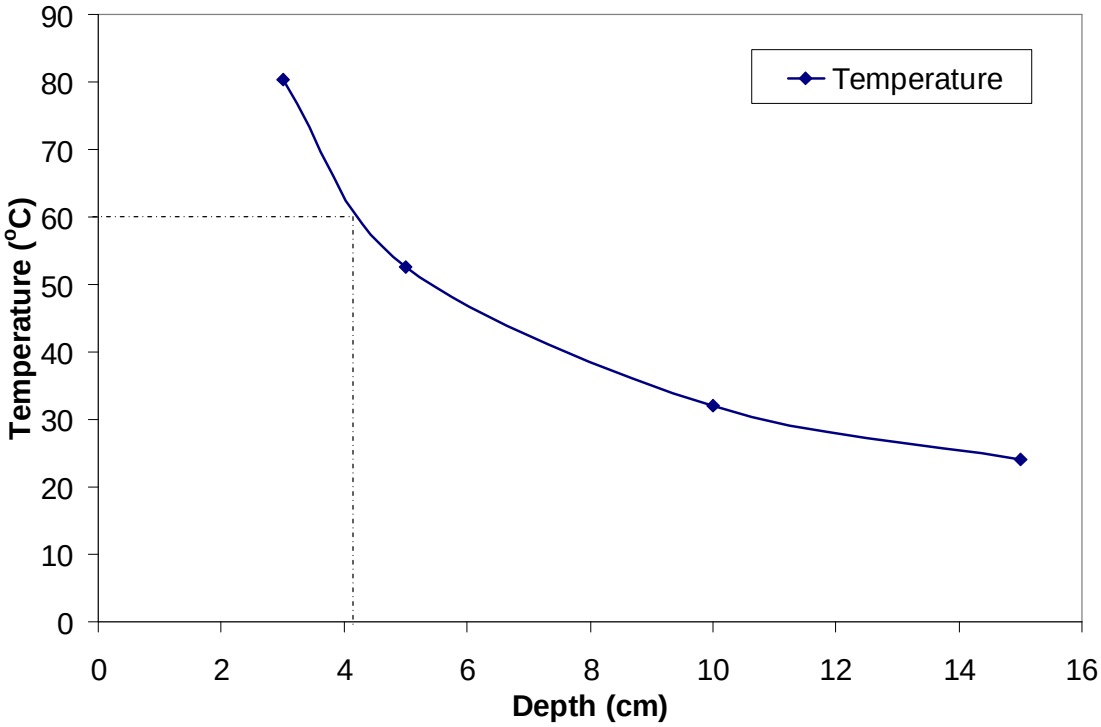

Figure 4.12: Example of Determining Depth of Lethal Heat Penetration for Exposure to 50 kW/m^2 for 5 Minutes.

Figure 4.13 shows the temperature profiles for various depths for an exposure of 25 kW/m^2. The trend of temperature profiles and maximum temperatures are similar to that of the 50 kW/m^2. Table 4.2 gives the maximum temperatures at various depths for exposure to heat fluxes of 25 and 50 and 75 kW/m^2. As can be seen from the data in the Table, with increasing heat flux, there is an increase in the maximum temperature measured at every depth. Table 4.3 gives the values of the depth of lethal heat penetration for the various heat fluxes. As can be seen from the figures in the Table, there is an increase in the depth of lethal heat penetration with increase in heat flux. This is consistent with basic heat transfer theory and with the literature (e.g., [2, 5, 22]).

Table 4.4 gives the maximum temperatures at various depths for exposure to heat flux of 50 kW/m^2 for three different times of exposure. As can be seen from the Table, with an

increase in exposure time, there is an increase in the maximum temperatures measured. Table 4.5 gives the corresponding depths of lethal heat penetration for different exposure times and as can be seen, the depth of lethal heat penetration increases with increase in time of exposure. These results are also consistent with basic heat transfer theory. Data from Richon [5] also showed a trend of increase in depths of lethal heat penetration with increase in measured heat flux at surface of sand.

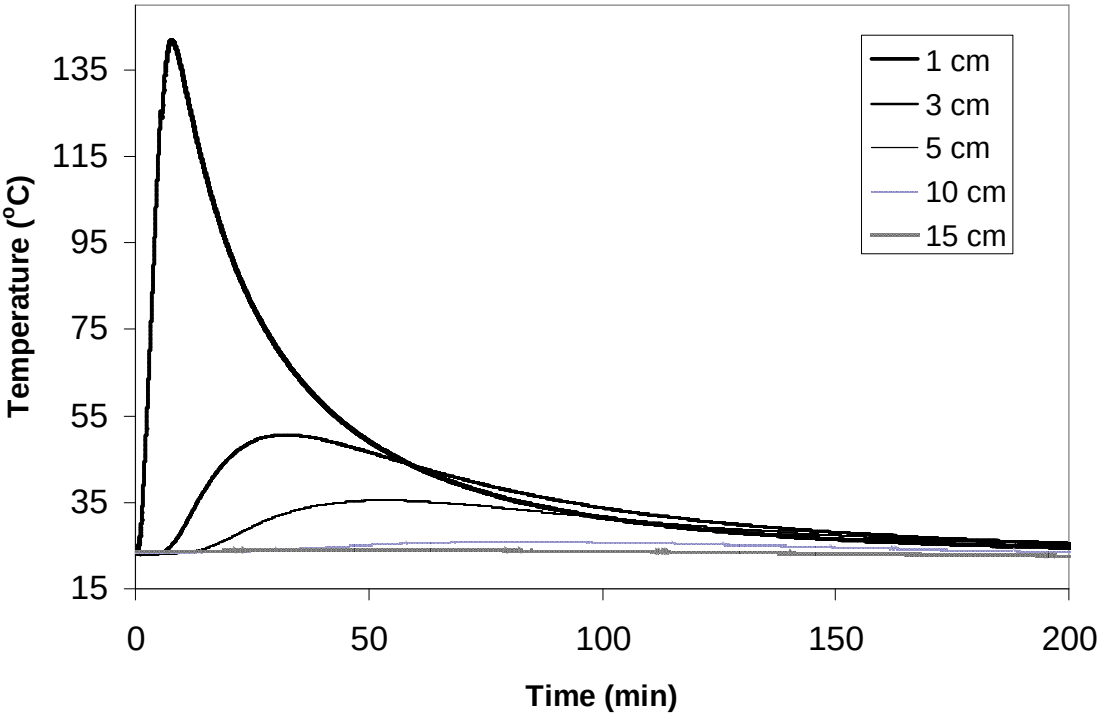

Figure 4.13: Temperature Profiles at Various Depths in Dry Sand During and After 5 Minutes Exposure to Heat Flux of 25 kW/m^2

Table 4.2: Measured Maximum Temperatures at Various Depths in Dry Sand for Different Heat Flux Values for 5 Minutes Exposure

Depth (cm)	Temperatures (^{o}C)		
	70 kW/m^2	50 kW/m^2	25 kW/m^2
1	471.1	273.0	141.8
3	136.0	80.3	50.6
5	76.5	52.6	35.5
10	32.5	32.1	25.9
15	28.4	24.6	24.1

Table 4.3: Depths of Lethal Heat Penetration in Dry Sand at Three Different Heat Fluxes

Heat Flux (kW/m^2)	Depth of Lethal Heat Penetration (cm)
25	2.8
50	4.2
75	6.2

Table 4.4: Maximum Temperatures Measured at Various Depths in Dry Sand for Different Times of Exposure to Heat Flux of 50 kW/m^2

Depth (cm)	Temperatures (^{o}C)		
	5 Minutes	7 Minutes	10 Minutes
1	273.0	411.7	447.7
3	80.3	106.0	127.0
5	52.6	54.7	64.9
10	32.1	32.1	33.6
15	24.6	28.2	28.3

Table 4.5: Depths of Lethal Heat Penetration in Dry Sand at Heat Flux of 50 kW/m^2 for Different Exposure Times

Time of Exposure (min)	Depth of Lethal Heat Penetration (cm)
5	4.2
7	4.7
10	5.3

4.4.3 Two-layer soil

Figure 4.14 gives the temperature profiles measured at depths of 1 cm, 5 cm and 10 cm in the dry two-layer soil exposed to a heat flux of 25 kW/m^2 for 10 minutes. It should be

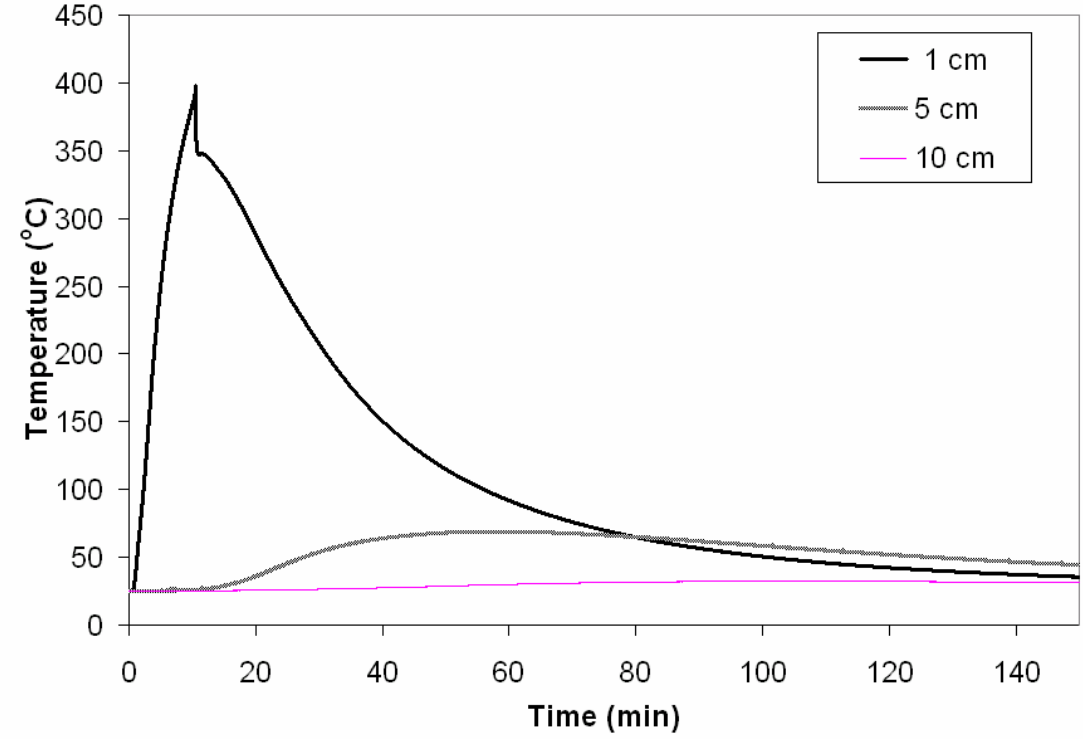

Figure 4.14: Temperature Profiles Measured at Depths of 1 cm, 5 cm and 10cm in a Dry Two-layer Soil During and After 10 Minutes Exposure to Heat Flux of 25 kW/m^2

noted here that smoldering combustion was observed to be taking place in the top soil as smoke could be seen coming out of the soil sample during the experiments. Further investigation carried out after the test by gently scooping off top portions of the top soil showed that charring had taken place in the top soil to a depth of about 1.5 cm. There was a reduction in cooling rate depicted by the change in the temperature profile during cooling at 350^{o}C. This is an indication that after the heat source had been removed there was internal heat generation due to the smoldering combustion and the 350^{o}C temperature was the temperature persisting within the smoldering soil. This explains why the temperature at a depth of 1 cm persisted over 200^{o}C for close to 20 minutes as depicted in Figure 4.14.

Figure 4.15 gives the temperature profiles at depths of 1, 5 and 10 cm for exposure to a heat flux of 50 kW/m^2 for a period of 5 minutes. Similar to the case of exposure to a heat flux of 25 kW/m^2 for 10 minutes, smoldering combustion occurred in the top soil resulting in high temperature persisting over 20 minutes at a depth of 1 cm. A reduction in the rate of cooling at 1 cm depth is observed to commence around 420^{o}C. Table 4.6 gives the maximum temperatures at depths of 1, 3, 5 and 10 cm. From the Table, the 25 kW/m^2 heat flux exposure produced a smaller temperature at a depth of 1 cm than the exposure to a heat flux of 50 kW/m^2. However higher temperatures were observed at the other internal depths due to the longer period of exposure of the heat flux of 25 kW/m^2. Consequently the 25 kW/m^2 exposure produced a greater depth of lethal heat penetration than the 50 kW/m^2 exposure due to the longer period of exposure to the heat flux of 25 kW/m^2.

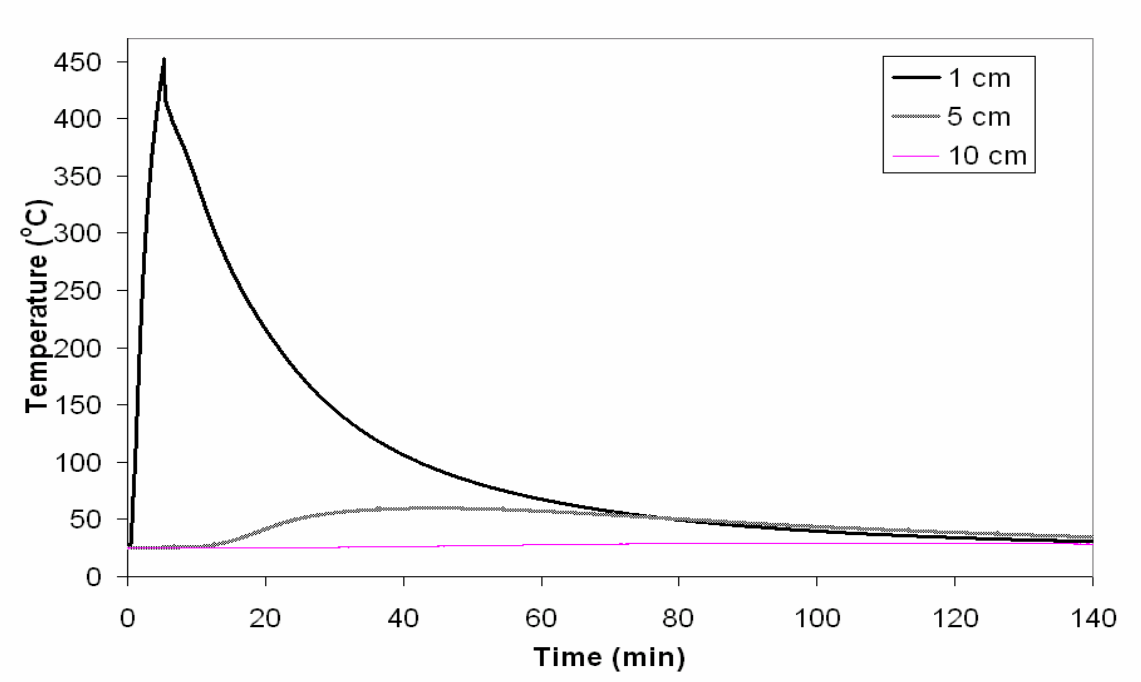

Figure 4.15: Temperature Profiles Measured at Depths of 1 cm, 5 cm and 10cm in a Dry Two-layer Soil for Exposure to Heat Flux of 50 kW/m^2 for 5 Minutes

Table 4.6: Maximum Temperatures Measured at Various Depths in Dry Two-layer Soil Exposed to Heat Flux of 25 kW/m^2 for 10 Minutes and 50 kW/m^2 for 5 Minutes

Heat Flux	Maximum Temperatures (°C)				
	1 cm	3cm	5 cm	10 cm	Depth of Lethal Heat Penetration (cm)
25 kW/m^2	397.8	114.5	69.0	32.4	5.8
50 kW/m^2	452.8	103.6	59.8	29.4	5.0

4.4.4 Moist sand

Figure 4.16 shows the temperature profiles measured at five depths for sand with a moisture content of 5% exposed to heat flux of 50 kW/m^2 for a period of 5 minutes. Similar to dry sand, there is a reduction in temperature with increasing depth as

expected. For the 1 cm depth temperature profile, there is a gradual deviation of the trend of temperature increase to a semi-pseudo state around 70^{o}C possibly due to commencement of emission of steam within the sand. The maximum temperatures are considerably smaller than that for the dry sand. For example, at a depth of 1 cm, the maximum temperature measured in the dry sand is reduced by 173% in the moist sand. This clearly depicts the effect of moisture reducing the rate of heat transfer in sand as discussed in Chapter One.

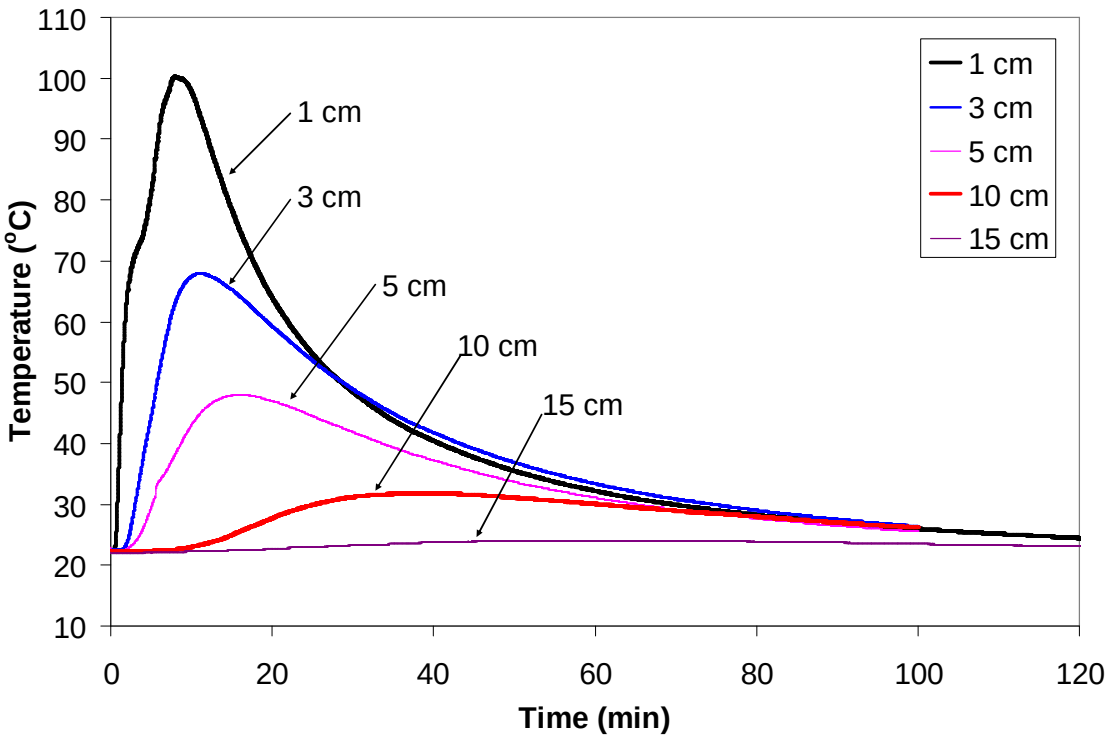

Figure 4.16: Temperature Profiles at Various Depths in Sand With 5% Moisture Content During and After 5 Minutes Exposure to Heat Flux of 50 kW/m^2

Figure 4.17 gives the temperature profiles measured at a depth of 1 cm for sand of various moisture contents. The profiles indicate that there is a decrease in the maximum temperatures with increasing moisture content. This is also consistent with findings on the effects of moisture as catalogued by various authors (e.g., [5, 22, 30, 32, 45]). The

maximum temperature measured at 1 cm depth was 100^{o}C. This is consistent with Scotter [23] finding that the temperature at a point in a moist soil does not rise above 100^{o}C until all the water at that point had been boiled off. The maximum temperatures measured at each of the depths and the depths of lethal heat of penetration for all the moist sands as well as the dry sand exposed to a heat flux of 50 kW/m^2 for 5 minutes are presented in Table 4.7. As can be seen from the values obtained, the depth of lethal heat penetration decreases with increasing moisture content. Again this is consistent with what has been found in the literature [5, 22, 30, 32, 45].

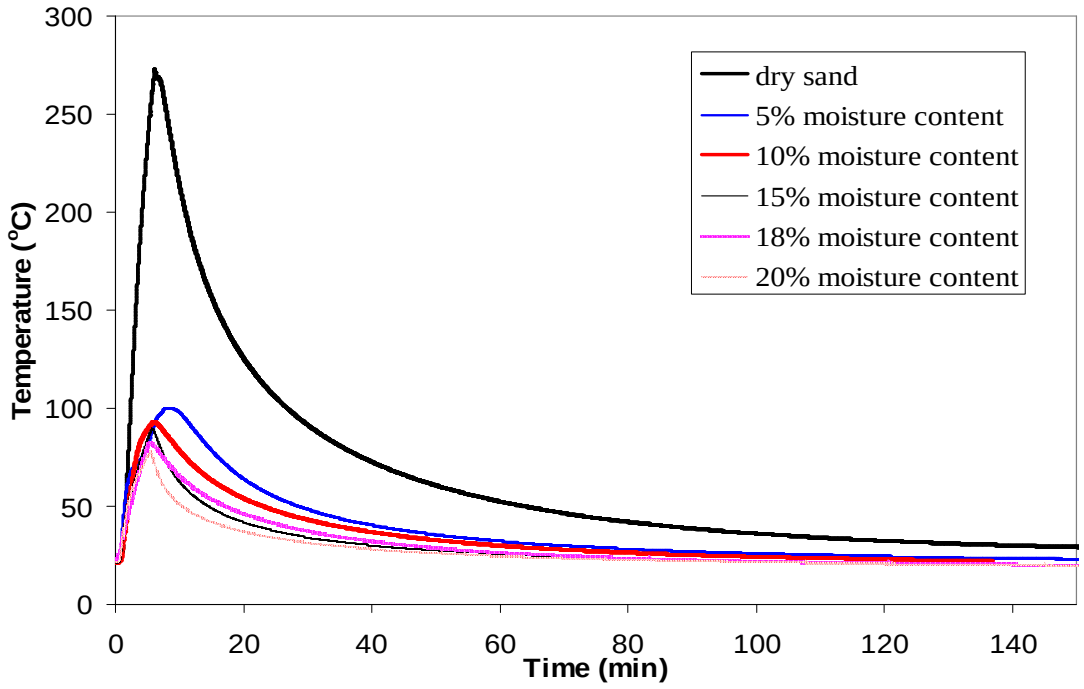

Figure 4.17: Temperature profiles for Various Moisture Contents in Dry Sand at Depth of 1 cm for 5 Minutes Exposure to Heat Flux of 50 kW/m^2

Table 4.7: Maximum Temperatures at all Measured Depths and Depths of Lethal Heat Penetration in Sand of Various Moisture Contents Exposed to Heat Flux of 50 kW/m^2 for 5 Minutes.

Moisture Content	Maximum Temperatures (^{o}C)					Depth of Lethal Heat Penetration (cm)
	1 cm	3 cm	5 cm	10 cm	15 cm	
0%	273	80.3	52.6	32.1	24.6	4.2
5%	100	67.9	48	31.8	24.0	3.7
10%	93.2	63.2	46.5	29.4	24.9	3.3
15%	89.7	47.3	35.6	26.1	24.2	2.4
18%	82.6	41.3	26.7	25.6	23.9	2.1
20%	78.4	39.0	25.1	24.7	23.8	1.9

4.4.5 Inherent organic content

The inherent inorganic content of the peat moss by weight as determined over three tests was 7.5%. The value of 7.5% obtained for this study falls within the range of values found by Hartford [56]. Hartford obtained an inorganic content averaging 4% for Green Thum brand peat and 8% for Sunshine brand peat. The preliminary tests with the DSC to determine the temperature of phase change in the peat moss showed that phase change occurred around 175^{o}C. Hence 175^{o}C is an approximate temperature at which combustion of the peat moss commences.

4.4.6 Effect of moisture on smoldering combustion of peat moss

Recall that peat moss with moisture contents of 0, 30, 100, 110 and 120% were subjected to a heat flux of 50kW/m^2 and allowed to undergo sustained combustion. With the inclusion of moisture, burns were sustained for all moisture contents except 120%. This is consistent with Frandsen [46] finding that for low inorganic contents, there would be no sustained burning for moisture contents of about 120%. Generally, the maximum temperatures achieved decreased with increasing moisture content. This is also consistent with Frandsen and Ryan [33] in which they found moist duff covering reduced temperatures in the mineral soil below. This is due to the high specific heat of

water absorbing some of the thermal energy as the water is boiled off before the organic material is brought to ignition temperature. Table 4.8 gives the values of the maximum temperatures obtained for the various moisture contents at the various depths as the peat moss underwent sustained smoldering combustion.

Table 4.8: Maximum Temperatures (^{o}C) Measured at Various Depths in Peat Moss of 6 Different Moisture Contents Exposed to Heat Flux of 50 kW/m^2 for 2 Minutes and Allowed to Undergo Sustained Smoldering Combustion.

Depth (cm)	Moisture Content				
	0%	30%	100%	110%	120%
1	493	481	475	394	406
3	589	485	454	440	65.8
5	582	560	523	505	46.2
10	619	512	521	508	24.4
15	599	521	567	556	24.3

4.4.7. Effect of Inorganic content on smoldering

The effects of inorganics on smoldering were analysed in the following ways:

- effect of inorganic content on average maximum temperatures for each inorganic content
- effect of inorganic content on duration of smoldering combustion
- effect of inorganic content on time to reach ignition temperature.

A consistent trend was observed in the variation of the average maximum temperatures for the inorganic contents tested. The average maximum temperature is the average of all the temperatures obtained for the various depths for a particular inorganic content. This gives a measure of the total heat that will be given off by the peat moss. Table 4.9 gives the values of the maximum average temperatures for the inorganic contents tested. As can be seen from the trend shown in the table, the maximum average temperatures decrease with increasing inorganic content. This may be due to the fact that peat moss,

after igniting, gives of heat as against sand which does not give off heat when the ignition temperature of peat moss is achieved. Thus with a reduction in the amount of peat moss through an increase in inorganic content (sand), the total heat that can be evolved by the mixture is reduced. This results in a reduced maximum average temperature. There is however, no sustained combustion at 82% inorganic content which agrees with the work of Frandsen [46].

Table 4.9: Average Maximum Temperatures Measured for Various Inorganic Contents Exposed to Heat Flux of 50 kW/m^2 for 2 Minutes and Allowed to Undergo Sustained Smoldering Combustion.

Inorganic Content (%)	Maximum Average Temperatures (^oC)
7.5	576
30	562
44	547
60	464
80	288

Recall that in Chapter One it was mentioned that Selving [22] used TGA to obtain the ignition temperature of peat moss used in his study as 169^{o}C. In this study, 175^{o}C was the value obtained for commencement of phase change using the Differential Scanning Calorimeter which compares closely with that of Selving [22]. The temperature of 175^{o}C will be used as the temperature at which smoldering combustion starts hence whenever the temperature of the peat mixture is above 175^{o}C, it will be assumed that smoldering combustion is taking place. Table 4.10 shows the trend of time above ignition temperature, which represents sustained smoldering combustion, for the various inorganic contents tested. From Table 4.10, apart from the inherent inorganic content (7.5%) which showed a high duration of burn above 170^{o}C at depths of 1 cm and 3 cm, there was a general trend of increasing duration of smoldering burn with increasing inorganic content.

Table 4.10: Effect of Inorganic on Time for Sustained Smoldering Combustion (Periods During Which Burn Temperatures Stood Above 170^{o}C)

Depth (cm)	Duration (min) of Temperature Above 170^{o}C at all Depths				
	7.5%	30%	44%	60%	80%
1	55.8	51.0	52.7	53.4	68.3
3	93.6	78.0	98.6	103.3	176.3
5	134.7	147.3	148.1	172.0	186.2
10	87.5	323.4	326.0	456.3	465.2
15	431.8	530.2	546.1	588.0	No Combustion

Table 4.11 gives the times required for samples at the various inorganic contents to achieve the ignition temperature of 175^{o}C. It is assumed here that once a temperature of 175^{o}C and above is achieved, sustained smoldering combustion is taking place.

Table 4.11: Time to Reach Ignition Temperatures for Percentages of Inorganics in Peat Moss Tested at 50 kW/m^{2}

Depth (cm)	Time (min) of Peat and Sand Mixture to Reach Ignition Temperature at All Depths				
	7.5%	30%	44%	60%	80%
1	3.4	1.8	1.5	2.3	2.7
3	17.5	15.6	16.9	19.1	29.4
5	42.2	55.3	42.1	48.8	79.0
10	87.5	96.8	123.4	146.9	289.8
15	149.8	170.7	204.0	275.2	495.4

There is a reduction in time to reach the ignition temperature from the inherent inorganic contents to 44% inorganic content and then a reversal in the trend is seen from 60% upwards. Sand has a lower heat capacity than peat moss and a higher thermal conductivity than peat moss, in effect, sand has a higher thermal diffusivity compared to

peat moss and would thus transmit heat faster than peat moss. This could be the reason why inclusion of sand between 30% and 44% causes a reduction in the times to reach the ignition temperatures especially as the average maximum temperatures are also high for those values of inorganics, generally above 500^{o}C. Recall that with increasing inorganic content, there is a decrease in the average temperatures at 60% and 80% inorganic content. The reduced average temperatures, which would lead to lower temperature gradients, could be the reason for the reversal in the trend of reduced ignition temperatures for 60% and 80% inorganic content.

4.4.8 Correlation for effect of inorganics on smoldering spread rate of peat moss

In this section, data from time to reach ignition temperature from the smoldering peat moss experiments detailed above will be used to obtain a correlation to account for effect of the presence of inorganics on the spread rate of peat moss. This correlation will be compared to that developed by Frandsen [48]. Frandsen [48] developed an expression for load loss rate in peat moss as:

$$w = 0.27 - 0.097R_M - 0.033(R_1 - D), \quad (4.1)$$

where w = load loss rate, g /cm^{2}h

D = R_I if $R_I < 1.0$

D = 1.0 if $R_I \geq 1.0$

R_M = moisture ratio of fuel array (ratio of water mass to organic mass)

R_I = inorganic ratio of the fuel array (ratio of inorganic mass to organic mass)

The maximum load loss rate $w_{\max}$ is given by

$$w_{\max} = 0.62 - 0.22R_M - 0.076(R_I - D), \text{ g/cm}^2\text{h} \quad (4.2)$$

From this the rate of spread was given as:

$$R = w_{\max} / \rho \quad (4.3)$$

where R = smoldering rate of spread, cm/h

ρ = density in g/cm^3

According to Frandsen [48], the rate of spread as given in Equation (4.3) carries a 33% error as a result of the median and mean values of the observed maximum mass loss rate from Equation (4.2).

In the experimental results given on effect of inorganics on smoldering rate in Table 4.12, it was assumed that the time to reach ignition temperature was the time for the mixture to reach a temperature of 175^{o}C. From the data, the spread rate from 3 cm to 15 cm is determined in cm per minute. The spread rate at 1 cm is neglected to avoid errors that could be introduced as a result of the direct effect of the incident heat flux. Steady state smoldering spread rate is expected to have been achieved at a depth of 3 cm. A plot of spread rate versus percentage of inorganic yields a fourth order graph shown in Figure 4.18.

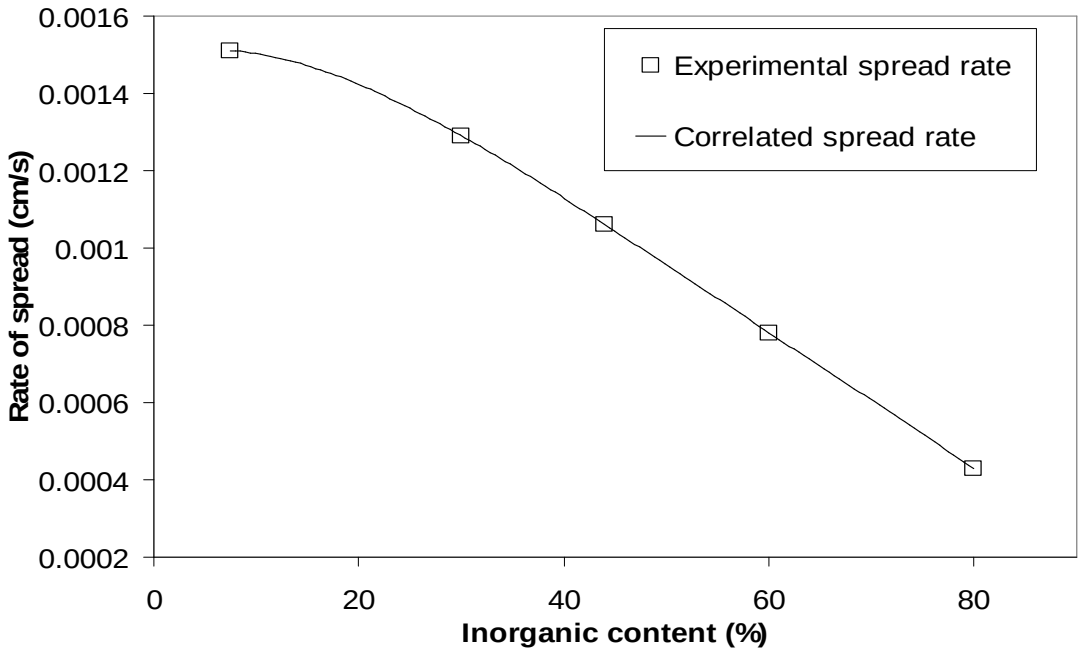

Figure 4.18: Spread Rate (cm/s) of Peat Moss and Sand Mixtures (Zero Percent Moisture Content) Exposed to a Heat Flux of 50 kW/m^2.

The trend of variation of spread rate of peat with percentage inorganic material is depicted in Figure 4.18. A fourth order polynomial trend is observed. The observed trend is given as:

$$w = -3\times10^{-11} IC^4 + 7\times10^{-9} IC^3 - 6\times10^{-7} IC^2 + 6\times10^{-6} IC + 0.0015 \qquad (4.4)$$

where w = spread rate of mixture, cm/s

IC = inorganic content = mass of inorganic/total mass of mixture, %

Equation (4.4) is compared against Frandsen's [43] model (Equation (4.3)) at zero percent moisture ratio. This is to investigate the possibility of estimating the smoldering spread rate of organic material using only the percentage of the inorganic content of the organic material. From Equation (4.2), for zero percent moisture ratio, $R_M = 0$, w_{max} thus becomes:

$$w_{\max} = 0.62 - 0.076(R_I - D) \qquad (4.5)$$

Table 4.12 gives a comparison of results from Equation (4.4) and Frandsen's model for various percentages of inorganics. Sample calculations are given in Appendix D.

Table 4.12: Comparison of Smoldering Spread Rate (cm/s) from Frandsen's Model and Experimental Correlation

Percentage Inorganic	Frandsen's Model [43]	Experimental Correlation (Equation (4.4))
7.5%	4.84	5.45
30%	4.15	4.69
44%	3.96	4.03
60%	3.9	2.97

The experimental correlation does an adequate job of predicting the smoldering spread rate of peat moss with a given percent of inorganic content in comparison with Frandsen's [48] model. It should be noted here that Frandsen's [48] model inherently has an error of ±33% as stated previously. The edge effects from the use of the kaowool insulating board are assumed to be negligible in the analysis of the results. This is

because the smoldering spread being simulated in the study is downward and not lateral. Also, from the literature in which similar sample holders were used for holding organic material (e.g., [43, 48, Anderson) for simulating lateral smoldering spread, edge effects were said to minimal.

4.4.9 Forest soils and laboratory soils.

The forest floor material had inorganic content and moisture content values that, based on the work of Frandsen [48], suggest that sustained combustion would not take place. Such was the case as there was no sustained combustion in all the tests conducted, for both the forest floor samples and the laboratory constructed soils. Comparison of the response of the two types of soils, forest floor and laboratory constructed, exposed to similar heat fluxes showed very good agreement in temperatures measured at the various depths. Graphs depicting comparison of the temperature responses of both the forest floor and laboratory constructed soils for samples 1 and 2 are shown in Figures 4.19 and 4.20. Temperature profiles measured for other samples are shown in Appendix E.

The temperature profiles for depths of 1 cm, 3 cm and 5 cm for both the forest and laboratory constructed soils for sample one are shown in Figure 4.19. From the graph, the temperature profiles between the two types of soils are very similar. At a depth of 1 cm, the difference in the temperature rises of the forest and laboratory soil is 0.7%. At a depth of 3 cm, the difference was 5.4% and at 5 cm the variation was 7.8%. Figure 4.201 also depicts the temperature profiles at depths of 1 cm, 3 cm and 5 cm for the forest and laboratory constructed soils for sample 2. The variation in the temperature rises for both the forest and laboratory constructed soils are 1.1% at 1 cm, 5.7% at 3 cm and 15.2% at 5 cm.

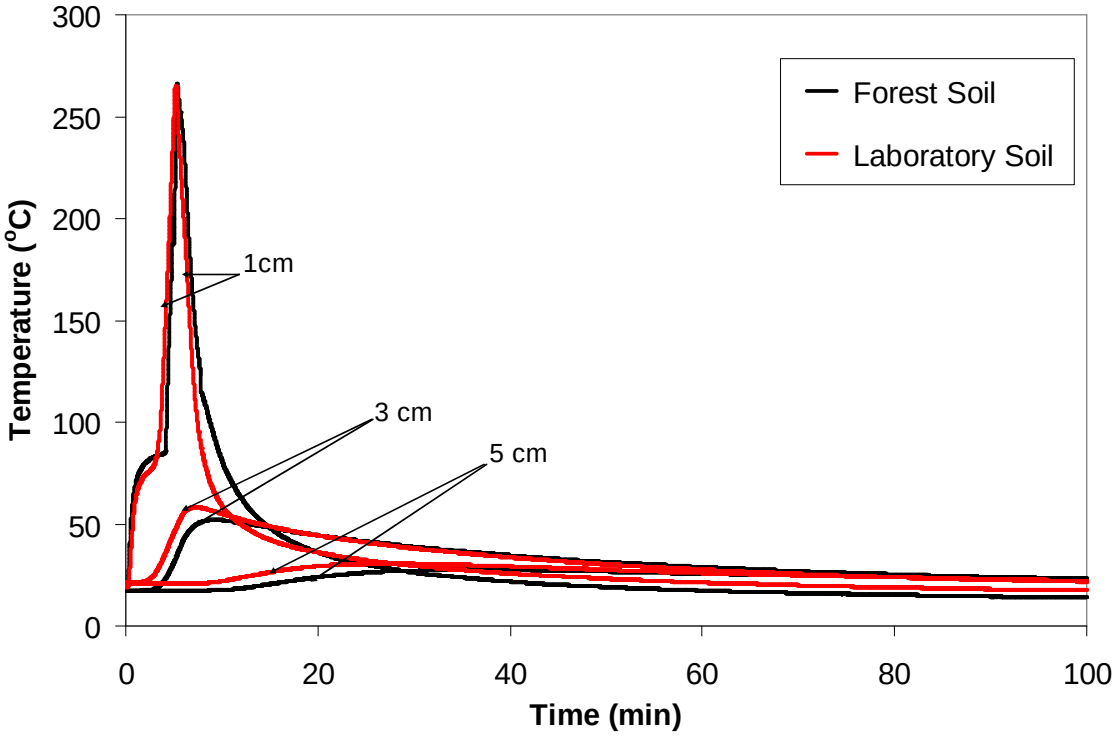

Figure 4.19: Comparison of Temperature Profiles for Forest Soil and Laboratory Constructed Soil for Sample 1 Exposed to a Heat Flux of 80 kW/m^2 for 8 Minutes

There is, however, a considerable time lag between the profiles for the laboratory constructed soil and the forest soil especially during cooling at a depth of 1 cm. This is probably due to the inability to exactly match the thermal properties of the forest soil samples. Also the presence of grass and other materials on the surface of the forest soil could affect the heating and cooling rates but these could not be reconstructed on the laboratory soil.

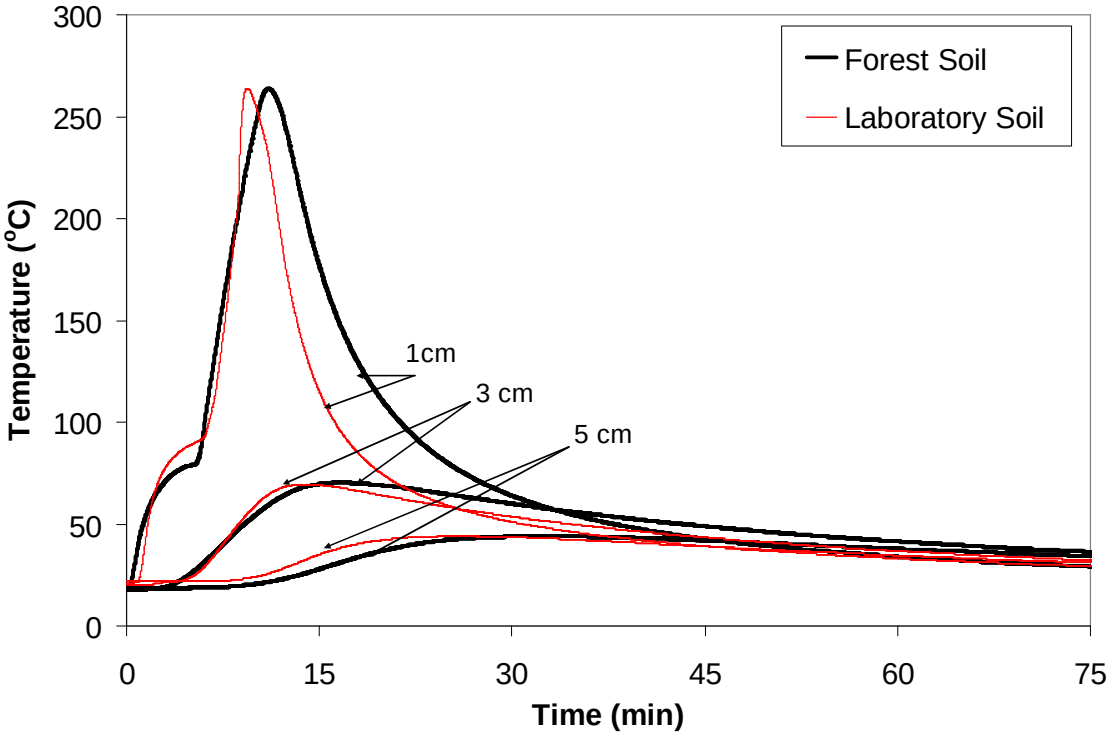

Figure 4.20: Comparison of Temperature Profiles for Forest Soil and Laboratory Constructed Soil for Sample 2 During and After 8 Minutes Exposure to Heat Flux of 80 kW/m^2

Table 4.13 gives the values of differences in maximum temperature rises between the laboratory constructed soils and the forest soils. In the analysis, temperature rises are being used instead of absolute temperatures. This is because the use of absolute temperatures could lead to erroneous conclusions especially if the initial temperatures are not the same. The values obtained for the difference in maximum temperatures are small and the time lag that exists in most cases between the two types of soil could be due to slight difference in material properties, both physical and thermal as explained previously. However with the maximum temperatures being well depicted, the laboratory soil could be used very well to aid in determining the depth of lethal heat penetration since that depends on maximum temperatures and not when those

temperatures are achieved. The laboratory created soils in all cases gave slightly higher values than the forest floor and was thus conservative.

Table 4.13: Percentage Difference in Maximum Temperature Rises Measured at Different Depths Between the Forest Floor Soils and Laboratory Constructed Soil.

Sample	Percentage Difference Between Maximum Temperatures Rises Measured in Forest and Laboratory Soil Specimens at Various Depths					
	1 cm	3 cm	5 cm	7 cm	10 cm	15 cm
1	0.7	5.4	7.3	15.5	19.2	6.6
2	10.2	5.7	15.1	7.1	7.2	6.3
3	2.1	5.3	10.5	20.0	8.5	3.4
4	1.1	4.6	1.8	4.1	2.3	7.1
5	2.7	2.1	25.6	15.9	25.7	11.7

Table 4.14 gives the depths of lethal heat penetration for both the forest soil and the laboratory constructed soil. As can be seen from the figures, the depths of lethal heat penetration determined from both types of soil are very close with a maximum percentage difference of 4.2%.

Table 4.14: Comparison of Depth of Lethal Heat Penetration for Various Samples of Forest Soil and Laboratory Constructed Soil

Sample	Depth of Lethal Heat Penetration (cm)		
	Forest soil	Laboratory soil	Percentage difference
1	2.9	3.0	3.4%
2	3.75	3.75	0%
3	3.65	3.70	1.4%
4	2.6	2.65	1.9%
5	2.5	2.4	4.2%

4.5 Summary of chapter

The experimental procedure and apparatus used to obtain results to validate the model developed in Chapter Two have been detailed in this chapter. Brief backgrounds and functions of the various apparatus were described. The experiments conducted include:

- heat transfer in dry homogenous sand exposed to various heat fluxes
- heat transfer in moist homogenous sand,
- heat transfer in dry two-layer soil,
- heat transfer in peat moss of various moisture contents,
- smoldering spread rate in peat moss with different inorganic contents,
- heat transfer in forest floor soil and laboratory constructed soil.

Methods of collecting and conditioning of samples including soil samples from the forest were described as well as methods of determining the physical properties of the forest soil and creation of similar soils in the laboratory. The results obtained have been discussed including the estimation of the depth of lethal heat penetration. The intensity and duration of heat flux was found to impact on the depth of lethal heat penetration and maximum temperatures, the presence of moisture was also found to limit the flow of heat in soil. These findings are consistent with findings from other authors in the literature and basic heat transfer theory. The presence of inorganics in peat moss was found to reduce average maximum temperatures but increase the duration of smoldering combustion. Good agreement was observed between the heat response of forest floor and laboratory created soils, especially in the determination of depth of lethal heat penetration.

CHAPTER FIVE: COMPARISON OF NUMERICAL AND EXPERIMENTAL RESULTS

In this Chapter the predictions of temperature profiles, maximum temperatures and depth of lethal heat penetration by the temperature dependent thermal properties model, constant thermal properties model, and the two layer constant thermal properties model given in Chapter Three will be compared to experimental results obtained in Chapter Four. The main discussion in this chapter will include the following.

- A comparison of numerical and experimental results for dry sand exposed to heat fluxes of 25, 50 and 75 kW/m^2 for various periods of exposure.
- A comparison of numerical and experimental results for two-layer soil exposed to a heat flux of 25 kW/m^2 for 10 minutes and a heat flux of 50 kW/m^2 for 5 minutes.

5.1 Comparison of experimental and numerical results of dry sand

In Chapter Four, temperature profiles measured in dry sand of 0.4 mm mesh size exposed to heat fluxes of 75, 50 and 25 kW/m^2 were presented. The depths of lethal heat penetration were also determined. These experimental measurements will now be compared against numerical predictions.

5.1.1 Comparison of predictions for single-layer soil

Temperature profiles from numerical predictions by the TDTP and CTP models and measured in the experiments for exposure of dry sand to a heat flux of 25 kW/m^2 for 5 minutes are compared in Figure 5.1. The Figure gives the temperature profiles at depths of 1 cm and 3 cm. Table 5.1 also gives a comparison of the predicted and measured maximum temperature rises at 1, 3, 5 and 10 cm as well as the depths of lethal

heat penetration. The temperature rise is computed from the difference between the initial temperature of soil and the maximum temperature measured.

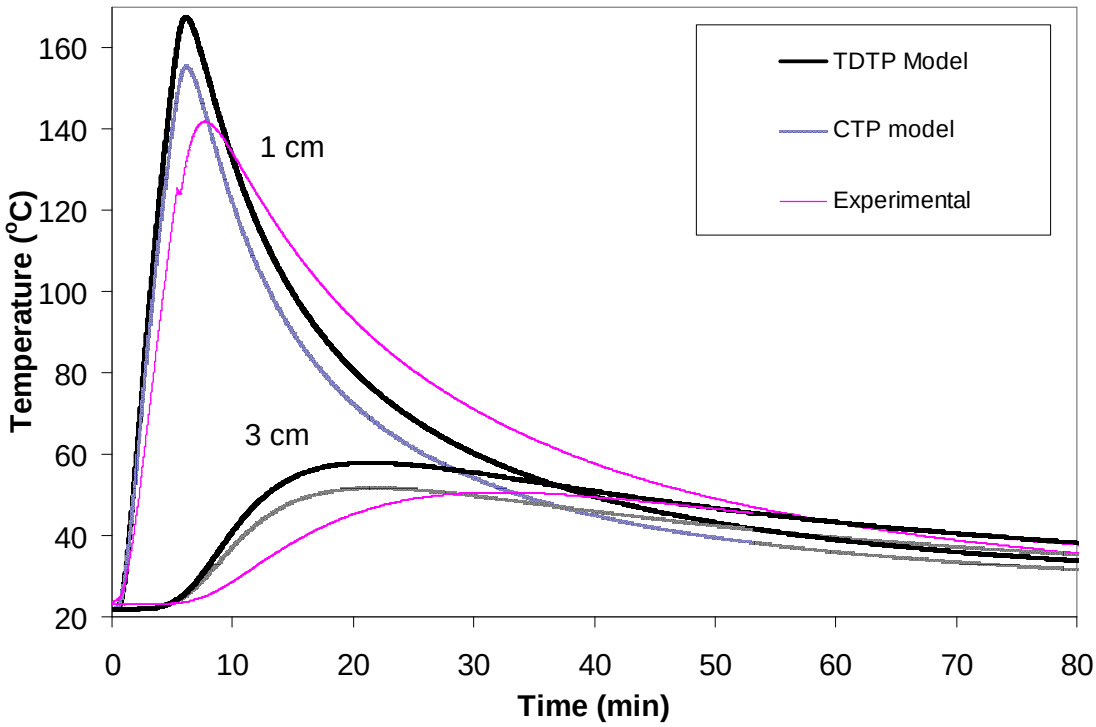

Figure 5.1: Comparison of Temperature Profiles Predicted by the TDTP and CTP Models with Temperatures Measured at Depths of 1 cm and 3 cm During and after 5 Minutes Exposure to a Heat Flux of 25 kW/m^2

Table 5.1: Comparison of Maximum Temperature Rises at Various Depths and Depth of Lethal Heat Penetration Predicted by the TPTD and CTP Models with Temperature Measurements for Exposure To 25 kW/m^2 for 5 Minutes

Type of Prediction	Maximum Temperature Rise (°C) at Various Depths				
	1 cm	3 cm	5 cm	10 cm	Depth of Lethal Heat Penetration (cm)
CTP Model	131.6	28.3	11.7	2.0	2.6
TDTP Model	143.4	34.3	14.5	2.5	3.0
Experimental	118.8	27.4	12.3	2.8	2.8

From Figure 5.1 both the TDTP and CTP over-predict the temperature profiles and maximum temperatures at 1 cm and 3 cm during heating. The profiles are under-predicted during cooling. From Table 5.2, both models over-predicted the temperature rises at all depths. The TDTP over-predicted the depth of lethal heat penetration by about 7% whilst the CTP model under-predicted the depth of lethal heat penetration by about 7%. Recall that in Chapter 3 it was explained that the TDTP model predicts higher internal temperatures and thus larger values of depth of lethal heat penetration than the CTP model. It was mentioned again in Chapter Three that a curve fitting method was used to determine the depth of lethal heat penetration. Due to the high nodal size resolution available in the numerical results, the depth of lethal heat penetration determined is more accurate than the experimental value for which spatial resolution is low. This could account for the higher depth of lethal heat penetration estimated for the experimental measurement than the CTP model though the CTP model recorded higher temperature rises at all depths. An experimental depth of lethal heat penetration less than 2.8 cm will have been obtained had a higher nodal resolution been used. This will then have been consistent with the temperature rises obtained for both experimental and numerical works.

The percentage difference between predicted maximum temperature rises and temperature measurements was 12% for CTP model and 22% for TDTP model. The predicted profiles had higher rates of heating and cooling than the experimental measurements.

Predicted temperature profiles from the TDTP and CTP models and temperature measurements for an exposure to a heat flux of 50 kW/m^2 for 5 minutes are presented in Figure 5.2. The maximum temperature rises at various depths and resultant depth of lethal heat penetration for exposure to a heat flux of 50 kW/m^2 for 5, 7 and 10 minutes are also given in Tables 5.2, 5.3 and 5.4.

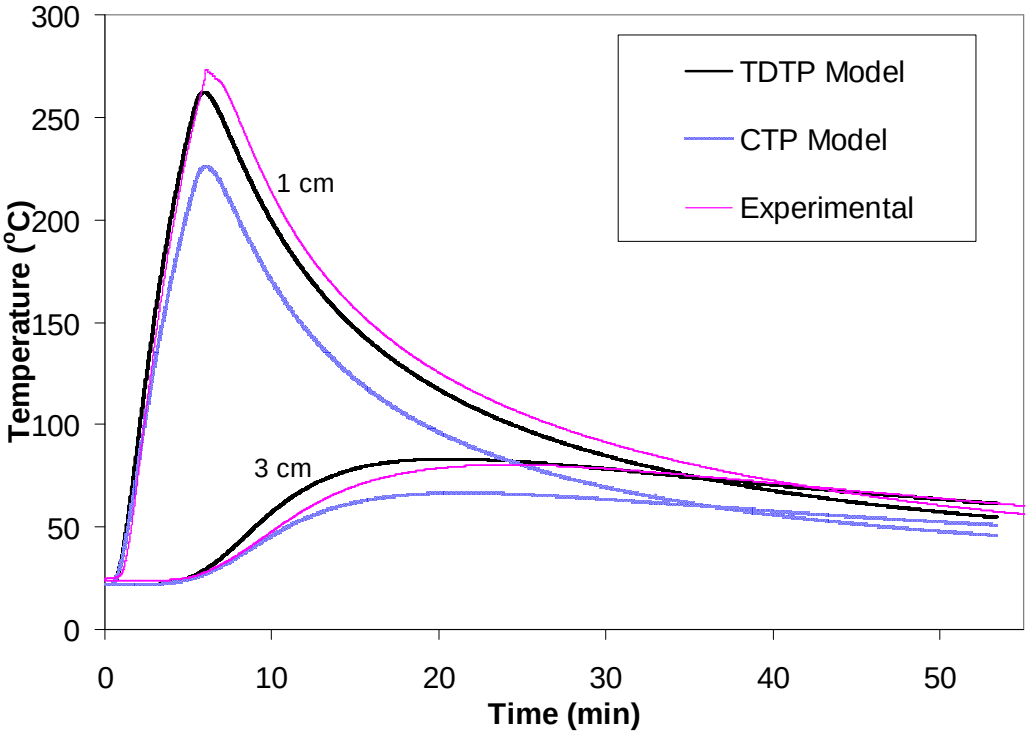

Figure 5.2: Comparison of Temperature Profiles Predicted by the TDTP and CTP Models with Temperatures Measured at Depths of 1 cm and 3 cm During and after 5 Minutes Exposure to a Heat Flux of 50 kW/m^2

From the Figure, the temperature profiles and maximum temperatures at a depth of 1 cm are under-predicted by both models. At a depth of 3 cm, the TDTP model over-predicts the maximum temperatures and profiles whilst the CTP model under-predicts the profiles and maximum temperature. From Table 5.2, at a depth of 1 cm, the TDTP model under-predicts the maximum temperature rise by 4% and over-predicts the maximum temperature rise at 3 cm by 8%. The CTP model under-predicts the maximum temperature rise by 18% at 1 cm depth and 21% at 3 cm depth.

Similar to the data from Table 5.2, the TDTP model over-predicts the depth of lethal heat penetration whilst the CTP model under-predicts the depth of lethal heat penetration. The TDTP model over-predicts the depth of lethal heat penetration by 2% whilst the CTP under-predicts the depth of lethal heat penetration by 16%. From Table 5.3 which shows data for exposure to heat flux of 50 kW/m^2 for 7 minutes, the TDTP model over-predicts

the depth of lethal heat penetration by about 13% whilst the CTP model under-predicts by 10%. From Table 5.4 which shows data for exposure to heat flux of 50 kW/m^2 for 10 minutes, the TDTP model over-predicts the depth of lethal heat penetration by about 17% whilst the CTP model under-predicts the depth of lethal heat penetration by 6%.

Table 5.2: Comparison of Maximum Temperature Rises and Depth of Lethal Heat Penetration Predicted by the TDTP and CTP Models with Measured Values at Various Depths Exposure to Heat Flux of 50 kW/m^2 for 5 Minutes

Type of prediction	Maximum Temperature Rise in (^{o}C) at Various Depths				
	1 cm	3 cm	5 cm	10 cm	Depth of Lethal Heat Penetration (cm)
CTP Model	203.0	43.4	18.1	4.1	3.5
TDTP Model	238.5	59.7	26.0	6.2	4.3
Experiment	248.4	56.4	28.7	7.4	4.2

Table 5.3: Comparison of Maximum Temperature Rises and Depth of Lethal Heat Penetration Predicted by the TDTP and CTP Models with Measured Values at Various Depths Exposure to Heat Flux of 50 kW/m^2 for 7 Minutes

Type of prediction	Maximum Temperature Rise in (^{o}C) at Various Depths				
	1 cm	3 cm	5 cm	10 cm	Depth of Lethal Heat Penetration (cm)
CTP Model	246.6	56.6	23.9	5.8	4.2
TDTP Model	286.5	79.02	35.0	8.8	5.3
Experiment	386.7	80.0	28.8	9.6	4.7

Table 5.4: Comparison of Maximum Temperature Rises and Depth of Lethal Heat Penetration Predicted by the TDTP and CTP Models with Measured Values at Various Depths for Exposure to Heat Flux of 50 kW/m^2 for 10 Minutes

Type of Prediction	Maximum Temperature Rise (^{o}C) at Various Depths				
	1 cm	3 cm	5 cm	10 cm	Depth of Lethal Heat Penetration (cm)
CTP Model	294.2	76.0	32.3	7.8	5.0
TDTP Model	336.4	106.4	47.8	12.2	6.2
Experiment	421.7	102.0	39.1	7.6	5.3

Table 5.5 gives the maximum temperature rises and the depths of lethal heat penetration for a 5 minute exposure to a heat flux of 75 kW/m^2. The trend of the data is different from that observed for the other predictions as both models under-predict the temperature rises and the depth of lethal heat penetration. The TDTP model under-predicts the depth of lethal heat penetration by 18% whilst the CTP under-predicts the depth of lethal heat penetration by 35%.

Table 5.5: Comparison of Maximum Temperature Rises and Depth of Lethal Heat Penetration Predicted by the TDTP and CTP Models with Measured Values at Various Depths Exposure to Heat Flux of 75 kW/m^2 for 5 Minutes

Mode of Prediction	Maximum Temperature Rise in ^{o}C at Various Depths (cm)				
	1 cm	3 cm	5 cm	10 cm	Depth of Lethal Heat Penetration (cm)
CTP Model	249.3	53.1	22.3	6.9	4.0
TDTP Model	307.8	79.2	35.0	10.3	5.1
Experiment	445.6	110.5	51.3	7.3	6.2

5.1.2 Reasons for variation between numerical and measured values

The following reasons can be put forward to account for the differences in measured and predicted temperature profiles, values of maximum temperatures and depths of lethal heat penetration.

- For the exposure to a heat flux of 25 kW/m^2 for 5 minutes, the differences in the profiles can be due to the value of the convective heat transfer coefficient used in the model. A high value of the convective heat transfer coefficient, *h*, will cause a faster rate of cooling due to a larger value of convective heat flux. This is especially so as the temperatures measured with exposure to a heat flux of 25 kW/m^2, are lower than the average temperatures used in determining the value of *h* in Chapter Three. Further deductions to support this reason can be made from Figure 5.2 which gives the temperature profiles for five minutes exposure to a heat flux of 50 kW/m^2. It can be seen from the predicted and measured temperature profiles at a depth of 1 cm from Figure 5.2 that during cooling, the slopes and shapes of the profiles are similar, implying that the convective heat transfer coefficient value used in this study was more representative of the temperatures achieved with a heat flux of 50 kW/m^2.

- For exposure to a heat flux of 75 kW/m^2 it was seen that the differences in maximum temperature rise between predicted and measured values resulted in differences in the depth of lethal heat penetration of 18% by the TDTP model and 35% by the CTP model. Recall that the thermal conductivity relation used for the model, Equation (3.5) was obtained over a limited temperature range, between 17.5^{o}C and 37.5^{o}C, and then linearly extrapolated. Recall also that in Chapter Three, the thermal conductivities used in this study and that measured by Pourhashemi, et. al. [61] in quartz and sea sands were compared and in the comparison, it was realised that between 500K and 650K, the quartz sand showed an increase of 0.46 W/m·K representing about 90% increase in the thermal conductivity at 300K, the sea sand showed an increase of 0.33 W/m·K representing approximately 50% increase in the thermal conductivity at 300K whilst that used in this study showed an increase of only 0.09 W/m·K representing about 35% of the value at 300K. This implies that at high temperatures the thermal conductivity relationship used in the model will likely be generating and using thermal conductivity values less than what it should actually be.

Recall again that in the sensitivity analyses carried out in Chapter Three, it was pointed out that a decrease in thermal conductivity results in a decrease in maximum temperatures and depth of lethal heat penetration. Hence, the fact that the thermal conductivity was generated over a limited temperature range resulting in possible smaller values being used in the numerical prediction at high temperatures, could be the cause of low values of maximum temperatures and depths of lethal heat penetration predicted by the models at 75 kW/m^2.

- The assumption of convective cooling during heating at high heat fluxes could also lead to lower predictions by the model. Practically, during heating in the experiments, the temperature immediately above the soil (and beneath the heater) will not be ambient and convective cooling will not be effective. Recall that it was mentioned in Chapter Four that during the experiments, after heating the sand, the heated sand was moved away from beneath the cone heater to an area where temperature was more representative of the ambient. This was to ensure practical convective cooling. Recall that in the sensitivity analysis carried out in Chapter 3, neglecting convective cooling during heating causes about 17% and 15% increase in predicted depth of lethal heat penetration by the TDTP and CTP model respectively. The CTP model predicted a depth of lethal heat penetration of 6.1 cm when there was no convective cooling during heating and 4.7 cm was predicted by the CTP model.

- Recall that one of the reasons stated for choosing a heat flux boundary condition in this study was due to the fact that high temperature gradients could exist in soils. Thus, in the experiments carried out, the possibility of the thermocouple not being exactly at the targeted position exists. For example, the TDTP model predicts a maximum temperature variation of 15% between depths of 0.9 mm and 1 cm.

It is obvious from the literature that predicting exact values of depth of lethal heat penetration and temperature profiles in a soil is generally difficult due to the inability to accurately measure the thermal properties of the soil. In comparing the results of this study with the literature, Richon [5] measured and predicted four depths of lethal heat penetration with six different boundary conditions in dry Ottawa sand. For a boundary condition similar to this study (constant heat flux exposure and convective cooling at all times), variations obtained by Richon [5] between predicted and measured depths of lethal heat penetration ranged from 12% to 47%. Steward, et. al. [16] also measured several depths of lethal heat penetration in dry Ottawa sand. For a constant heat flux boundary condition, predicted and measured depths of lethal heat penetration obtained by Steward, et. al. [16] had variations of more than 100% in some cases. Scotter [23] obtained variations of about 33% between predicted and measured maximum temperatures. Pourhashemi, et. al. [61] obtained variations of 15% between measured and predicted temperatures during transient periods.

In this study, apart from the variations observed at an exposure to a heat flux of 75 kW/m^2 variations between predicted and measured depths of lethal heat penetration (maximum of 18%) were better than that reviewed in the literature. It must be also noted that the values of depth of lethal heat penetration are generally small hence a small variation in the value could translate into large percentage variations.

5.1.3 Comparison of results for two-layered soil

Table 5.6 gives a comparison of predicted and measured maximum temperatures at depths of 1, 3, 5 and 10 cm for an exposure of a dry two-layer soil to a heat flux of 25 kW/m^2 for 10 minutes. The values of thermal properties of slightly moist topsoil from Uscowicz [76] were used directly in the numerical model. The thermal values used are thermal conductivity, k = 0.42 W/mK, specific heat, c = 908.6 W/m^2K and density, ρ = 662.2 kg/m^3. The soil from which data was adapted had a moisture ratio of 0.056 m^3/m^3.

Table 5.6: Comparison of Maximum Temperatures and Depth of Lethal Heat Penetration Predicted by the CTP Model with Measured Values at Various Depths for Exposure to Heat Flux of 25 kW/m^2 for 10 Minutes

Type of prediction	Maximum Temperature Rise (^{o}C) at Various Depths				
	1 cm	3 cm	5 cm	10 cm	Depth of Lethal heat penetration (cm)
CTP Model	316.8	152.0	84.4	30.5	6.0
Experimental	397.8	114.5	69.0	32.4	5.8

As can be seen from Table 5.6, the temperature measured at 1 cm is considerably higher than the numerical value. Recall that in discussing the experimental results in Chapter Four, it was mentioned that smoldering combustion had taken place in the top soil and charring to a depth of about 1.5 cm had been observed, hence the high temperatures at a depth of 1 cm. Since the model does not take into account internal heat generation that takes place in smoldering combustion, the measured temperatures at and near points where smoldering combustion took place should be higher than the predicted temperatures. This is the case in Table 5.6. The temperature at 3 cm is lower than predicted by the model probably due to the fact that the thermal conductivity value used in the model, which is for slightly moist soil, will be higher than for dry soil. As was discussed in Chapter Three, a higher thermal conductivity will cause faster heat flow within soil and create smaller temperature gradients than a smaller value of thermal conductivity. The experimental results showed higher temperature gradients probably due to a lower value of thermal conductivity that exists for a dry soil compared to a wet soil. The depth of lethal heat penetration predicted by the model was larger than the experimental value by about 3%.

Table 5.7 gives the predicted and measured maximum temperatures for a 5 minute exposure to a heat flux of 50 kW/m^2. Similar to the case of 25 kW/m^2, the effects of smoldering combustion on the maximum temperatures are seen at a depth of 1 cm. Similarly, the effect of using a possibly higher thermal conductivity value in the model is seen in smaller temperature gradients for the numerical results than the experimental

results. This results in higher internal temperatures being predicted by the numerical model than measured in the experiments. The model over-predicts the depth of lethal by about 12%.

Table 5.7: Maximum Temperatures at Various Depths from Numerical Prediction and Experimental Measurements for a Two-Layered Soil Exposed to Heat Flux of 50 kW/m^2

Type of Prediction	Maximum temperature (^{o}C) at Various Depths				
	1 cm	3 cm	5 cm	10 cm	Depth of Lethal Heat Penetration (cm)
Numerical Prediction	369.5	138.0	74.0	29.0	5.6
Experimental Measurement	452.8	103.6	59.8	29.4	5.0

5.2 Implication of results to forest/wildland fire research

A review of the comparison of numerical and experimental results in this Chapter as well as the sensitivity analyses carried out in Chapter 3 shows that there are varying effects on the temperatures and depths of lethal heat penetration in a soil under wildland fire conditions arising from the properties of the soil and the boundary conditions prevailing. The effects of thermal conductivity is such that high thermal conductivity values create high depths of lethal heat penetration whilst large values of specific heat and density causes a reduction in the depth of lethal heat penetration. The effects of convective heat transfer coefficient on temperature rises especially at lower depths and depth of lethal heat penetration were not as large as the effect of the thermal properties. The effects of incident heat flux and the time of exposure of the heat flux were both found to cause large temperature rises and depths of lethal heat penetration. Typically, since the thermal properties of a soil cannot be changed (without changing the moisture state of the soil), the most important parameters that can be varied are the incident heat flux and the times of exposure. This implies that the size of fire and the burning time of fire in a forest/wildland are parameters that can be practically varied in a prescribed fire

to obtain desired results in terms of temperature rises and depths of lethal heat penetration. Fuels like slash, litter, grass etc. can be used in various loadings to obtain targeted incident heat fluxes and times of burning. However, one problem that still remains is the inability to accurately measure the thermal properties of the soil.

From a comparison of the two models developed in this study, that is the temperature dependent thermal properties (TDTP) and constant thermal properties (CTP) models, with experimental measurements, it is seen that the TDTP model over-predicts the depth of lethal heat penetration whilst the CTP model under-predicts the depth of lethal heat penetration. Moreover, the TDTP model predicts values that are closer to the experimental measurements than the CTP model. In making predictions, it is important to include a factor of safety and be conservative, hence the TDTP model which over-predicts the depth of lethal heat penetration is more conservative than the CTP model. The TDTP model is thus chosen as a better model to use than the CTP model.

The study has also shown that the dependence of thermal conductivity on temperature can be determined using available heat flow meters such as was used in this study, the Fox heat flow meter. Such temperature dependent properties will help in better predicting temperature profiles and depth of lethal heat penetration. Similarly, the dependence of other thermal properties such as the specific heat can be determined using equipments such as a Differential Scanning Calorimeter. Hence for any soil, the dependence of thermal properties on temperatures can be determined.

Generally, the depth of seeds and shoots of plants in soil can be predicted by soil scientists within an accuracy of 1 cm [5]. Hence predictions of depth of lethal heat penetration in soil should at worst be within this accuracy of 1 cm. All the predicted depths of lethal heat penetration by both models, except at 75 kW/m^2 were less than 1 cm and hence within the 1 cm accuracy of predicting depths of seeds and shoots of plants.

Practically, the model can be used to determine the depth of lethal heat penetration as well as temperature in soil to determine effect on seeds and plant tissues deep within soil. The temperature data that can be obtained from the model can also be used by forest managers to estimate when certain biological, chemical and physical activities related to temperature will occur in soil. For example, it is believed that when temperatures exceed 300^{o}C in the organic material, over half of the nitrogen within the affected organic material may be lost in gaseous form to the atmosphere. Also at temperatures above about 375^{o}C, more than 25% of the sulfur (an important plant nutrient and soil acidifier) within the affected organic material may be lost in gaseous form to the atmosphere and, temperatures between 175-200^{o}C can effectively distil organic matter into hydrocarbons that condense around soil particles, altering the physical character of soil and resulting in reduced infiltration[2, 10, 11].

Temperatures and depths of lethal heat penetration in dry soil are higher than that obtained in moist soils. Soils in forest settings will contain some amount of moisture and will rarely be completely dry. This implies that predictions made with the model in this study, which neglects the presence of moisture in soil, will generally be conservative in nature and will predict the maximum possible values of maximum temperatures and depth of lethal heat penetration.

In this study, a method has been developed for small scale tests involving the use of the cone calorimeter for wildland fire research, specifically, for studies on heat transfer in soil exposed to sources of heat. The mode of heating available from the cone calorimeter and used in this study has been purely radiative, this mode of heat transfer is typical of high temperature fires. The results from the experimental measurements, which are consistent with basic heat transfer principles and with literature implies that the cone calorimeter can be used effectively for small scale tests on the soil. This will help in limiting the dependence on large scale tests since unlike other small scale tests where forest fuels are used to generate heat with uncontrollable heat inputs into soil, the heat input from the cone calorimeter can be controlled to desired values.

5.3 Summary of chapter

A comparison between numerical predictions and experimental results has been carried out here for cases of:

- heat transfer in a dry single-layer sand, and
- heat transfer in a dry two-layer soil.

In both cases, good agreement has been obtained between numerical predictions and experimental values especially in the prediction of the depth of lethal heat penetration except at very high heat fluxes. Reasons have been given for variations between predicted and measured values of temperature profiles and depth of lethal heat penetration especially at high heat fluxes as well as implications of this study for wildland fire research.

CHAPTER SIX: CONCLUSIONS AND RECOMMENDATIONS

6.1 Conclusions

In this study two types of models of heat transfer in soil have been developed: a temperature dependent thermal properties model and a constant thermal properties model. The heat transfer model based on temperature dependent properties of soil can be easily developed once a relation between the thermal properties and temperature can be obtained. The inputs to the models are:

- temperature dependent thermal properties relations of soil for temperature dependent thermal properties models,
- constant thermal properties of soil for constant thermal properties model,
- density of soil,
- a constant heat flux and time of exposure of such heat flux and
- heat transfer coefficient at surface of heated soil.

The results from comparison of the two types of one-layer heat transfer models in dry sand with the experimental measurements have shown that a temperature dependent properties model does a better job of predicting temperature profiles and depths of lethal heat penetration than a model that uses constant thermal properties model. In this study the temperature dependent properties model over-predicted depths of lethal heat penetration in a dry singly layer sand by a margin ranging from 6% to 18% whilst the constant properties model under-predicted the experimental results by 2 to 35%. In the literature, variations obtained ranged from 15% to 47%. The temperature dependent thermal properties model in general was conservative in predictions of the depth of lethal heat penetration. For the two-layer model using constant properties, the model over-predicted the depth of lethal heat penetration by 3% in the first test and 12% in the

second test. The model developed in this study thus does a very good job of predicting temperature profiles and depth of lethal heat penetration compared to variations observed in the literature. Predicted depths of lethal heat penetration, apart from that for exposure to heat flux of 75 kW/m^2 were within 1 cm accuracy. Recall that depth of seeds and plant shoots in the soil can be predicted within an accuracy of 1 cm.

Apart from predictions made at exposure to a heat flux of 75 kW/m^2, the numerical models, especially the TDTP model did a good job of predicting the temperature profiles and depth of lethal heat penetration. The models did not do a very good job at high heat fluxes due to the following.

- The relationship used for the temperature dependence of thermal conductivity of sand was obtained from a limited temperature range which might not be representative of the actual relationship at high temperatures which were obtained at exposure to a heat flux of 75 kW/m^2
- The relationship used for dependence of specific heat on temperature of sand was adapted from literature and might thus not be very representative of that of the sand used in the experiment and
- The assumption of convective cooling during heating up of sand which in practice might not be the case or not of the degree used in the model. Neglecting the effect of convective cooling during heating up in the models showed better agreement with the experimental results at high heat flux of 75 kW/m^2.

The effect of moisture on the rate of heat transfer in soil as catalogued by many authors was also observed in this study. The maximum temperatures and depths of lethal heat penetration obtained experimentally decreased with presence of moisture and were far less than that obtained for dry sand. With just a 5% moisture content in sand, there was a reduction in temperature at depth of 1 cm from the dry sand exposed to heat flux of 50 kW/m^2 for five minutes by as much as 170%. There was a reduction in the depth of lethal heat penetration by 13% with the same 5% moisture content. The effect of

moisture on the maximum temperatures and depth of lethal penetration in sand was observed to increase with increasing moisture content.

Practically, there will be some amount of moisture in soil, since the maximum temperatures and depths of lethal heat penetration obtained in dry soil is higher than that obtained in moist soil (as was depicted in this study with sand), the model of heat transfer in dry soil developed in this study will predict values of maximum temperatures and depths of lethal heat penetration that are higher than real values and will thus be conservative. This makes the use of such a model very ideal in situations where predictions are desired to be conservative.

The presence of inorganics in peat moss was found to decrease the maximum average temperatures obtained in smoldering combustion of peat moss. The presence of inorganics was also found to retard the spread rate of smoldering combustion in peat moss. The retardation in spread rate of smoldering combustion with increasing inorganic content ultimately leads to a point where smoldering combustion is not sustained. This limit of inorganic content in peat moss where smoldering combustion is not sustained has been catalogued by researchers in the literature (e.g., Fransden [46]). The effect of the presence of inorganics on spread rate and maximum temperatures is expected to cause a reduction in temperatures transmitted to mineral soils with increasing organic matter.

The effect of moisture on spread rate and temperatures achieved in smoldering organic matter (peat moss) was also presented in this study. The maximum temperatures at various depths were found to decrease with increase in moisture content similar to the case of sand. This implies that the amount of heat transmitted to the mineral soil by a smoldering organic matter in the forest will decrease with increase in moisture content of the organic layer. This is consistent with findings by Frandsen and Ryan [33] who recorded heat fluxes in soil with moist peat moss coverings of 2.1 kW/m^2 as against 3.3 kW/m^2 recorded in soils with dry peat moss coverings.

In the experiments, it was observed that due to the slow spread rate of peat moss, temperatures of over 200^{o}C persisted at various depths for long periods of time. Practically, this implies that will certainly be an increase in the total thermal energy transmitted to the mineral soil and consequently the depth of lethal heat penetration when organic material burns. This is consistent with findings in literature (for e.g.,[2]) that a ground fire is the most destructive of all forest/wildland fires due to the high temperatures that persist over long periods of time.

Methods have been developed in this study to use available garden materials such as peat moss and fine sand, to represent forest floor soil by matching the physical properties, such as the organic and moisture contents and bulk densities, of the various layers of the forest soil. The cone calorimeter has also been shown to be capable of being used in wildland fire studies as a source of heat by providing a controllable radiative heat flux in terms of magnitude and time of exposure. These together can be used extensively in wildland fire studies to validate models of heat transfer and limit the dependence on full scale tests to validate such models of heat transfer in the soil. These stem from the results obtained from comparing the temperature responses of forest floor and laboratory constructed soils to heat inputs. The laboratory created soil did a very good job of mimicking the temperature profiles and depth of lethal heat penetration measured in the forest soil.

Recall that in developing the model, a few assumptions were made including:

- a constant heat flux boundary condition
- absence of moisture

These will have to be borne in mind when applying results from this model and are therefore applicable to similar prevailing conditions. Practically, the heat flux generated in a forest fire is not constant as assumed in the model. Also the effect of moisture was not considered in the model hence for the case where there is moisture in the soil, the

actual depth of lethal heat penetration will be less than predicted. The result obtained with the model will thus be conservative.

6.2 Recommendation for future work

Based on the results of the experiments and the numerical work, the following recommendations for future work are made.

- Since it is believed that the relationship expressing the dependence of thermal properties, that is the specific heat and thermal conductivity, on temperature was not very representative of the thermal properties of the sand used in this study, especially at high temperatures, and could be the cause of the variations in numerical and measured values of temperatures and depths of lethal heat penetration, an investigation of methods such as the use of the Differential Scanning Calorimeter to obtain the temperature dependence of thermal properties of the soil over a large temperature range is recommended. This can then be used in the temperature dependent thermal properties model with higher accuracy.
- Since it has been shown that a numerical model that incorporates temperature dependent thermal properties has better predictive abilities than a constant thermal properties model, extension of the single-layer temperature dependent thermal properties model to several layers is highly recommended.
- The use of the DSC to obtain relationships for the variation of thermal properties with temperature for dry peat moss is also recommended. This can be used in developing a numerical model of smoldering combustion in peat moss. Such a model can be incorporated into the two-layer numerical model developed in this study to represent a model of organic layer over mineral soil. This model will do a better job of predicting temperature profiles and depth of lethal heat penetration in cases where smoldering combustion will take place than the two-layer model developed in this study.

- The use of DSC and Heat Flow Meter to obtain correlations for the dependence of thermal properties on temperature of moist soil is also recommended. Such a correlation can be used to develop a simple model of heat transfer in moist soils. Such a model together with that for smoldering peat moss can be incorporated in a two-layer model that will do a very good job of predicting temperatures and depths of lethal heat penetration in a real forest floor soil as it would account for the presence of moisture.

REFERENCES

[1] Davis, P. K., Byram, G. M. and Krumm, W.R. 1959. Forest Fire, Control and Use. McGraw Hill, New York.

[2] Ryan, K. C. 2002. Dynamic Interactions Between Forest Structure and Fire Behaviour in Boreal Ecosystems, Silva Fennica, 1: 13-39.

[3] Natural Resources Canada,2005, Forest Fire, Facts and Questions, Canadian Forest Service, http://www.nofc.forestry.ca/fire/facts_e.php. Assessed on 12th April, 2006.

[4] McNabb, D. H., and Cromack, K.Jr. 1990. Effects of Prescribed Fire on Nutrients and Soil Productivity 125-141. In: Natural and Prescribed Fire in Pacific Northwest Forests. Walstad, John D., ed., et al. Corvallis, OR, Oregon State University Press.

[5] Richon, J. B. 1987. Heat Transfer in Soils Exposed to Fires. M.Sc. Thesis, Department of Chemical Engineering, University of New Brunswick, Fredericton, NB.

[6] DeBano, L. F., Savage, S. M. and Hamilton, D. M. 1976. The Transfer of Heat and Hydrophobic Substances During Burning. Soil Science Society of America Journal 40:779-782.

[7] Neary, D. G., Klopatek, C. C., DeBano, L. F. and Ffolliott, P. F. 1999. Fire Effects on Below-ground Sustainability: A Review and Synthesis. Forest Ecology and Management 122: 51-71.

[8] Natural Resources Canada. 2005. Forest Fire, Facts and Questions, Canadian Forest Service, http://www.nofc.forestry.ca/fire/facts_e.php. Assessed on 12th April, 2006.

[9] Stanhope, R. 2003. Forest Management. Logging and Sawmill Journal, http://www.forestnet.com. Accessed on 20th June, 2005.

[10] DeBano, L. F., Savage, S. M. and Hamilton, D. M. 1976. The Transfer of Heat and Hydrophobic Substances During Burning. Soil Science Society of America Journal 40:779-782.

[11] Neal J. L., Wright E. and Bollen W. B. 1965. Burning Douglas-Fir Slash:Physical, Chemical and Microbial Effects on Soil. Oregon State University Forest Research Laboratory No.1. Corvallis, Oregon.

[12] Kohnke H. 1968. Soil Physics. McGraw Hill, New York.

[13] Ghildyal , B.P and Tripathi R. P. 1987. Soil Physics. John Wiley and Sons Incorporated, New York.

[14] Steila, D. and Pond, E. T. 1989. The Geography of Soils, Second Edition. Rowman and Littlefield Publishers Incorporated, Savage, Maryland.

[15] Baver, L. D. 1956. Soil Physics, Third Edition. John Wiley and Sons. New York.

[16] Steward, R.F. Peter, S. and Richon, J. B. 1990. A Method for Predicting the Depth of Lethal Heat Penetration Into Mineral Soils Exposed to Fires of Various Intensities. Canadian Journal of Forest Research 20: 919-26.

[17] Preisler, H. K., Haase, S.M. and Sackett, S.S. 2000. Modeling and Risk Assessment for Soil Temperatures Beneath Prescribed Forest Fires. Environmental and Ecological Statistics 7: 239-254.

[18] Schimmel J. and Granstrom, A. 1996. Fire severity and Vegetation Response in the Boreal Swedish Forest. Ecology 77: 1436-1450.

[19] Bradstock, R. A. and Auld, T. D. 1995. Soil Temperatures During Experimental Bushfires in Relation to Fire Intensity: Consequences for Legume Germination and Fire Management in South-Eastern Australia. Journal of Applied Ecology 32: 76-84.

[20] British Columbia Ministry of Food and Agriculture. 2004. Fire Effects on Grasses and Forbs, Factsheet of Fire Effects on Rangelands. Victoria, B.C.

[21] Feller, M.C. 1998. The Influence of Fire Severity, Not Fire Intensity, on Understory Vegetation Biomass in British Columbia. In: Proceedings, 13th Conference on Fire and Forest Meteorology. 1996. Lorne, Australia. International Journal of Wildland Fire.

[22] Selving, J. P. 1992. Heat Transfer Beneath a Spreading Fire. Ph.D. Thesis, Department of Chemical Engineering, University of New Brunswick, Fredericton, NB.

[23] Scotter, D. R. 1970. Soil Temperatures Under Grass Fires, Australian Journal of Soil Research 8: 273 -9.

[24] Feddes, R. A. 1973. Some Physical Aspects of Heat Transfer in Soil. Journal of International Society for Horticulture Science 27: 189-196

[25] Kiaviany, M. 2005. Principles of Heat Transfer in Porous Media, Second Edition. Springer- Verlag, New York.

[26] Krarti, M. Claridge, D. E., and Kreider J. F. 1995. Analytical Model to Predict Non-Homogeneous Soil Temperature Variation. Journal of Solar Energy Engineering 117:100-107.

[27] Beadle N.C.W. 1940. Soil Temperatures During Forest Fires and Their Effect on the Survival of Vegetation. Journal of Ecology 28:180-192.

[28] Archibold, O.W., Nelson, L. J., Ripley, E., A., and Delanoy, L. 1998. Fire Temperatures in Plant Communities of the Northern Mixed Prairie. Canadian Field-Naturalist 112:234-240.

[29] Http://www.msc-smc.ec.gc.ca/msb/manuals/soiltemp/introduction_e.html: Website of the Meteorological Services of Canada. Accessed on 2nd February 2006.

[30] Chandler C., Cheney P., Thomas P., Trabaud, L and William, D. 1983. Forest Fire Behaviour and Effects. Fire and Forestry. John Wiley and Sons, New York.

[31] Pafford, D. Dhir, V. J., Anderson, E. B., Cohen, J. 1985. A Model for Ground Surface Heating During a Prescribed Burn, Symposium on Fire and Forest Meteorology. Detroit, MI. Washington, DC: 24-32.

[32] Chinanzvavana S., Grosshandler, W. L. and Davis D.C. 1986. Analysis of Heat Transfer in Soil During Open Field Burning, Transactions of the American Society of Agricultural Engineers. 29:1797-1801.

[33] Frandsen, W.H. and Ryan, K.C.1986. Soil Moisture Reduces Belowground Heat Flux and Soil Temperatures Under a Burning Fuel Pile. Canadian Journal of Forest Research. 16: 244-248.

[34] Enninful E.K. and Torvi D. A. 2005. Effect of Moisture on Heat Release and Smoke Production of Vegetation. In Proceedings: Spring Technical Meeting, Combustion Institute Canadian Section. Halifax, NS.

[35] Simmerman, D., Arno, S. and Harrington, M. 1991. A Comparison of Dry and Moist Fuel Underburns in Ponderosa Pine Shelterwood Units. In Proceedings: 11th Conference on Fire and Forest Meteorology, Missoula, MT. 387-397.

[36] Wondafrash, T.T., Sancho M.I., Miguel V. G. and Serrano R.E. 2005. Relationship Between Soil Color and Temperature in the Surface Horizon of Mediterranean Soils: A Laboratory Study. Soil Science 170: 495-502.

[37] Campbell, G. S., Jungbauer, J, D. Bristow K. L and Hungerford D. R. 1995. Soil Temperature and Water Content Beneath a Surface Fire. Soil Science 159: 363-374.

[38] Pyne, S.J., Andrew, P.L. and Laven, R.D. 1996. Introduction to Wildland Fire. John Wiley and Sons, New York.

[39] Rideout, S. Oswald, B.P. and Legg, M. H. 2003. Ecological, Political and Social Challenges of Prescribed Fire Restoration in East Texas Pineywoods Ecosystems: A Case Study, Forestry 76: 261-269.

[40] Patterson, W. B., Sword-Sayer, M. A. Haywood, J. D. and Brooker, S. 2003. Effects of Vegetation Management with Prescribed Fire on Soil Physical Properties in a Young Longleaf Pine Stand. In Proceedings: 12th Biennial Southern Silvicultural Research Conference, Biloxi, MS: 74-79.

[41] Xavier U., Marc L., Luis R. O., Sara, B. and Marc, C. 2005. Effects of Prescribed Fire on Soil Quality in Mediterranean Grassland (Prades Mountains, North-East Spain), International Journal of Wildland Fire 14: 379–384.

[42] Cohen, J. 2004. Relating Flame Radiation to Home Ignition Using Modeling and Experimental Crown Fires. Canadian Journal of Forestry Research, 34, 1616-1626.

[43] deVries, D. A. 1963. Thermal Properties of Soil. In: Physics of Plant Environment, North-Holland, Amsterdam: 210-235.

[44] Hungerford, R.D., Frandsen, H.F., Ryan, K.C., Heat Transfer into Duff and Organic Matter. 1996. Final Project Report for United States Fish and Wildlife Service, Ogden, UT.

[45] Ohlemiller, T. J.1995. Smoldering Combustion, SFPE Handbook of Fire Protection Engineering. Second Edition. Section 2. Chapter 11, National Fire Protection Association, Quincy, MA: 171-179.

[46] Frandsen, W. H. 1997. Ignition Probability of Organic Soils. Canadian Journal of Forest Research. 27: 1471-1477.

[47] Albini F., Amin R. M., Hungerford, R. D., Frandsen, W. H. and Ryan, K. C. 1996. Models for Fire-Driven Heat and Moisture Transport in Soils. United States Department of Agriculture, General Technical Report INT-GTR-335, Ogden, UT.

[48] Frandsen, W. H. 1991. Smoldering Spread Rate: A Preliminary Estimate. In:11th Conference on Fire and Forest Meteorology, April 16-19, Missoula, MT.

[49] Wein R.W., 1983. Fire Behaviour and Ecological Effects in Organic Terrain. In: SCOPE 18: The Role of Fire in Northern Circumpolar Ecosystems. John Wiley and Sons, New York.

[50] Sheshukov, M. A. 1974. Features of Sward (turf) Fires. Lesovedenie 5:81-83

[51] Shearer, R.C. 1975. Seedbed Characteristics in Western Larch Forests After Prescribed Burning. USDA Forest Service General Technical Report INT-167, Ogden UT.

[52] Norum, F. A. 1977. Preliminary Guidelines for Prescribed Burning Under Standing Timber in Western Larch/Douglas-Fir Forests. USDA Forest Servive General Technical Report INT-229. Ogden, UT.

[53] Frandsen, W. H. 1987. The Influence of Moisture and Mineral Soil on the Combustion Limits of Smoldering Forest Duff. Canadian Journal of Forest Research. 17: 1540-1544.

[54] Frandsen, W. H. 1985. Soil Moisture Reduces Belowground Heat Flux and Soil Temperatures Under a Burning Fuel Pile. Canadian Journal of Forest Research. 16:244-248.

[55] Reinhardt, E.D., Keane, R.E., Brown, J.K. and Turner, D. L. 1991. Duff Consumption for Prescribed Fire in the U.S. and Canada: A Broadly Based Empirical Approach. In Proceedings: 11th Conference of Fire and Forest Meteorology, Missoula, MT, April 16-19: 362-370.

[56] Hartford, R. A. 1989. Smoldering Combustion Limits in Peat as Influenced by Moisture, Mineral Content and Organic Bulk Density. In Proceedings: 10th Conference on Fire and Forest Meteorology, Ottawa, ON, April 17-21: 282-286.

[57] Anderson K. R. 2000a. Incorporating Smoldering Into Fire Growth Modelling. In: 3rd Symposium on Fire and Forest Meteorology. Long Beach, CA: 31–36.

[58] Cromer, R.N. and Vines, R. G. 1996. Heat Transfer Under a Burning Windrow. Australian Forestry Research 2: 29-34.

[59] Janssens M, Parker WJ. 1996. Oxygen consumption calorimetry. Heat release in fires. Chapman & Hall: 31-59.

[60] Keith, P.1993. Uses of the Cone Calorimeter. Rapra Technology Limited, Shropsire, SY4 4NR, UK.

[61] Pourhashemi, S. A., Hao, O. J. and Chawla, C. R. 1999. An Experimental and Theoretical Study of the Non-Linear Heat Conduction in Dry Porous Media. International Journal of Energy Research: 389-401.

[62] Flinn, M. A. and Wein, R. W. 1977. Depth of Underground Plant Organs and Theoretical Survival During Fire. Canadian Journal of Botany 55: 2550-2554.

[63] Rowe, J. S. 1983. Concepts of Fire Effects on Plant Individuals and Species. In: DeBano, R. W. and Maclean, D. A.(eds.). The Role of Fire in Northern Ecosystems Circumpolar, Scope 18. John Wiley and Sons, New York: 135-154.

[64] Staggs J. E., Whiteley, R. H. 1999. Modelling the Combustion of Solid-Phase Fuels in Cone Calorimeter Experiments. Fire and Materials: 23.

[65] Janssens, M. L. 1991. Thermophysical Characteristics of Wood and Their Role in Enclosure Fire Growth. Ph.D. Thesis, University of Gent, Belgium.

[66] Myers, G. E.1971. Analytical Methods in Heat Conduction Transfer. McGraw Hill, New York.

[67] Carslaw H. S. and Jaeger J. C.1959. Conduction of Heat in Solids. Second Edition, Oxford University Press, UK.

[68] Incropera, F.P. and DeWitt D. P.1996. Fundamentals of Heat and Mass Transfer. John Wiley and Sons Incorporated, New York.

[69] Torvi, D.A. 1997. Heat Transfer in Thin Fibrous Materials Under High Heat Flux Conditions. Ph.D. Thesis, Department of Mechanical Engineering, University of Alberta, Edmonton, AB.

[70] Torvi, D. A. 1992. A Finite Element Model of Heat Transfer in Skin Subjected to a Flash Fire. MSc. Thesis, Department of Mechanical Engineering, University of Alberta, Edmonton, AB.

[71] Nidal H., Abu, H., and Randall, C. R. 2000. Soil Thermal Conductivity: Effects of Density, Moisture, Salt Concentration, and Organic Matter. Soil Science Society of America Journal, 64:1285-90

[72] Flynn, D. R. and Watson, T. W. 1968. High Temperature Thermal Conductivity of Soils, In: Thermal Conductivity, Proceedings of the 8th Conference., C. Y. Ho and R. E. Taylor (Eds.), Plenum Press, New York, NY : 913-939.

[73] LaserComp . 2004. FOX200 and FOX300 Series Instrument Manual and Guide. LaserComp, Saugus, MA.

[74] Hiraiwa Y. and Kasubuchi T.2000. Temperature Dependence of Thermal Conductivity of Soil Over a Wide Range of Temperature (5 – 75^{o}c). European Journal of Soil Science, 51: 211-218.

[75] Touloukian, Y. S. and Buyco, E. H. 1970. Thermophysical Properties of Matter, Specific Heat of Nonmetallic Solids, IFI/Plenum, New York, NY.

[76] Usowicz, B. 1996. Thermal Properties of Topsoil Layer in an Olive Orchard, Institute of Agrophysics, Polish Academy of Sciences, Doswiadczalna 4, 20-280, Lublin Poland.

[77] Thermal Ceramics. Kaowool Low Temperature Boards Product Information. www.thermalceramics.com. Accessed on 4th September, 2005.

[78] Saskatchewan Environment and Resource Management Forest Ecosystems Branch. 2000. Nisbet Provincial Forest, Integrated Forest Land Use Plan, Background Document.

[79] American Society for Testing and Materials. 1997. Standard Test Method for Heat and Visible Smoke Release Rates for Materials and Products Using an Oxygen Consumption Calorimeter. Designation E 1354-97. West Conshohocken, PA.

[80] Schneider P. J. 1955. Conduction Heat Transfer. Addison-Wesley Publishing Company, Massachusetts.

APPENDIX A

Finite-difference solution of the heat transfer equations

The equations required for the formulation of the model are given in Chapter 2, Equation (2.16)

$$k\frac{\partial T}{\partial x} = q_o^{"} - \varepsilon\sigma T_{x=0}^4 - h(T_{x=0} - T_a) - E_{sm} \quad \text{at } x = 0 \text{ for } 0 < t \le t_{exposure}$$

$$k\frac{\partial T}{\partial x} = -\varepsilon\sigma(T_{x=0}^4 - T_a^4) - h(T_{x=0} - T_a) - E_{sm} \quad \text{at } x = 0 \text{ for } t > t_{exposure}$$

$$\rho c\frac{\partial T}{\partial t} = \frac{\partial}{\partial x}\left(k\frac{\partial T}{\partial t}\right) \quad \text{at } x > 0 \text{ and } t \ge 0 \text{ (temperature dependent properties)}$$

$$\frac{\partial T}{\partial t} = \alpha\frac{\partial^2 T}{\partial x^2} \quad \text{at } x > 0 \text{ and } t \ge 0 \qquad \text{(constant properties)}$$

$$T_{x=L} = T_a \quad \text{for} \quad 0 < t \le \infty$$

(1A1)

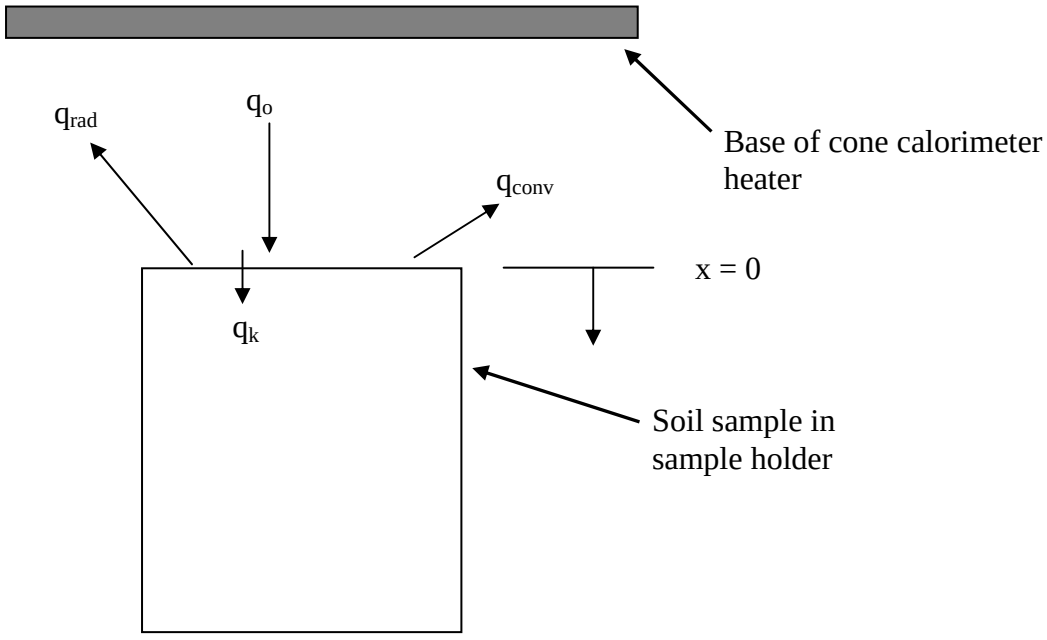

From the diagram above, for energy exchange at the surface of the soil is given by:

$$q''_{net} = q''_k + E_{sm} \qquad (1A2)$$

where $q''_{net} = q''_0 + q''_{rad} + q''_{conv}$ = net heat flux at the surface of the soil

q''_k = conducted heat flux through surface to node 1

q''_{conv} = conductive heat losses

q''_{rad} = radiative heat losses

E_{sm} = thermal energy storage in soil.

As given by Equation (1A1)

$$k\frac{\partial T}{\partial x} = q_o^{"} - H_R T_{x=0} - h(T_{x=0} - T_a) - E_{sm} \quad \text{at } x = 0 \text{ for } 0 < t \le t_{exposure} \tag{1A3}$$

$$k\frac{\partial T}{\partial x} = q_o^{"} - H_{TOTAL}(T_{x=0} - T_a) - E_{sm} \quad \text{at } x = 0 \text{ for } t > t_{exposure} \tag{1A4}$$

where $T_{x=0}$ is the surface temperature,

T_a is the ambient temperature

$$H_R = \varepsilon\sigma(T_{x=0}^3) \tag{1A5}$$

$$H_{TOTAL} = \varepsilon\sigma(T_{x=0}^2 + T_a^2)(T_{x=0} + T_a) + h$$

Referring to $T_{x=0}$ as T_o for surface temperature for convenience, then from Equation (1A3), for $0 < t \le t_{exposure}$

$$K\frac{T_o - T_1}{\Delta x} = q_o^{"} - H_R(T_o) - h(T_o - T_a) - E_{sm}$$

$$q_o = K\frac{T_o - T_1}{\Delta x} + h(T_o - T_a) + H_R(T_o) + \rho C\frac{\Delta x}{2}\frac{dT_o}{dt}$$

$$\frac{dT_o}{dt} = \frac{2\alpha}{k\Delta x}q_o - \frac{2\alpha}{\Delta x^2}(T_o - T_1) - \frac{2\alpha H_R}{k\Delta x}(T_o) - \frac{2\alpha h}{k\Delta x}(T_o - T_a) \tag{1A6}$$

From the Euler method of marching ahead in time

$$T_o^{i+1} = T_o^i + \left.\frac{dT}{dt}\right|^i \Delta t \tag{1A7}$$

where i is the old time step and i+1 is the new time step. From Equations (1A6) and (1A7)

$$T_o^{i+1} = T_o^i + \frac{\alpha\Delta t}{(\Delta x)^2}\left[\frac{2\Delta x}{k}q_o - 2(T_o - T_1) - 2\frac{H_R\Delta x}{k}(T_o) - 2\frac{h\Delta x}{k}(T_o - T_a)\right]^i$$

Rearranging gives

$$T_o^{i+1} = T_o^i(1-2\alpha-2\alpha PH_{total}\frac{\Delta x}{k}) + 2\alpha PT_1^{\ i} + 2\alpha P\frac{\Delta x}{k}q_o + 2\alpha Ph\frac{\Delta x}{k}T_a \quad (1A8)$$

where $\alpha = \frac{k}{\rho C}, P = \frac{\Delta t}{\Delta x^2}$

$$H_{total} = h + \varepsilon\sigma(T_{x=0}^3)$$

For t > $t_{exposure}$

$$T_o^{i+1} = T_o^i(1-2\alpha-2\alpha PH_{total}\frac{\Delta x}{k}) + 2\alpha PT_1^{\ i} + 2\alpha P\frac{\Delta x}{k}q_o + 2\alpha PH_{TOTAL}\frac{\Delta x}{k}T_a \quad (1A9)$$

where $H_{total} = h + \varepsilon\sigma(T_{x=0}^2 + T_a^2)(T_{x=0} + T_a)$

Interior nodes

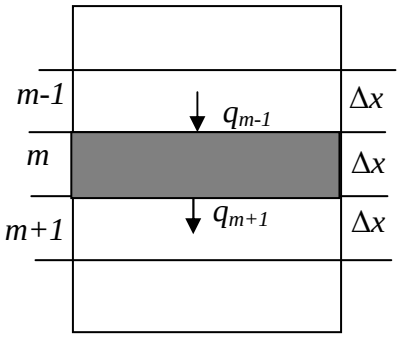

$$q_{m-1,m} = q_{m,m+1} + E_{sm} \quad (1A10)$$

$$\frac{k}{\Delta x}(T_{m-1} - T_m) - \frac{k}{\Delta x}(T_m - T_{m+1}) = \rho C\Delta x\frac{dT_m}{dt}$$

$$\frac{dT_m}{dt} = \frac{\alpha}{(\Delta x)^2}(T_{m-1} - T_m) - \frac{\alpha}{(\Delta x)^2}(T_m - T_{m+1})$$

Applying the explicit method of moving ahead in time and rearranging we have:

$$T_M^{i+1} = T_M^i(1-2\alpha P) + \alpha PT_{M-1}^{\ i} + \alpha PT_{M+1}^i \quad (1A11)$$

For the bottom node, for a semi infinite medium, equation is of form:

$$T_{Last}^{i+1} = T_{Last}^i \quad (1A12)$$

Putting the three equations in the matrix form yields

$$\begin{bmatrix} T_o \\ T_1 \\ - \\ - \\ T_{last-1} \\ T_{last} \end{bmatrix}^{i+1} = \begin{bmatrix} 1-2\alpha P(1+H_{total}\Delta x/k) & 2\alpha P & & & & \\ \alpha P & 1-2\alpha P & \alpha P & & & \\ & - & & & & \\ & & - & & & \\ & & \alpha P & 1-2\alpha P & \alpha P & \\ & & & & 1 & \end{bmatrix} \begin{bmatrix} T_o \\ T_1 \\ - \\ - \\ T_{last-1} \\ T_{last} \end{bmatrix}^{i} +$$

$$\begin{bmatrix} 2\alpha P\Delta x(q_o + hT_a)/k \\ 0 \\ - \\ - \\ 0 \\ 0 \end{bmatrix} \qquad (1A13)$$

For the case of variable properties as adapted from [65]

$$q_{m-1,m} = \frac{k_{m-1}+k_m}{2} A \frac{t_{m-1}-t_m}{\Delta x}$$
$$q_{m,m+1} = \frac{k_m+k_{m+1}}{2} A \frac{t_m-t_{m+1}}{\Delta x} \qquad (1A14)$$
$$E_{sm} = (\rho c)_m A\Delta x \frac{dT_m}{dt}$$

At the surface, considering energy exchange as was done for the constant properties case:

$$q_o'' = \frac{k_o+k_1}{2\Delta x}(T_o - T_1) + h(T_o - T_a) + H_R T_o + (\rho C)_o \frac{\Delta x}{2}\frac{dT_o}{dt}$$

$$\frac{dT_o}{dt} = 2P\left[\frac{q_o''\Delta x}{(\rho c)_o} - \frac{k_o+k_1}{2(\rho c)_o}(T_o - T_1) - \frac{h\Delta x}{(\rho c)_o}(T_o - T_a) - \frac{H_R\Delta x}{(\rho c)_o}(T_o)\right]$$

Employing the explicit method of moving ahead in time given in Equation (1A15)

$$T_o^{i+1} = (1 - P\frac{k_o+k_1}{(\rho c)_o} - 2P\frac{H_{total}\Delta x}{(\rho c)_o})T_o^i + P\frac{k_o+k_1}{(\rho c)_o}T_o^i + \frac{2P\Delta x}{(\rho c)_o}[q_o + hT_a] \quad (1A16)$$

where $H_{total} = h + \varepsilon\sigma(T_{x=0}^3)$.

For $t > t_{exposure}$,

$$T_o^{i+1} = (1 - P\frac{k_o + k_1}{(\rho c)_o} - 2P\frac{H_{total}\Delta x}{(\rho c)_o})T_o^i + P\frac{k_o + k_1}{(\rho c)_o}T_o^i + \frac{2P\Delta x}{(\rho c)_o}[q_o + H_{total}T_a] \qquad (1A17)$$

where $H_{total} = h + \varepsilon\sigma(T_{x=0}^2 + T_a^2)(T_{x=0} + T_a)$

For the interior nodes from Equation (1A10)

$$\frac{k_{m-1} + k_m}{2}\frac{T_{m-1} - T_m}{\Delta x} = \frac{k_m + k_{m+1}}{2}\frac{T_m - T_{m+1}}{\Delta x} + (\rho c)_m \Delta x \frac{dT_m}{dt}$$

Rearranging to obtain an expression in $\frac{dT_m}{dt}$ and applying the explicit method of moving ahead in time:

$$T_m^{i+1} = \frac{k_{m-1} + k_m}{2(\rho c)_m}T_{m-1}^i + (1 - \frac{k_{m-1} + 2k_m + k_{m+1}}{2(\rho c)_m})T_m^i + \frac{k_{m+1} + k_m}{2(\rho c)_m}T_{m+1}^i \qquad (1A18)$$

At the last node, from semi-infinite assumption:

$$T_{last}^{i+1} = T_{last}^i \qquad (1A19)$$

Putting the three equations in the matrix form yields the matrix below:

$$\begin{bmatrix} T_o \\ T_1 \\ - \\ - \\ T_{last-1} \\ T_{last} \end{bmatrix}^{i+1} =$$

$$\begin{bmatrix} 1-\frac{k_o+k_1}{(\rho c)_o}P-\frac{H_{total}P\Delta x}{(\rho c)_o}2P & P\frac{k_o+k_1}{(\rho c)_o} & & & \\ \frac{k_{m-1}+k_m}{2(\rho c)_m}P & 1-\frac{k_{m-1}+2k_m+k_{m+1}}{2(\rho c)_m}P & \frac{k_m+k_{m+1}}{2(\rho c)_m}P & & \\ & - & & & \\ & & - & & \\ & & & - & \\ & & & & 1 \end{bmatrix}$$

$$\begin{bmatrix} T_o \\ T_1 \\ - \\ - \\ T_{last-1} \\ T_{last} \end{bmatrix}^{i} + \begin{bmatrix} \frac{2P\Delta x}{(\rho c)_o}(q_{ot}+hT_a) \\ 0 \\ - \\ - \\ 0 \\ 0 \end{bmatrix} \qquad (1A20)$$

For the two-layer model, the surface node will have the same equations as that given by Equation (1A9) with subscript 1. The middle nodes will also have the same equation given by Equation (1A11) with subscript 1 to represent first layer.

$$T_o^{i+1} = T_o^i(1-2\alpha_1-2\alpha_1 P_1 H_{total}\frac{\Delta x_1}{k_1}) + 2\alpha_1 P_1 T_1^i + 2\alpha_1 P_1 \frac{\Delta x_1}{k_1} q_o + 2\alpha_1 P_1 h \frac{\Delta x_1}{k_1} T_a$$

(1A21)

The interior nodes of the first layer will have an equation similar to that of Equation (1A11) with subscript 1 as:

$$T_{1,M}^{i+1} = T_{1,M}^i(1-2\alpha_1 P_1) + \alpha_1 P_1 T_{1,M-1}^i + \alpha P T_{1,M+1}^i \qquad (1A22)$$

At the bottom of the first node,

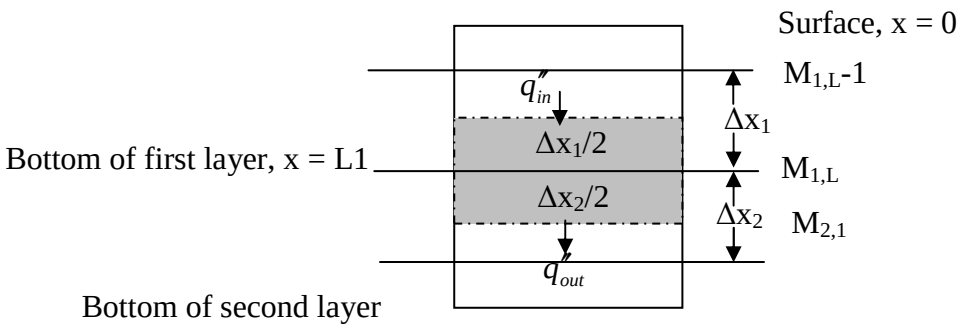

From the figure, considering energy exchange at the bottom of the last node

$$q''_{in} = k_1 \frac{T_{M1,L-1} - T_{M1,L}}{\Delta x_1}$$

$$q''_{out} = k_2 \frac{T_{M1,L-1} - T_{M2,1}}{\Delta x_2}$$

$$E_{sML,1} = (\rho c)_1 \frac{\Delta x_1}{2} \frac{dT_{ML,1}}{dt}$$

From Equation (1A10)

$$k_1 \frac{T_{M1,L-1} - T_{M1,L}}{\Delta x_1} = k_2 \frac{T_{M1,L-1} - T_{M2,1}}{\Delta x_2} + (\rho c)_1 \frac{\Delta x_1}{2} \frac{dT_{ML,1}}{dt} \qquad (1A23)$$

$$\frac{2\alpha_1}{(\Delta x)^2}\left(T_{M1,L-1} - T_{M1,L}\right) - \frac{2k_2}{(\rho c)_1} \frac{(T_{M1,L} - T_{M2,1})}{\Delta x_1 \Delta x_2} = \frac{dT_{M1,L}}{dt} \qquad (1A24)$$

From the Implicit method of moving ahead in time given in Equation (1A7),

Equation (1A24) becomes

$$T^{i+1}_{M1,L} = T^{i}_{M1,L} + \left(\frac{2\alpha_1}{(\Delta x_1)^2}(T_{M1,L} - T_{ML,1}) - \frac{2k_2}{(\rho c)_1} \frac{(T_{M1,L} - T_{2,1}}{\Delta x_1 \Delta x_2} \right)^i \Delta t \qquad (1A25)$$

Rearranging Equation (1A25) gives for the bottom node of the first layer:

$$T^{i+1}_{ML,1} = 2\alpha_1 P_1 T^{i}_{M1,L-1} + T^{i}_{M1,L}\left(1 - 2\alpha_1 P_1 - 2\frac{k_2}{(\rho c)_1} \frac{\Delta t}{\Delta x_1 \Delta x_2}\right) + 2\frac{k_2}{(\rho c)_1} \frac{\Delta t}{\Delta x_1 \Delta x_2} T^{i}_{M2,1}$$

(1A26)

The top node of the second layer will have a temperature boundary condition and the temperature is the same as that of the bottom of the first node given by Equation (1A26). The interior nodes of the second layer will be the same as that of the single layer give by Equation (1A10) with subscript 2

$$T_{2,M}^{i+1} = T_{2,M}^{i}(1-2\alpha_2 P_2) + \alpha_2 P_2 T_{2,M-1}^{i} + \alpha_2 P_2 T_{2,M+1}^{i}$$

where $P_2 = \dfrac{\Delta t}{(\Delta x_2)^2}$

The last node will have an equation similar to that of the single layer given by Equation (1A11) but with subscript 2 to represent the second layer. This is given as:

$$T_{Last}^{i+1} = T_{Last}^{i}$$

APPENDIX B

Solution of the one-dimensional Fourier field equation with constant properties and convective cooling but without surface radiative heat losses

Recall that the one-dimensional Fourier Equation, for a given uniform initial temperature is given by:

$$\frac{\partial T}{\partial t} = \alpha \frac{\partial^2 T}{\partial x^2} \qquad \text{(2B1)}$$

$T = T_o$ at time $t = 0$

For the boundary conditions

At the bottom of soil, $T\big|_{x=L} = T_o$

For the surface of the soil

$q'' = q''$ for time $t \leq t_{exposure}$ and

$q'' = 0$ if $t > t_{exposure}$

$$-k \frac{\partial (T_{x=0} - T_o)}{\partial t}\bigg|_{x=0} + h(T_{x=0} - T_o) = q''$$

The solution is obtained by the use of Laplace transform. Combining methods from Richon [5], Carlslaw and Jaeger [66] and Schneider [80], the Laplace transform is obtained for the left hand side of Equation (2B1)as:

$$L\left(\frac{\partial^2 T}{\partial x^2}\right) = \int_0^\infty \frac{\partial^2 T}{\partial x^2} e^{-st} dT$$

$$= \frac{\partial^2 T}{\partial x^2}$$

where $T = T_{x=0} - T_o$

Similarly, for the right hand side of equation (2B1):

$$L\left(\frac{\partial T}{\partial t}\right) = \int_0^\infty \frac{\partial T}{\partial t} e^{-st} dt$$

$$= \left[Te^{-st}\right]_0^\infty + s\int_0^\infty Te^{-st} dt$$

Integrating by parts gives

$$L\left(\frac{\partial T}{\partial t}\right)=\mathrm{s}\,\overline{T}$$

Therefore from Equation (2B1)

$$\alpha\left(\frac{\partial^2 T}{\partial x^2}\right)=s\overline{T}$$
$$\Rightarrow \frac{\partial^2 T}{\partial x^2}-\frac{s}{\alpha}\overline{T}=0 \qquad (2B2)$$

Equation (2B2) is an ordinary differential equation for which the solution is

$$\overline{T}=Ae^{\sqrt{\frac{s}{\alpha}}x}+Be^{-\sqrt{\frac{s}{\alpha}}x}$$

Given that the temperature at the bottom of soil does not change, then

$$T_{x=L}=T_o-T_o=0$$

Therefore $\overline{T}=Be^{-\sqrt{\frac{s}{\alpha}}x}$ (2B3)

Differentiating Equation (2B3) with respect to *x* yields

$$\frac{\partial\overline{T}}{\partial t}=-B\sqrt{\frac{s}{\alpha}}e^{-\sqrt{\frac{s}{\alpha}}x} \qquad (2B4)$$

Substituting Equation (2B4) into boundary condition at surface gives:

$kB\sqrt{\frac{s}{\alpha}}+hBe^{-\sqrt{\frac{s}{\alpha}}x}=\frac{q''}{s}$ from which B is given by:

B = $\frac{q''}{s\left(k\sqrt{\frac{s}{\alpha}}+h\right)}$ which upon substituting in Equation (5B3) gives

$$\overline{T}=\frac{q''}{s\left(k\sqrt{\frac{s}{\alpha}}+h\right)}e^{-\sqrt{\frac{s}{\alpha}}x} \qquad (2B5)$$

Let $Y=\sqrt{\frac{s}{\alpha}}$ and $H = h/k$

From which 2B5 becomes

$$\bar{T} = \frac{\frac{q''}{k}}{s(Y+H)} e^{-Yx}$$

Carlslaw and Jaeger provides a table of Laplace transform pairs from which obtaining the inverse transfer of $\bar{T}$ yields:

$$T(x,t) = \frac{Y}{kH}\left[erfc\left(\frac{x}{2\sqrt{\alpha t}}\right) - e^{Hx+\alpha t H^2} erfc\left(\frac{x}{2\sqrt{\alpha t}} + H\sqrt{\alpha t}\right)\right] \quad \text{(2B6)}$$

APPENDIX C1

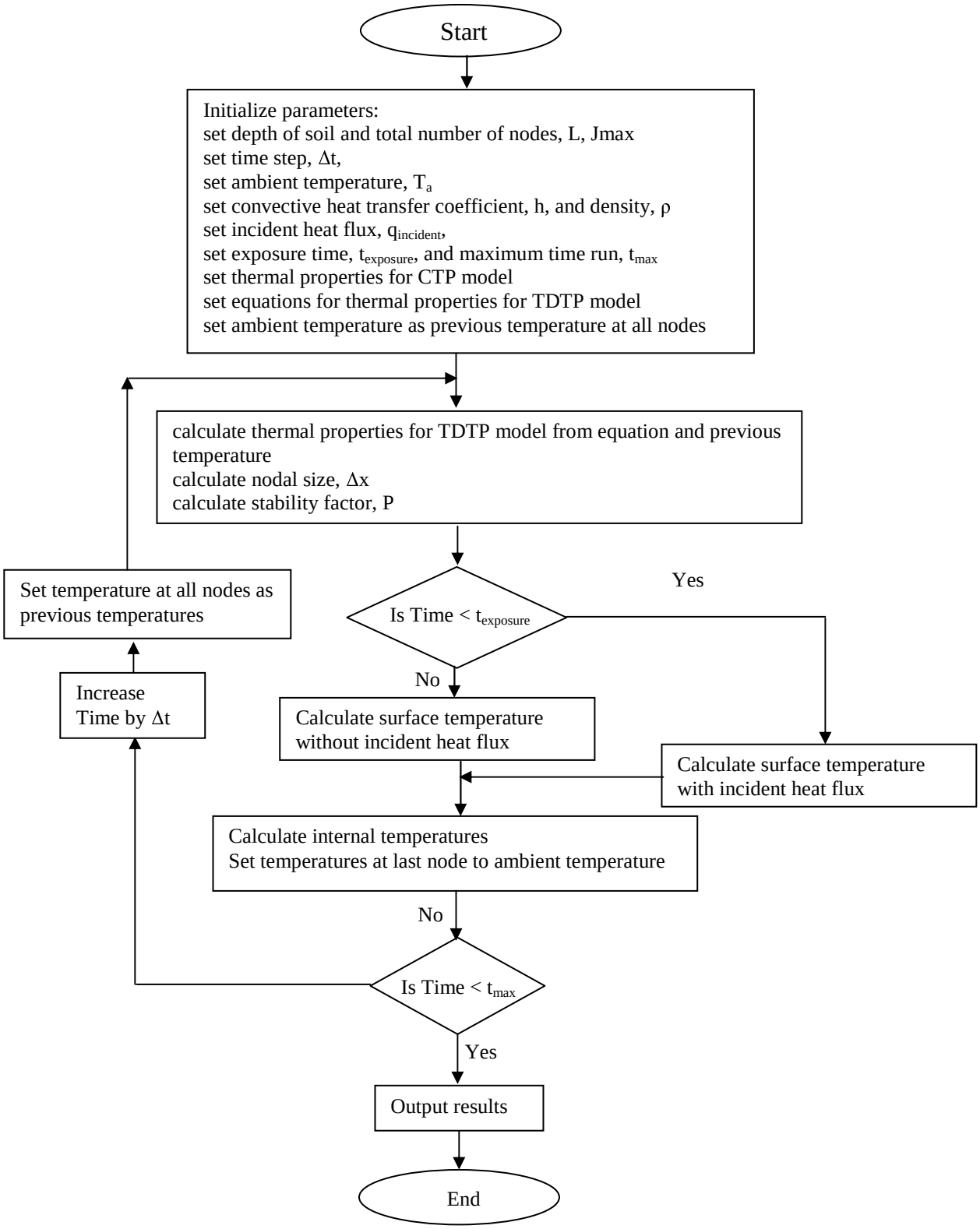
Start
Initialize parameters:
set depth of soil and total number of nodes, L, Jmax
set time step, Δt,
set ambient temperature, T_a
set convective heat transfer coefficient, h, and density, ρ
set incident heat flux, $q_{incident}$,
set exposure time, $t_{exposure}$, and maximum time run, t_{max}
set thermal properties for CTP model
set equations for thermal properties for TDTP model
set ambient temperature as previous temperature at all nodes
calculate thermal properties for TDTP model from equation and previous temperature
calculate nodal size, Δx
calculate stability factor, P
Is Time < $t_{exposure}$
Yes
No
Calculate surface temperature without incident heat flux
Calculate surface temperature with incident heat flux
Calculate internal temperatures
Set temperatures at last node to ambient temperature
No
Is Time < t_{max}
Yes
Output results
End
Increase Time by Δt
Set temperature at all nodes as previous temperatures

APPENDIX C2

Flow chart for computer program for two-layer model

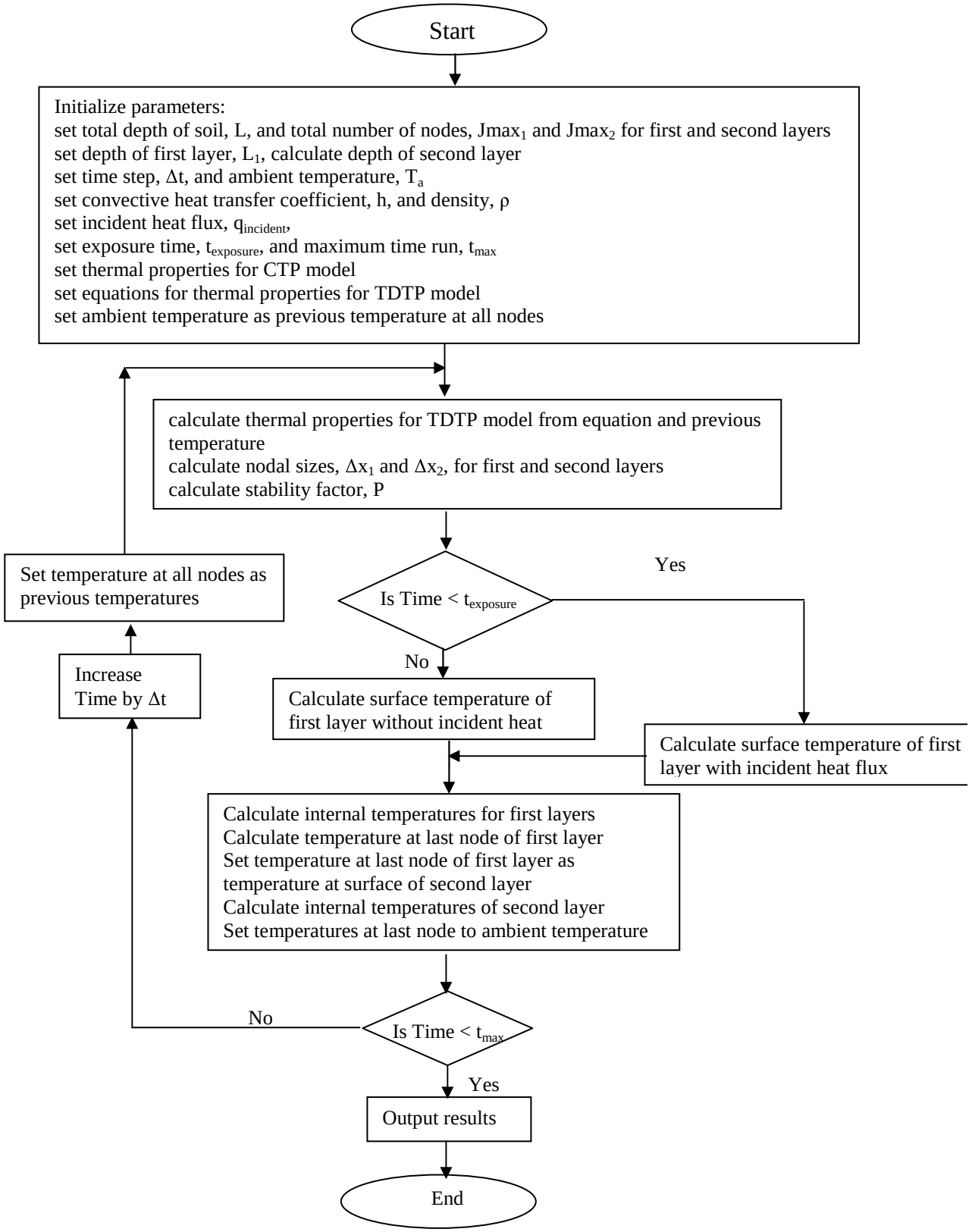

APPENDIX C3

Computer code for single layer TDTP and CTP models

THIS COMPUTER CODE SOLVES ONE-DIMENSIONAL TRANSIENT HEAT CONDUCTION EQUATION FORMULATED FROM A FINITE DIFFERENCE APPROACH THAT USES THE EULER METHOD OF MOVING AHEAD IN TIME

```
REAL TN,TOLD

DIMENSION TN(500), TOLD(500)
DIMENSION HC(500),THK(500),ALPH(500)
C    IHPUT DATA;
C  TA =AMBIENT TEMPERATURE
C    JMAX = THE NUMBER OF COMPUTATIONAL NODES IN THE SOIL
C    ALPH = THE THERMAL DIFFUSIVITY
C    S    = ALPH*DELT/DELX/DELX
C    TMAX = THE MAXIMUM TIME
C   TN  = TEMPERATURE ARRAY
C   DELX = NODAL STEP
C   DELT = TIME STEP
C  SL = TOTAL DEPTH OF SOIL
C   RHO= DENSITY
C   H= CONVECTIVE HEAT TRANSFER COEFFICIENT
C   QINCIDENT = INCIDENT HEAT FLUX
C  TAU=EXPOSURE TIME
C SIGMA = STEFAN BOLTZMANN'S CONSTANT
C  EMISSIVITY = EMISSIVITY OF SOIL

          IINPF = 1
           IOFLE = 6
```

```
      JMAX=341
      NMAX=5000
      SL = 0.17
      DELT=0.1
      RHO=1588.0
      TMAX=7000.0
      H=13
      TA=298.3
      QINCIDENT=75000.0
      TAU = 300.0
      SIGMA=5.671E-08
      EMISSIVITY=0.9

C     CALL INPUT(JMAX,SL,DELT,ALPH,RHO,S,TMAX
C     H, TA,QINCIDENT, TAU)

      JMAP = JMAX - 1
C     ALPH = THK/(RHO*HC)
      DELX = SL/(JMAX-1)
      P=DELT/(DELX*DELX)
      S = ALPH*DELT/(DELX*DELX)
      WRITE(IOFLE,3)DELT,DELX
    3 FORMAT('      DELT =',E10.3,/,'         DELX =',E10.3,//)
      WRITE(IOFLE,4)S

C     SET INITIAL CONDITIONS
      DO 5 J = 1,JMAX
      5 TN(J) = TA
      N = 0.
      T = 0.
```

```
C       SET BOUNDARY CONDITIONS
        WRITE(IOFLE,20)

        DO 999 T = 0,TMAX,DELT
        DO 11 J = 1,JMAX
                TOLD(J) = TN(J)

11      CONTINUE

        DO 7 J=1,JMAX
C     THIS SECTION INPUTS THE THERMAL CONDUCTIVITY AND HEAT
C     CAPACITY
C     FOR THE TEMPERATURE DEPENDENT PROPERTIES MODEL, COMMENT
C      OUT THE CONSTANT VALUES OF HC(J) AND THK(J). FOR THE
C     CONSTANT PROPERTIES MODEL, COMMENT OUT THE EQUATIONS FOR
C     THK(J) AND C  HC(J) AND USE THE CONSTANT HC(J) AND THK(J)
       THK(J)= 0.0006*TOLD(J)+0.0661
       HC(J)=(4186.8*0.0097*TOLD(J)**0.52)
        HC(J)=781.6
        THK(J)=0.2431

C      FOR SURFACE BOUNDARY CONDITION
        IF(J.EQ.1) THEN
             IF(T.GT. TAU) THEN
             QINCIDENT = 0.0
          ELSE
             QINCIDENT= QINCIDENT
         ENDIF
       HR=EMISSIVITY*SIGMA*(TOLD(1)*TOLD(1)+TA*TA)*(TOLD(1)+TA)
       HTOTAL=HR+H
C     THIS SECTION COMPUTES THE SURFACE TEMPERATURE, THE FIRST
```

```
C    PART IS FOR THE TEMPERATURE DEPENDENT PROPERTY MODEL,
C    COMMENT OUT IF NEED TO USE THE CONSTANT PROPERTY MODEL

          TN(1)=TOLD(1)*((1-P*(THK(1)+THK(J+1))/(RHO*HC(1)))
     &    -(2.0*P*HTOTAL*DELX/(RHO*HC(1))))
     &    +(THK(1)+THK(J+1))*P*TOLD(J+1)/(RHO*HC(1))
     &    +2.0*P*DELX*(QINCIDENT+HTOTAL*TA)/(RHO*HC(1))

C         THIS IS THE PART FOR THE CONSTANT PROPERTIES MODEL,
C         COMMENT IT OUT WHEN USING THE VARIABLE PROPERTIES MODEL
                    TN(1) =
     &              TOLD(1)*(1.- 2.0*S- 2.0*S*DELX*HTOTAL/THK)
     &              +2.0*S*TOLD(J+1)
     &              +2.0*S*DELX*(QINCIDENT+HTOTAL*TA)/THK
                    ENDIF

C         THIS SECTION COMPUTES THE INTERNAL TEMPERATURES
                    IF((J.GT.1).AND.(J.LT.JMAX)) THEN
C         THE FIRST PART IS THE TEMPERATURE DEPENDENT PROPERTY
C        MODEL, COMMENT OUT WHEN USING THE CONSTANT PROPERTY
C         MODEL
          TN(J) = TOLD(J-1)*P*(THK(J-1)+THK(J))/(2*RHO*HC(J))
         &  + TOLD(J)*(1-P*(THK(J-1)+2.0*THK(J)+THK(J+1))/(2.0*RHO*HC(J)))
          &  + TOLD(J+1)*(THK(J)+THK(J+1))*P/(2.0*RHO*HC(J))

C         THIS PART IS FOR THE CONSTANT PROPERTY MODEL, COMMENT
C         OUT WHEN USING TEMPERATURE DEPENDENT PROPERTY MODEL

          TN(J) = (1.- 2*S)*TOLD(J) + S*TOLD(J-1) + S*TOLD(J+1)
                    ENDIF
C         THIS SECTION COMPUTES THE TEMPERATURE AT THE LAST NODE
```

```
            IF(J.EQ.JMAX) THEN
                TOLD(JMAX) = TA
                TN(JMAX)=TOLD(JMAX)
            ENDIF
7       CONTINUE

        WRITE(IOFLE,21) T,(TN(J)-273.2,J=1,JMAX,10)
        21 FORMAT(F10.1,180F14.2)
        999 CONTINUE

 STOP
  END
```

APPENDIX D

Convective heat transfer coefficient.

The convective heat transfer coefficient, *h*, will be obtained by considering the soil as a horizontal plate with hot surface up or cold surface down. For such a plate, the recommended correlation for the average Nusselt number is given by [70] as:

$$\overline{Nu_L} = 0.54 Ra_L^{1/4} \quad (10^4 \le Ra_L \le 10^7) \text{ - - - - - - -} \tag{D1}$$

$$\overline{Nu_L} = 0.15 Ra_L^{1/3} \quad (10^7 \le Ra_L \le 10^{11}) \text{ - - - - - - - -}$$

where Ra_L is the Raleigh's number and is given by:

$$Ra_L = \frac{g\beta(T_s - T_\infty)L^3}{\alpha\nu} \text{ - - - - - - - -} \tag{D2}$$

where g = acceleration due to gravity, 9.81 m/s^2

$\beta = 1/T_f$ = expansion coefficient of air K^{-1}

T_s = surface temperature of soil ^{o}C or K

T_∞ = ambient temperature ^{o}C or K

α = thermal diffusivity of air m^2/s

ν = kinematic viscosity of air m^2/s

L = ratio of surface area to perimeter of plate.

An average surface temperature of 255^{o}C and ambient temperature of 22^{o}C are chosen for determining the heat transfer coefficient. The average of the two for temperature of fluid film, T_f is (270+22)/2 = 146^{o}C which corresponds to 419 K.

From Table A.4 in [67] using T_f = 400 K, properties of air obtained are:

- k = 33.8x10^{-3} W/m.K,
- ν = 26.41 x 10^{-6} m^2/s,
- α = 38.3 x 10^{-6} m^2/s,
- Pr = 0.690,
- $\beta = (1/T_f)$ = 0.0025 K^{-1}.

For the sample holder being used, the surface area measures 10 cm x 10 cm. Hence

$$L = \frac{100}{40}\frac{cm^2}{cm} = 2.5 \text{ x } 10^{-2} \text{ m.}$$

Hence from Equation (D2)

$$Ra_L = \frac{9.81 \times 0.0025(270-22) \times (2.5 \times 10^{-2})^3}{38.3 \times 10^{-6} \times 26.41 \times 10^{-6}} = 93953.6 = 9.4 \text{ x } 10^4.$$

From equation (D1), $Nu_L = 0.54\ Ra_L^{1/4} = 0.54 \text{ x } 9.4^{1/4} = 9.5$

$$\bar{h} = \frac{\overline{Nu_L}.k}{L} = \frac{9.5 \times 33.8 \times 10^{-3}}{0.025} = 12.87 \text{ W/m}^2\text{.K}$$

A value of h = 13 W/m^{2}K is used in this study.

APPENDIX E

Sensitivity analyses for the Constant Thermal Properties Model

The effect of thermal conductivity on predicted maximum temperatures are depicted in Table E1. The symbol "↑" implies an increase and "↓" implies a decrease.

Table E1: Effect of Thermal Conductivity on the Maximum Temperatures at Various Depths of Soil Column Predicted By the Constant Thermal Properties Model

Depth (cm)	Temperature (^{o}C)				
	Nominal value of thermal conductivity k = 0.2431 W/mK	10% increase in k	20% increase in k value	10 % decrease in k	20% decrease in k value
0	589.1	0.5 ↓	1 ↓	0.6 ↑	1 ↑
1	225.2	4 ↑	7 ↑	4 ↓	9 ↓
3	65.6	5 ↑	10 ↑	5 ↓	11 ↓
5	40.3	4 ↑	8 ↑	4 ↓	9 ↓
10	26.3	4 ↑	7 ↑	3 ↓	6 ↓

The effect of thermal conductivity on predicted temperatures is a decrease in surface temperature and an increase in the internal temperatures for an increase in thermal conductivity. The exact opposite occurs when there is a decrease in the thermal conductivity values. The trend is similar to the case of the temperature dependent thermal properties model (TDTP). The surface temperatures predicted here are higher than that of the TDTP model.

The effects of specific heat on predicted maximum temperatures are given in Table E2.

Table E2: Effect of Specific Heat on the Maximum Temperatures at Various Depths Predicted By The Constant Thermal Properties Model.

Depth (cm)	Percentage Change in Temperature				
	Temperature (^{o}C) at Nominal value c=781.9 W/m^{2}K	10% increase in c value	20% increase in c value	10% decrease in c value	20% decrease in c value
0	589.1	↓0.6	↓1	↑0.6	↑1
1	225.2	↓5	↓10	↑6	↑13
3	65.6	↓5	↓9	↑6	↑12
5	40.3	↓4	↓6	↑4	↑9
10	26.3	↓3	↓5	↑4	↑7

The effects of specific heat on predicted temperatures are similar to that of the TDTP model as there is a decrease in predicted temperatures with an increase in specific heat and an increase in predicted temperatures with a decrease in specific heat.

The effects of density on predicted temperatures are given in Table E3. As can be seen from the data from the Table, with an increase in density, there is a decrease in predicted temperatures similar to the effect of specific heat.

Table E3: Effect of Density on Predicted Maximum Temperatures at Various Depths Predicted By the Constant Thermal Properties Model

Depth (cm)	Percentage Change in Temperature				
	Temperature (^{o}C) at Nominal value ρ = 1588 kg/m^3	10% increase in ρ value	20% increase in ρ value	10 % decrease in ρ value	20% decrease in ρ value
0	589.1	↓0.6	↓1	↑0.6	↑1
1	225.2	↓5	↓10	↑6	↑13
3	65.6	↓5	↓9	↑6	↑12
5	40.3	↓4	↓6	↑4	↑9
10	26.3	↓3	↓5	↑4	↑7

The effect of convective heat transfer coefficient are given in Table E4. From the data, the effect of convective heat transfer coefficient on predicted temperatures are not significant compared to the effect of the thermal properties.

Table E4: Effect of Heat Transfer Coefficient on the Maximum Temperatures at Various Depths Predicted By the Constant Thermal Properties Model.

Depth (cm)	Temperature (^{o}C)				
	Nominal value of h = 12.87 W/m^{2}K	10% increase in h value	20% increase in h value	10 % decrease in h value	20% decrease in h value
0	589.1	↓0.7	↓1	↑0.7	↑1
1	225.2	↓0.6	↓1	↑0.7	↑1
2	65.6	↓1	↓2	↑1	↑2
3	40.3	↓1	↓2	↑1	↑2
4	26.3	↓0.3	↓0.7	↑0.7	↑1

The effect of incident heat flux on predicted temperatures are given in Table E5.

Table E5: Effect of Incident Heat Flux on the Maximum Temperatures at Various Depths Predicted By the Constant Thermal Properties Model.

Depth (cm)	Temperature (^{o}C)				
	Nominal value of q'' = 50 kW/m^2	10% increase in q'' value	20% increase in q'' value	10 % decrease in q'' value	20% decrease in q'' value
0	589.1	↑5	↑9	↓5	↓10
1	225.2	↑5	↑9	↓5	↓11
2	65.6	↑3	↑6	↓4	↓8
3	40.3	↑2	↑5	↓3	↓5
4	26.3	↑1	↑2	↓1	↓2

The data from the figure indicate that with an increase in the value of the incident heat flux, there is an increase in predicted temperatures similar to that of the TDTP model

The effect of no convective cooling during heating on predicted temperatures is given in Table E6.

Table E6: Effect of no convective cooling during heating on Predicted Temperatures

Nominal Temp(^{o}C)	Temp (^{o}C) for no convective cooling during heating	Percentage difference
589.1	631.3	↑7%
225.2	241.2	↑7%
65.6	74.2	↑13%
40.3	46.8	↑15%
26.3	28.1	↑6%

As can be seen from the data in the Table, neglecting convective cooling during heating causes significant changes in the predicted temperatures.

APPENDIX F1

Calculation of moisture content of moist soils

Moisture content is defined by :

$$MC = \frac{M_{moist} - M_{dry}}{M_{dry}} \qquad \text{(F1)}$$

where M_{moist} = mass of the moist sample

M_{dry} = mass of the dry sample

For a sand sample of mass 2700 g or 2.7 kg, for a 5% moisture content, from Equation (F1)

$$M_{moist} = MC \text{ x } M_{dry} + M_{dry} \qquad \text{(F2)}$$

M_{moist} = 0.05(2700)+2700 = 2835 g

Mass of water required $M_{water} = M_{moist} - M_{dry}$ (F3)

= 2835 – 2700 = 135 g

This is also simply equal to $MC \text{ x } M_{dry}$

Hence 135 g of water will be required to be added to a dry sand of 2700 g to obtain a 5% moisture content.

Similarly for peat moss, for a 30% moisture content with a dry sample weight of 250g

Mass of water required will be:

M_{water} = 0.30 x 250 = 75 g

APPENDIX F2

Determination of Inherent Inorganic Content of Peat Moss

A mass of dried peat moss M_1 was burnt until only ashes remained with mass M_2. It is assumed here that all the organic portion of the peat moss will burn off and leave the inorganic portion.

The inherent inorganic content then becomes:

$$IC = \frac{M_2}{M_1} \qquad \text{(F2-1)}$$

Table F2-1 gives the results of three tests used to determine the inherent inorganic content of peat moss.

Table F2-1: Determination of Inherent Inorganic Content

Test Number	Mass (g)		
	M_1	M_2	M_1/M_2
1	52.1	4	0.076
2	59.3	4.1	0.069
3	53.4	4.3	0.08

The average of the inherent inorganic contents (M_1/M_2) is:

$$\frac{0.076 + 0.069 + 0.080}{3} = 0.075 = 7.5\%.$$

Thus the inherent inorganic content of the peat moss used in this study is thus 7.5%

APPENDIX F3

Determination of mass of sand required to give a targeted total inorganic content of peat moss and sand mixture.

It is assumed here that the inorganic content of sand is 100%

Recall that the inherent inorganic content of peat moss is 7.5%.

For any peat moss and fine sand mixture, the total inorganic content in percentage is given by

$$\text{IC} = \frac{M_{inorganic}}{M_{total}} \tag{F3-1}$$

where $M_{inorganic}$ = total mass of inorganics (sand and inherent inorganic in peat moss)

M_{total} = total mass of mixture

Since peat moss comprises 7.5% inorganics by mass,

$M_{inorganic} = M_{sand} + 0.075M_{peat}$

where M_{sand} = mass of sand required

M_{peat} = mass of peat moss required

Equation (F3-1) thus becomes:

$$IC = \frac{M_{sand} + 0.075M_{peat}}{M_{total}} = \frac{M_{sand} + 0.075M_{peat}}{M_{peat} + M_{sand}}$$

From which the M_{sand} is given as:

$$M_{sand} = \frac{(IC - 0.075)M_{peat}}{1 - IC} \tag{F3-2}$$

From Equation (F3-2), with any mass of peat moss, M_{peat} and the desired inorganic content of the mixture *IC*, the mass of sand required can be determined.

For example, for a total inorganic content of 44% with a peat moss mass of 250g, the mass of sand required is

$$M_{sand} = \frac{(0.44 - 0.075)250}{1 - 0.44} = 163 \text{ g}$$

Hence 163 g of sand is required to be mixed with 250 g of peat moss in order to obtain an inorganic content of 44% for the total mixture.

APPENDIX G

Calculating of spread rate of peat moss with inorganic content.

From Chapter Four, the correlation obtained for spread rate of peat moss with inorganics is given by:

$$w = -3\times10^{-11} IC^4 + 7\times10^{-9} IC^3 - 6\times10^{-7} IC^2 + 6\times10^{-6} IC + 0.0015 \quad \text{(G1)}$$

where w = spread rate of smouldering combustion in cm/s

IC = inorganic content in percent

For the peat moss in this study, at an inorganic content of 44%

$$w = -3\times10^{-11}44^4 + 7\times10^{-9}44^3 - 6\times10^{-7}44^2 + 6\times10^{-6}44 + 0.0015$$

w = 0.001086 cm/s

w = 0.001086 cm/s x 3600 s/hr

w = 3.9096 cm/hr

w = 3.9 cm /hr

For the mixture at 44% inorganic content, the mass of peat used was 283 g. Recall that the inorganic content of peat was 7.5% implying that the organic mass within the peat is

283 x 0.925 = 261.8 g

For a volume of 1700 cm^3, the organic density ρ, now becomes 261.8/1700

$\rho = 0.154\ g/cm^3$

From Frandsen's model, for zero percent moisture content, the spread rate from Equation (4.3) becomes:

$$w_{max} = 0.62/\rho \quad \text{(G2)}$$

$w_{max} = 0.62/0.154 = 4.025$ cm/hr

This compares very well with the correlation smouldering spread rate value of 3.9 cm/hr The percentage variation is 3%.

APPENDIX H

Comparison of Forest and Laboratory Constructed Soils

Figure H1 shows the temperature profiles at depths of 1 cm, 3 cm and 7 cm for the laboratory and forest soils for sample 5. Figure H2 shows the temperature profiles at depths of 1 cm, 3 cm and 5 cm for sample 3.

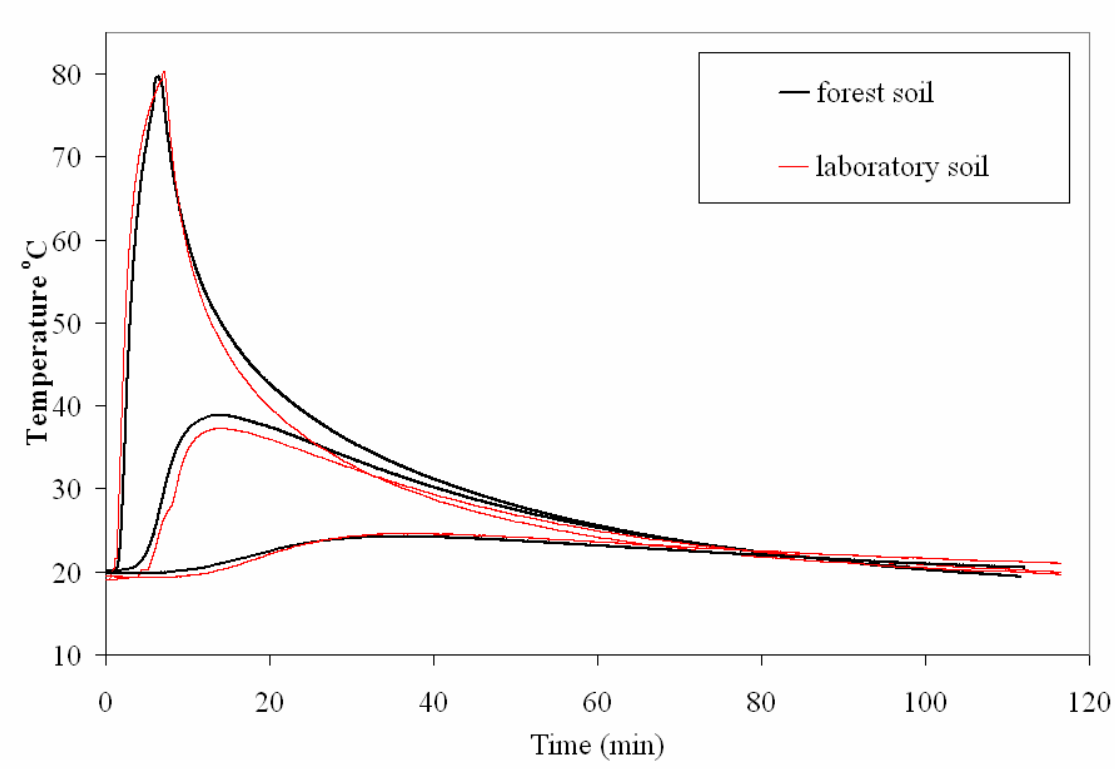

Figure H1: Comparison of Temperature Profiles at Depths of 1 cm, 3 cm and 7 cm for Forest and Laboratory Constructed Soils (Sample 5) Exposed to a Heat Flux of 50 kW/m^2 for 5 minutes

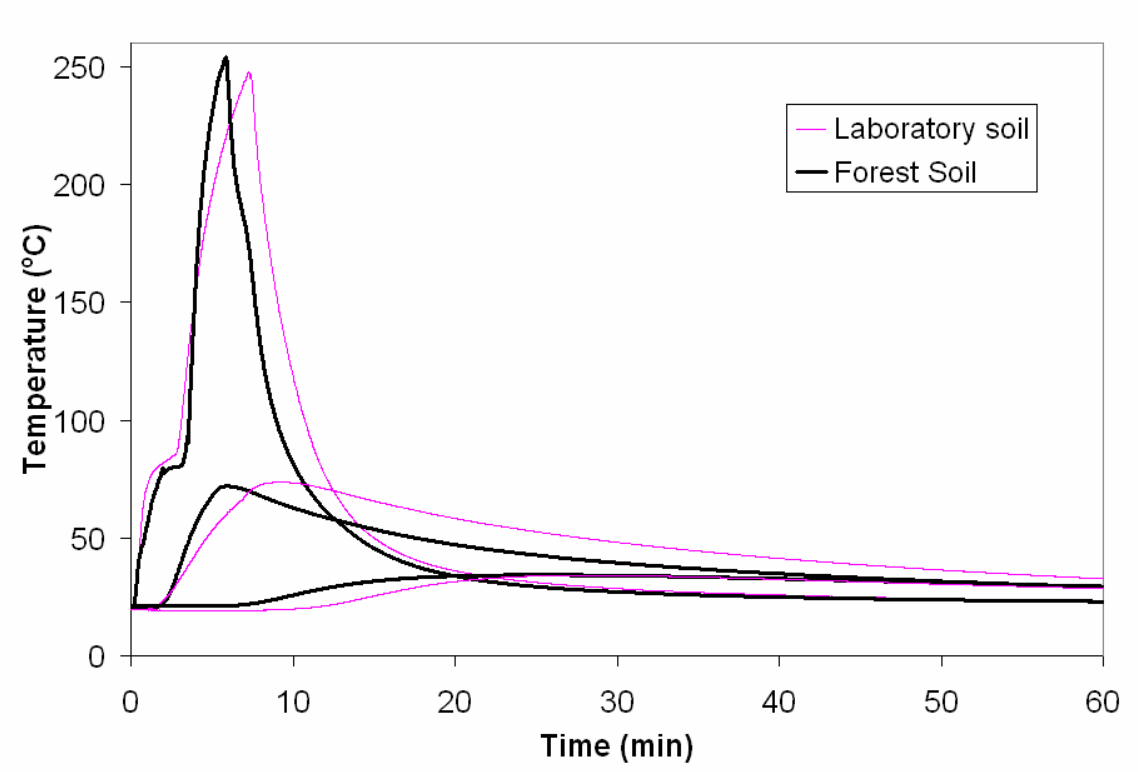

Figure H2: Comparison of Temperature Profiles at Depths of 1 cm, 3 cm and 5 cm for Forest and Laboratory Constructed Soils Exposed to a Heat Flux of 80 kW/m^2 for 8 Minutes